

Stochastic Terrain and Soil Modeling for Off-Road Mobility Studies

Richard Chan Lee

Thesis submitted to the faculty of the Virginia Polytechnic Institute and
State University in partial fulfillment of the requirements for the degree of

Master of Science
In
Mechanical Engineering

Dr. Corina Sandu

Dr. Mehdi Ahmadian

Dr. Dennis Hong

28 April 2009

Blacksburg, Virginia

Keywords: stochastic terrain modeling, finite difference method, stochastic soil properties,
wheel-soil interaction, off-road mobility studies

© Copyright 2009

Richard C. Lee

Stochastic Terrain and Soil Modeling for Off-Road Mobility Studies

Richard Chan Lee

ABSTRACT

For realistic predictions of vehicle performance in off-road conditions, it is critical to incorporate in the simulation accurate representations of the variability of the terrain profile. It is not practically feasible to measure the terrain at a sufficiently large number of points, or, if measured, to use such data directly in the simulation. Dedicated modeling techniques and computational methods that realistically and efficiently simulate off-road operating conditions are thus necessary. Many studies have been recently conducted to identify effective and appropriate ways to reduce experimental data in order to preserve only essential information needed to re-create the main terrain characteristics, for future use.

This thesis focuses on modeling terrain profiles using the finite difference approach for solving linear second-order stochastic partial differential equations. We currently use this approach to model non-stationary terrain profiles in two dimensions (i.e., surface maps). Certain assumptions are made for the values of the model coefficients to obtain the terrain profile through the fast computational approach described, while preserving the stochastic properties of the original terrain topology. The technique developed is illustrated to recreate the stochastic properties of a sample of terrain profile measured experimentally.

To further analyze off-road conditions, stochastic soil properties are incorporated into the terrain topology. Soil models can be developed empirically by measuring soil data at several points, or they can be created by using mathematical relations such as the Bekker's pressure-sinkage equation for homogeneous soils. In this thesis, based on a previously developed stochastic soil model, the polynomial chaos method is incorporated in the soil model.

In a virtual proving ground, the wheel and soil interaction has to be simulated in order to analyze vehicle maneuverability over different soil types. Simulations have been created on a surface map for different case studies: stepping with a rigid plate, rigid wheel and flexible wheel, and rolling of a rigid wheel and flexible wheel. These case studies had various combinations of stochastic or deterministic terrain profile, stochastic or deterministic soil model, and an object to run across the surface (e.g., deterministic terrain profile, stochastic soil model, rolling rigid wheel).

This thesis develops a comprehensive terrain and soil simulation environment for off-road mobility studies. Moreover, the technique developed to simulate stochastic terrain profile can be employed to simulate other stochastic systems modeled by PDEs.

Acknowledgements

First and foremost, I give my deepest gratitude to my advisor Dr. Corina Sandu. Without her guidance and support, I would not have been able to complete the research for this thesis. She taught me many technical details regarding my research and gave me the opportunity to learn how to present the information to different audiences by writing various journal articles and presenting at a number of conferences. Under Dr. Sandu's advice, I was able to conduct and present research at a high level, and I am deeply grateful for it.

Next, I would like to acknowledge and thank Dr. Mehdi Ahmadian, who is one of my committee members and the director of CVESS. Dr. Ahmadian was my first advisor in graduate school. He gave me the flexibility to ask different faculty members within CVESS in order to choose the research project that I desired. Through bi-weekly NASA-VIPER meetings, I learned of the importance and skill of communication and leadership from Dr. Ahmadian.

I would also like to thank and acknowledge several people who highly influenced the research conducted in this thesis. I give my thanks to Dr. Adrian Sandu for giving me his insights on stochastic terrain modeling and Dr. John Ferris for providing me the data to verify the methodology. Many thanks go to Trey Smith, Lin Li, and Emmanuel Blanchard for their time in helping me further understand the theories and procedures behind this research.

I am grateful to all of the members of the NASA-VIPER meetings, including Dr. Sean Kenny, Dr. Luis, Crespo, Dr. Daniel Giesv, and Dr. Pushkin Kachroo, for their helpful discussions and suggestions for my research.

I have greatly enjoyed my time and experience at CVESS. I would like to thank Mrs. Sue Teel and recognize her efforts in handling all of the paper work and documents for graduate school. I also thank all of the members of the CVESS family for the great conversations and experiences, in particular, Brian, James, Anake, and Hyun, who have spent many long working nights with me in the office at Randolph.

The research accomplished in this thesis was supported in part by NASA Langley through the VIPER award, by TARDEC through the Automotive Research Center, and by the NSF GOALI award CMMI-0700278. I would like to acknowledge these agencies for providing me with the funding and support to allow me to spend more time on my research.

Finally, I would like to show my sincerest gratitude to my family for their never-ending encouragement and motivation. They have supported me throughout my life and I am indebted to them. They have inspired me to accomplish my achievements.

Contents

ABSTRACT.....	ii
Acknowledgements.....	iv
Contents	vi
List of Figures	viii
List of Tables	xi
Chapter 1 Introduction	1
1.1 Motivation.....	1
1.2 Problem Statement	1
1.3 Research Objectives	3
1.4 Research Approach	3
1.5 Thesis Outline	4
Chapter 2 Review of Literature.....	5
2.1 State of the art in terrain and soil modeling for off-road mobility studies.....	5
2.2 Background	11
2.3 Previous terrain and soil modeling at AVDL.....	12
Chapter 3 Stochastic Terrain Profile.....	14
3.1 Modeling terrain profiles using stochastic PDE method.....	14
3.2 Experimental analysis of model coefficients	22
3.3 Processing raw terrain data with Surfer	30
3.4 Validating the stochastic PDE method.....	33
Chapter 4 Stochastic Soil Model.....	42
4.1 Experimental tests to develop empirical soil models	42
4.2 Simulating stochastic soil models using the polynomial chaos approach.....	45
4.3 Comparison of results for stochastic soil models	47
Chapter 5 Integrated Terrain-Soil Simulation Environments	51
5.1 Parameters used for the simulation environment	51
5.2 “Stepping” with a rigid plate on a flat terrain profile	53
5.3 “Stepping” with a rigid wheel on a flat terrain profile	54
5.4 “Stepping” with a rigid wheel on a flat terrain profile	55

5.5 Rolling with a rigid wheel on a deterministic terrain profile	57
5.6 Rolling with a flexible wheel on a deterministic terrain profile	59
5.7 Rolling on a deterministic terrain profile with stochastic soil properties	62
5.8 Rolling on stochastic terrain profile with deterministic soil properties	64
5.9 Rolling on stochastic terrain profile with stochastic soil properties	66
Chapter 6 Conclusions	69
Chapter 7 Future Work	72
References	74
Appendix A	82
A.1 MATLAB m-file used to create stochastic terrain profiles	82
A.2 Tabulated values from experimental analysis of σ and K	86
A.3 MATLAB m-file used to parse the raw data	100
A.4 Procedures to obtained processed raw data	103
Appendix B	107
B.1 Raw data for lunar soil simulant GRC-1	107
B.2 Detailed procedures for the polynomial chaos approach.....	109
B.3 MATLAB m-file for creating stochastic soil models	111
Appendix C	116
C.1 MATLAB m-file for rigid plate “stepping” on deterministic surface	116
C.2 MATLAB m-file for rigid wheel “stepping” on deterministic surface	118
C.3 MATLAB m-file for flexible wheel “stepping” on deterministic surface.....	120
C.4 MATLAB m-file for rigid wheel rolling on deterministic surface.....	123
C.5 MATLAB m-file for rigid wheel rolling on deterministic surface.....	127
C.6 MATLAB m-file for rigid wheel rolling on deterministic surface with stochastic soil ..	130
C.7 MATLAB m-file for flexible wheel rolling on deterministic surface, stochastic soil ...	134
C.8 MATLAB m-file for rolling on stochastic surface with deterministic soil	138
C.9 MATLAB m-file for rolling on stochastic surface with stochastic soil	138

List of Figures

Figure 3-1	Coefficients $A-E$ corresponding to their relative points	16
Figure 3-2	Illustration of boundary condition assumption and simplified notations	17
Figure 3-3	Illustration of nine different sections with different surrounding nodes	18
Figure 3-4	System of equations of a 4 points by 4 points surface map in matrix form	19
Figure 3-5	Matrices within a sparse matrix of a 5 points by 5 points surface map (a) Matrix with coefficients A, B, D (b) Matrix with coefficient C (c) Matrix with coefficient E...	20
Figure 3-6	Sparse matrix of a 5 points by 5 points surface map.....	21
Figure 3-7	Realization of a 2-D terrain profile using stochastic PDEs	22
Figure 3-8	Parameter analysis of K value	23
Figure 3-9	Parameter analysis for K values less than 0.1	24
Figure 3-10	Parameter analysis for K values greater than 0.1	25
Figure 3-11	Realizations for parameter analysis of model coefficient K (a) K value equals 1 (b) K value equals 2 (c) K value equals 4 (d) K value equals 10	27
Figure 3-12	Parameter analysis of σ value	28
Figure 3-13	Realizations for parameter analysis of model coefficient σ (a) σ value equals 1 (b) σ value equals 10 (c) σ value equals 50 (d) σ value equals 100.....	29
Figure 3-14	Map of the parsed raw terrain data obtained from VTPL	31
Figure 3-15	Processed terrain profile from raw data set in Surfer (a) 10 points by 10 points (b) 20 points by 20 points (c) 40 points by 40 points (d) 80 points by 80 points	32
Figure 3-16	Processed terrain profile from raw data set read in MATLAB (a) 10 points by 10 points (b) 20 points by 20 points (c) 40 points by 40 points (d) 80 points by 80 points	33
Figure 3-17	Trial runs for input of σ while model parameters remain at 1 (a) Trial 1 (b) Trial 2 (c) Trial 3 (d) Trial 4	35
Figure 3-18	Trial runs for input of σ and K values (a) Trial 1 (b) Trial 2 (c) Trial 3 (d) Trial 4	36
Figure 3-19	Trial runs for input of σ and reduced K values (a) Trial 1 (b) Trial 2 (c) Trial 3 (d) Trial 4	37
Figure 3-20	Simulation with σ value and K value equal to 0.2	39

Figure 3-21 Definition of variables used in Table 3-7	40
Figure 4-1 Cone penetrometer experiments performed on Virginia Tech’s terramechanics rig ..	43
Figure 4-2 Image of the cone penetrometer CP40 II (a) Disassembled view (b) Assembled View	44
Figure 4-3 Pressure-sinkage relationship for GRC-1.....	44
Figure 4-4 Stochastic simulation of GRC-1 with $b = 0.076$ m and density = 1.64 g/cc (a) Pressure-sinkage relationships (b) Probability density function (PDF)	48
Figure 4-5 Stochastic simulation of GRC-1 with $b = 0.102$ m and density = 1.67 g/cc (a) Pressure-sinkage relationships (b) Probability density function (PDF)	49
Figure 4-6 Stochastic simulation of GRC-1 with $b = 0.19$ m and density = 1.75 g/cc (a) Pressure-sinkage relationships (b) Probability density function (PDF)	49
Figure 4-7 Stochastic simulation of dry sand (0% moisture) (a) Pressure-sinkage relationships (b) Probability density function (PDF)	50
Figure 5-1 Chart of all the case studies presented in this chapter	52
Figure 5-2 Rigid plate “stepping” on a deterministic flat surface	54
Figure 5-3 Elliptic pressure distribution of contact patch	54
Figure 5-4 Rigid wheel “stepping” on a deterministic flat surface	55
Figure 5-5 Flexible wheel “stepping” on a deterministic flat surface	56
Figure 5-6 Geometry of contact patch of rolling wheel	57
Figure 5-7 Rigid wheel rolling on deterministic flat surface	58
Figure 5-8 Deterministic terrain surface with semi-oval bump	59
Figure 5-9 Rigid wheel rolling on a surface with a semi-oval bump	59
Figure 5-10 Flexible wheel rolling on deterministic flat surface	60
Figure 5-11 Flexible wheel rolling on a surface with a semi-oval bump	61
Figure 5-12 Side view of all case studies on flat deterministic terrain profiles	61
Figure 5-13 Rigid wheel rolling over terrain with stochastic soil parameter	62
Figure 5-14 Side view of Figure 5-13	63
Figure 5-15 Flexible wheel rolling over terrain with stochastic soil parameter	63
Figure 5-16 Side view of Figure 5-15	64
Figure 5-17 Rigid wheel rolling over stochastic terrain with deterministic soil	65
Figure 5-18 Side view of Figure 5-17	65

Figure 5-19 Flexible wheel rolling over stochastic terrain with deterministic soil	66
Figure 5-20 Side view of Figure 5-19	66
Figure 5-21 Rigid wheel rolling over stochastic terrain with stochastic soil	67
Figure 5-22 Side view of Figure 5-21	67
Figure 5-23 Flexible wheel rolling over stochastic terrain with stochastic soil	68
Figure 5-24 Side view of Figure 5-23	68
Figure A-1 Print screen of “Grid” on Surfer Toolbar	104
Figure A-2 Print screen of pop-up window in Surfer	105
Figure A-3 Illustration of “Map” on Surfer Toolbar	106

List of Tables

Table 3-1	Maximum values for the region of the K values less than 0.1	25
Table 3-2	“Best fit” line for graphs in regions of K values greater than 0.1.	26
Table 3-3	Numerical values recorded from subplots in Figure 3-11.	27
Table 3-4	Recorded values for subplots of Figure 3-17.	35
Table 3-5	Recorded values for subplots of Figure 3-18.	37
Table 3-6	Recorded values for subplots of Figure 3-19.	38
Table 3-7	Comparison between correlation of boundary nodes	41
Table 4-1	Standard deviations of GRC-1 at specific depths.	45
Table 4-2	Pressure-sinkage parameters for numerical simulations.	48
Table 5-1	Pressure-sinkage parameters for Sandy Loam.	53
Table 5-2	Parameters for tire model.	53
Table A-1	Tabulated values for Figure 8, for $\sigma = 0.1$	87
Table A-2	Tabulated values for Figure 8, for $\sigma = 1$	88
Table A-3	Tabulated values for Figure 8, for $\sigma = 10$	89
Table A-4	Tabulated values for Figure 9, for $\sigma = 0.1$	90
Table A-5	Tabulated values for Figure 9, for $\sigma = 1$	91
Table A-6	Tabulated values for Figure 9, for $\sigma = 10$	93
Table A-7	Tabulated values for Figure 10, for $\sigma = 0.1$	96
Table A-8	Tabulated values for Figure 10, for $\sigma = 1$	97
Table A-9	Tabulated values for Figure 10, for $\sigma = 3$	97
Table A-10	Tabulated values for Figure 10, for $\sigma = 5$	98
Table A-11	Tabulated values for Figure 10, for $\sigma = 8$	98
Table A-12	Tabulated values for Figure 10, for $\sigma = 10$	99
Table A-13	Tabulated values for Figure 12.	100
Table A-14	X and Y coordinates for processed data	105
Table B-1	Raw data obtained at depths of 5mm to 55mm for GRC-1	107
Table B-2	Raw data obtained at depths of 65mm to 115mm for GRC-1	108
Table B-3	Slope of pressure and depth for each measurement.....	108
Table B-4	Calculated mean and standard deviation for every depth interval.....	109

Table B-5 Legendre polynomials to the 4 th order	110
---	-----

Chapter 1 Introduction

The scope of this thesis is to realistically and efficiently develop a simulation environment for off-road operating conditions which combines stochastic terrain profiles and stochastic soil models. This chapter provides the motivation and brings arguments for the importance of this research. Section 1.1 describes the motivation behind the current research. Section 1.2 defines the problem statement. Section 1.3 explains the research objectives. Section 1.4 introduces the approach used to achieve the research objectives. Section 1.5 gives an outline of the remaining chapters.

1.1 Motivation

Modeling the terrain in a realistic and efficient manner is critical in analyzing vehicle dynamics, especially in off-road conditions. Terrain geometry and soil characteristics highly affect vehicle mobility and handling. For off-road mobility studies, many uncertainties exist within the system, some of which could be the variability in the terrain heights, the variability in the soil types, and the variability in the tire forces. Hence, there have been sustained efforts to study the modeling and simulations of the stochastic properties in terrain profiles to accurately predict the vehicle performance.

Off-road studies on vehicle mobility can be categorized in three main areas: (1) real-life systems, (2) analytical models, (3) experimental studies. Real-life systems include the actual vehicle running across the terrain surface. Analytical models include mathematical or numerical representations of the vehicle and terrain. Experimental studies consist of physical depictions of the real-life systems. This thesis presents an original analytical model to illustrate the effects of the stochastic nature within the tire-soil interaction. The analytical model can be used to design real-life systems and validate experimental studies. Therefore, it is important to analyze the variability in recreating accurate representations of terrain profiles for off-road mobility studies.

1.2 Problem Statement

To have a complete understanding of the physics of off-road vehicle mobility, the stochastic nature of the terrain profile will have to be analyzed. Different operating conditions at a given

spatial location and a given time can greatly influence the performance of the vehicle. It is not practically feasible to measure the terrain at a sufficiently large number of points, or, if measured, to use such data directly in the simulation. Dedicated modeling techniques and computational methods are required to create accurate representations of virtual proving grounds to interpret vehicle dynamic simulations. Therefore, emphasis will have to be placed on stochastic terrain modeling in order to further examine vehicle dynamics.

To enhance the terrain models, stochastic soil models can be incorporated with it. Stochastic terrain profiles only present the topology of the terrain at a given time and location. Implementation of soil models is critical in realistically simulating off road conditions since different types of soil have different soil properties. Moreover, there is difficulty in predicting soil properties due to their dependence on environmental conditions and soil types. At any given spatial location, there can be variability in the soil due to its characteristics (e.g., moisture content, stiffness, cohesion). Similar to the terrain profiles, it is not practically feasible to measure soil properties at all desired locations and implement them directly into the simulation to be able to develop an accurate soil model. Therefore, computational methods will also be required to create stochastic soil models.

Combining the stochastic terrain profiles and the stochastic soil models yields a realistic virtual proving ground for off-road vehicle mobility studies. Many factors have to be considered when modeling the affects between the tire and soil interaction to have an accurate representation of the off-road mobility studies. Some factors may include the vertical force of the tire, the lateral dynamics of the tire, and the geometry of the contact patch. Dedicated modeling techniques will also be required to adequately present the simulation framework between a tire and the variability in the off-road terrain.

This study focuses on: (1) generating computational tools to model stochastic terrain topology, (2) incorporating stochastic soil characteristics in the terrain model, and (3) developing simulations for tire-soil interactions in the framework developed.

1.3 Research Objectives

Starting from the problem identified in the previous section, the following research objectives have been considered in this study.

1. Develop an efficient mathematical approach to treat the uncertainties in the terrain profiles and the soil models.
2. Use experimental data to verify the stochastic terrain modeling technique developed.
3. Process experimental terrain profile data and extract the key stochastic properties from the data collected.
4. Collect soil data to validate the stochastic soil models used.
5. Combine the terrain profiles with soil models to create a simulation framework for the tire-soil interaction.
6. Implement the mathematical models in MATLAB and run simulations with rigid plates, rigid wheels, and flexible wheels.

1.4 Research Approach

The computational approach used to achieve the research objectives is listed below.

1. Modeling stochastic 2-D terrain profiles.
 - Model a linear second order stochastic partial differential equations (PDE) driven by uncorrelated white noise.
 - Illustrate the technique on real terrain profile data.
2. Incorporate stochastic soil models in the simulation environment.
 - Use Bekker's pressure-sinkage equation for homogeneous soils to simulate relations specific to deformable soil types.
 - Validate the stochastic soil modeling technique using soil data collected in the terramechanics rig at AVDL.
3. Construct simulations to illustrate tire-soil interaction.
 - Create simulation scenarios to show different case studies of stochastic or deterministic terrain geometry, stochastic or deterministic soil model, and either a rigid plate, a rigid wheel, or a flexible wheel.

1.5 Thesis Outline

This thesis is organized in the following manner. Chapter 1 provides a brief introduction of the research, the motivation behind it, the problem statement and research objectives.

Chapter 2 presents a review of literature related to soil and terrain modeling, treatment of uncertainties, and tire-soil and terrain interaction.

Chapter 3 provides the methodology used to model the stochastic terrain profile. The finite difference is used to solve a linear second-order stochastic partial differential equation (PDE) to create terrain in two dimensions. This chapter also provides an experimental approach to obtain and process data to verify the methodology developed.

Chapter 4 presents a technique previously developed at AVDL which uses the Karhunen-Loeve expansion and the polynomial chaos theory to create the stochastic soil models. Some of the soil parameters in Bekker's pressure-sinkage equation are considered to be uncertain. This chapter also provides an experiment performed to obtain and process data to verify the stochastic soil model.

Chapter 5 illustrates the tire-soil interaction by creating different case scenarios in the integrated terrain-soil simulation environment. Several case studies were shown to examine the off-road mobility of rigid and flexible wheels in the off-road virtual proving ground developed.

Chapter 6 and chapter 7 present the conclusions of this study and recommendations for the future work, respectively.

Appendices are also attached to the end of this thesis with MATLAB codes and programs that were used to complete this work.

Chapter 2 Review of Literature

This chapter is organized in the following manner. Section 2.1 introduces a general review of literature. It consists of sources that relate to terrain modeling, numerical approaches to derive terrain models, soil modeling, and tire-soil interaction models. Section 2.2 discusses the sources that were highly relevant for this study. Section 2.3 describes the work accomplished by Dr. Lin Li, whose work closely relates to the topic of this thesis.

2.1 State of the art in terrain and soil modeling for off-road mobility studies

There have been recent efforts to model terrain profiles to create accurate simulations for vehicle dynamics. Studies show that methods to create terrain profiles can be grouped into two distinct categories: on-line and off-line.

On-line approaches of terrain modeling consist of collecting terrain data with improved technologies, such as high performance sensors, cameras, and lasers. Larson, Voyles, and Demir (2004) use a single camera to collect terrain data. The terrain data have spatial patterns which represent the characteristics of the terrain. Williams and Mahon (2004) also introduced an approach to collect terrain data of the sea floor by using a camera on an unmanned underwater vehicle (UUV). Laser scanning is a fairly new and popular technique that has been used in several research groups to recreate terrain models. One particular airborne laser scanner system is named TopEye. Data has been collected with this system to integrate terrain models with cartographic data (Elmqvist et al., 2001). Maas (2001) and Hyypä et al., (2000) used techniques to collect airborne laser scanner data of forestry terrain. Hatger (2005) also used laser airborne scanning techniques to record terrain data of areas in Northrhine Westphalia, Germany. Laser scanning collects large amounts of data, which allows highly accurate representations of the surface. However, it often results in complex data management and processing and long computational times.

After the laser scanning data is identified and processed, accurate digital terrain models (DTM) will be created using a specific approach. The fuzzy logic approach, which is used to analyze different soil classes in a spatial domain, was used to produce digital soil maps for parts of

Vestfold county in Norway (Debella-Gilo, Etzelmuller, and Klakegg, 2007). The fractional Brown motion approach was used to generate lunar simulation surfaces on PC or Silicon Graphics (Yang et al., 2008). Kamat and Martinez (2003) introduced ViTerra, a tool used to recreate 3D terrains. They used particular applications of construction jobsites. Although online approaches are proven to be very accurate, it usually includes high costs and complex assemblies.

Off-line approaches consist of generating algorithms and using mathematical tools to model the terrain profile. Many studies use statistical approaches to verify or model the terrain profiles. Statistical tests have been used to verify the linearity, Gaussianity, and stationarity of the terrain profile. The Belgian Block course and the Perryman3 profiles were used to verify this method (Chaika, Gorsich, and Sun, 2004). Two dimensional road profiles have also been characterized using the Autoregressive Integrated Moving Average (ARIMA) techniques, which examines the autocorrelation of the terrain models (Kern and Ferris, 2006; Kern et al., 2007).

Stochastic computational approaches are also popular in modeling terrain profiles and surfaces. Yeh, Lin, and Wang (2001) solved the Helmholtz wave equation with a stochastic approach to interpret wave propagation over an irregular terrain. The power spectral density is a function that is often used with a stationary stochastic process. There have been studies using the PSD approach to measure road roughness and approximate road profiles (Andrén, 2006; Ramji et al., 2006). The PSD approach has been used with the root mean square of elevation (RMSE) to characterize road/terrain roughness for ground vehicles. Howe et al., (2004) uses the International Roughness Index (IRI) and fatigue analysis to improve these measures.

There have also been several other numerical tests and approaches to model terrain profiles and surfaces. Yoon (2003) used the Delaunay triangulation and the T-search algorithm to model the terrain profile by searching for the resulting triangular polygons. Kim, Thompson, and Machiraju (2003) produced rough surfaces using discrete surface growth models. Compared to on-line approaches, off-line approaches are usually inexpensive, easy to handle for complex topologies, and are often created in real-time.

In this study, we propose solving stochastic partial differential equations as an off-line approach to model terrain profiles. There are several numerical methods that can be employed to solve for stochastic PDEs. The popular methods are the finite element method (FEM), the finite difference method (FDM), and the boundary element method (BEM). For many problems, BEM is the least efficient out of the three methods. Comparisons are usually made between FEM and FDM since both methods are categorized as volume discretization methods. FEM has the ability to precisely model surfaces and geometries in complex domains. Although FDM is only constrained to model rectangular shapes, the computational approach is easily implemented compared to FEM.

More sophisticated techniques can also be derived from these methods. Shen (1996) introduces the block finite difference scheme, which is derived from the finite element method to solve second-order differential equations. The method of lines (MOL) is another method in which the time, space, and randomness are treated separately to solve stochastic PDEs with forced additive noise. The MOL uses stochastic Runge-Kutta methods to solve the stochastic system (Rößler, Seaïd, and Zahri, 2008). The sparse grid stochastic collocation method is a collocation technique to approximate a solution for a stochastic PDE (Nobile, Tempone, and Webster, 2008).

Satisfying boundary conditions is essential in solving stochastic PDEs since it greatly influences the solution. One well known boundary condition is the Dirichlet boundary condition. Chantasiriwan (2005) introduces a global collocation method to solve stochastic PDEs with random Dirichlet boundary conditions. Another technique to solve the Dirichlet boundary value problem is the Adomian decomposition method (El-Sayed and Gaber, 2006). Duncan, Pasik-Duncan, and Zimmer (1996) use mathematical approaches to investigate stochastic PDEs with Dirichlet, Neumann, and mixed boundary conditions.

There are certain variables in the stochastic PDE that define the random signal, also known as the white noise. Kim et al., (2007) introduced a numerical method based on the integral equation to solve stochastic DEs with Poissonian white shot noise. Sandow and Trimper (1992) presented an approach to solve a stochastic DE, particularly the Kardar-Parisi-Zhang equation, with Gaussian white noise. Poissonian white shot noise and Gaussian white noise are specific mathematical models of noise. The stochastic Algorithm Refinement (AR) hybrid technique has

been studied in attempts to reduce the noise in stochastic systems (Alexander, Garcia, and Tartakovsky, 2005).

The Wiener process is a specific way to represent white noise in a stochastic system. It is used as a continuous time stochastic process. Gibson (1967) introduces an extensive solution to solve stochastic PDEs where the characteristic trajectories are modeled with the Wiener process. Schurz (2006) analyzes a stochastic DE driven by the Wiener process by solving it with an implicit backward Euler method. Lythe (1998) uses the finite difference solutions to solve for the Ginzburg-Landau stochastic PDE with the Wiener process. Other than mathematical methods, computer programs, such as Maple, have also been used to solve stochastic PDEs driven by the Wiener process (Cyganowski, 1995). Studies have shown that the applications of stochastic partial differential equations apply to problems dealing with a wide variety of subjects. Particular subjects include physics, biology, and chemical reactions.

There have also been studies to illustrate stochastic approaches to soil modeling. Fenton (1999) used statistical measures, such as sample covariance, spectral density, and wavelet variance functions, to analyze the uncertainties in soil properties. The Bayesian approach has also been used to estimate the uncertainties in soil moisture simulations. This approach is based on the Generalized Likelihood Uncertainty Estimation (GLUE) methodology (Hossain, Anagnostou, and Lee, 2004).

To create stochastic soil models, experiments must run to collect soil, moisture, and pressure-sinkage data. Van et al., (2008) compiled data from Tottori dry sand using bevameter techniques. Procedures were derived to extract the parameters for the Bekker's pressure-sinkage equation, which is a well known relationship for representing homogeneous soils. Many applications and studies have validated and implemented Bekker's equation. Another experimental technique used to estimate soil sinkage parameters is the multiplate penetration tests (Rashidi and Gholami, 2008). Bin et al., (2008) have also conducted experimental plate-sinkage tests to measure the properties of a lunar soil simulant made with volcanic ash that was obtained from the Jilin province, China. The plate-sinkage tests were conducted by PF2CD, a specific Distinct Element Method software.

Analysis of the behavior between tire and soil interaction is required to study off-road vehicle dynamics. Several studies show that this is a very challenging task and results vary depending on the type of terrain and the type of tire. One case scenario predicts behavior between three different flexible tires on soft soils using the finite element method (FEM) (Yong, Fattah, and Boonsinsuk, 1978). Chung and Lee (1975) utilize FEM to analyze the contact area by deriving the equations of motion underneath a moving rigid wheel. This study emphasizes the structure of the soil instead of the wheel. To efficiently simulate off-road conditions, the characteristics of the wheel will also have to be modeled. Shoop, Richmond, and Lacombe (2006) also model tire-terrain interactions using FEM simulations. Specific applications include tires running on cold regions terrains, such as snow. Zhang, Lee, and Liu (2005) have also studied tire and snow interactions using the ABAQUS computer software to solve finite element methods. The contact forces, the response of the tire, and the deformations in the snow were some of the parameters investigated in the study.

In addition to the use of numerical methods such as FEM, experimental tests are also performed to validate the studies of tire-soil interaction. Bauer, Leung, and Barfoot (2005) ran experiments on a single wheel rig to validate a single wheel model that was created in MATLAB. Experimental results that show a rigid wheel running on two different types of soil were also used to prove a tire-soil model created with the discrete element method (Khot et al., 2007). Nguyen et al., (2008) obtained experimental results to verify a method used to measure vertical soil reactions in contact areas of off-road tires. Wulfsohn and Upadhyaya (1992) conducted experiments on the UC Davis single wheel traction testing machine to develop a technique used to analyze the contact areas of several tires on different soil types.

Agricultural tractor tires have been popular in recent studies. Van et al., (2008b) created experiments to study the effects of tire inflation pressure for farm tractors. A relationship is derived between the tire inflation pressure, the rolling resistance, and the soil-tire stresses. Kumar and Dewangan (2004) have presented a study on power tiller tires. The study consisted of varying the normal loads and inflation pressures of the tire, and running it on a rigid flat surface. Garber and Wong (1981) studied the pressure distribution of a tracked vehicle, which highlight the idea of repetitive loading. Usually, the tractor tires are modeled and run in computer

simulation programs such as the Tractive Performance Prediction Model for Tracked Vehicles (TPPMTV) program (Park et al., 2008) and the MOSES program (Ferretti and Girelli, 1999). Using computer simulation programs can allow users to easily change the type of terrain that the tire model is being run on. MATLAB is used to create the simulation environment developed in this thesis. MATLAB allows a user-friendly interface in incorporating the stochastic terrain model and the stochastic soil model into the simulation framework.

Another common application of tire-soil interaction relates to planetary exploration. Studies have shown experimental results between rigid planetary rover wheels on dry sand (Shibly, Iagnemma, and Dubowsky, 2005). Patel, Scott, and Ellery (2005) suggested the use of the Rover Mobility Performance Evaluation Tool (RMPET), a computer program that simulates the interactions between tire and soil interaction for planetary exploration. Tracked and legged vehicles were also studied. Ishigami et al. (2007) focused on the steering aspects of the tire-soil contact area for a planetary exploration rover. Linear least square methods have also been used to determine the contact area for the applications of planetary rovers (Iagnemma et al., 2004).

For tire and soil interaction, different formulations and mathematical models are used to predict the forces and geometry in the contact patch. One study uses mathematical models to illustrate the pressure-sinkage, shear stress, and repetitive loading for a contact patch (Wyk, Spoelstra, and Klerk, 1994). Okello (1992) introduced a study that shows the contact area being split into two different sections: planar and spiral. The planar section is the section underneath the tire where the terrain is flat. The spiral section is the section between the planar section and the wheel-terrain entry point of contact. Formulations derived in these sections are functions of the angles that are created between the tire and the terrain. The deflection of the wheel can also be modeled as a function of the normal load, the inflation pressure, the carcass pressure, and specific constants that depend on the design of the tire (Sharma and Pandey, 1996b). There are many other techniques and methods used to analyze the contact area, and they are dependent on the type of tire and the terrain that the tire is rolling over.

Many different scenarios may be designed to illustrate a variety of effects in simulating the tire-soil interaction. One example of a case scenario is comparing a rigid wheel and a flexible wheel

running on a uniform terrain (Wang and Reece, 1984). Park, Popov, and Cole (2004) have also compared both flexible wheel models and rigid wheel models with a single point contact model. All three models were investigated with emphasis on soil deformation. In addition to the wheel, the terrain can also be modeled as either a rigid or a deformable surface (Sharma and Pandey, 1996a). Irregular terrains, such as curbs and potholes, influence the tire-terrain interaction very much. Studies have been done to model such effects by analyzing the radial spring of the tire, the sidewall impact, and the soil content (Day, 2005).

2.2 Background

The methodology used to model the terrain profiles in this paper is derived from the random forcing model presented by Constantinescu et al. (2007). The random forcing model consists of a second order PDE with an additive white noise process. In that study, the purpose was to construct autoregressive models of the background errors and apply it in the context of chemical transport models. The correlation length was determined in the random forcing model to be $\sqrt{K/L}$, in which K and L were parameters in the model. In this thesis, the finite difference method is used to solve the random forcing to model the stochastic terrain profiles. FDM is a numerical method that approximates the solution of a differential equation by discretizing the function on a grid. The solution is dependent on the surrounding nodes.

One way to characterize the soil properties is through the Bekker's pressure-sinkage equation for homogeneous soil (Wong, 2001). The pressure-sinkage parameters are n , k_c , and k_ϕ , and they vary depending on the type of soil and the moisture content. Soil modeling is not only limited to Bekker's equation. Other representations of soil models may include Reece's equation (Wong, 2001), which also includes pressure-sinkage characteristics. Van et al. (2008a) has shown that the experimental device used to obtain the parameters can also affect the value of the parameter (e.g., using a rectangular plate vs. a circular plate for the sinkage test).

The polynomial chaos theory was used to simulate stochastic processes by representing the unknown variable as a probability distribution (e.g., normal distribution). The Galerkin approach and collocation approach are two ways to solve for the polynomial chaos expansion (Sandu,

Sandu, and Ahmadian, 2006a). Applications that use the polynomial chaos theory include multibody dynamic systems with uncertain parameters. The Monte Carlo simulation was used to validate the polynomial chaos approach for multibody systems (Sandu, Sandu, and Ahmadian, 2006b). In this study, the polynomial chaos theory is used with the Karhunen-Loeve (KL) expansion to model stochastic soil parameters, as described by Sandu, Sandu, and Li (2005).

To realistically simulate the tire-soil interactions, the pressure distribution of the contact area, the geometry of the contact patch, and the characteristics of the tire will have to be modeled together. One way of calculating the pressure distribution in the contact patch was described by Chan (2008). The pressure distribution is a function of the shape change factor, the longitudinal slip ratio, the maximum pressure, the length of the contact patch, and the specific location of the contact patch. The maximum pressure is calculated as a function of the length and width of the contact patch and of the vertical load of the wheel. The geometry of the contact area can be displayed as a super-ellipse. Depending on the pressure or load of the wheel and the terrain characteristics, the super-ellipse can assume a wide variety of shapes (Hallonborg, 1996). Schwanghart (1991) discussed a study where the length of the contact area was derived using the sinkage, the radius of the wheel, and the deflection of the wheel. This equation can be modified to calculate the deflection of the wheel. Other important factors related to the contact patch are the slip ratio, the shear stress, and the shear displacement.

2.3 Previous terrain and soil modeling at AVDL

The work of Lin Li closely relates to the topic of this thesis. Li's work focused on the stochastic nature of vehicle dynamics and terramechanics (Li, 2008). Li also developed methodologies to create tire-soil interaction models for off-road mobility applications.

Lin Li has developed different methods to model terrain profiles. Li and Sandu (2007) have used both the Auto-Regressive Moving Average (ARMA) series method and the Autoregressive Integrated Moving Average (ARIMA) models to develop terrain profiles in one-dimension and two-dimensions. The linearity, stationarity, and Gaussianity of the terrain profile have been investigated to determine which method is of better use for modeling the different types of terrain. The ARMA model is better suited for well-paved roads, while the ARIMA model is

more appropriate for unprepared terrains. Lin Li also developed stationary and non-stationary, 1-D terrain profiles using the polynomial chaos approach. The Karhunen-Loeve expansion was used with the polynomial chaos approach to expand the stochastic terrain profile to two dimensions. For the 2-D case, there are two different algorithms in simulating the terrain profile (Li and Sandu, 2008). Compared to Li's approach to create terrain profiles, the method developed in this thesis has the capability to create as much terrain profiles as needed for the off-road vehicle dynamics simulation using a limited amount of data. The model can also be easily simulated by varying the model parameters in the stochastic PDE.

Lin Li has also developed stochastic soil models. The polynomial chaos method was applied to the parameters of Bekker's pressure-sinkage equation for homogeneous soils. The parameters for Bekker's equation were assumed to have a linear relationship in which the moisture content was the unknown variable (e.g., indirectly effects Bekker's equation). Both the uniform and normal distributions were also assumed for his case studies. The probability density function was displayed to validate his results (Sandu, Sandu, and Li, 2005). This stochastic soil model will be validated in the present study and incorporated in the off-road simulation environment. The soil modeling approach that Sandu, Sandu, and Li (2005) developed is used to incorporate into the simulation environment and used to validate the soil models obtained in this thesis. However, the soil model created in this thesis is not completely the same; here, the uncertain variable in Bekker's equation is considered one of the pressure-sinkage parameters (e.g., directly effects Bekker's equation).

Chapter 3 Stochastic Terrain Profile

This chapter describes a mathematical approach and validation for creating stochastic terrain profiles. It is organized in the following manner. Section 3.1 introduces the methodology in modeling the stochastic terrain profiles using a second-order stochastic partial differential equation. Section 3.2 shows the experimental analysis on the model coefficients. Section 3.3 displays the procedures and Surfer software to process raw terrain data. Section 3.4 shows procedures in matching the stochastic terrain profile to the processed raw data.

3.1 Modeling terrain profiles using the stochastic PDE method

A main focus of this thesis is to realistically and efficiently model terrain profiles using the finite difference approach to solve partial differential equations. The non-stationary terrain profiles are modeled and analyzed in two dimensions (e.g., surface map). Consider the second-order stochastic partial differential equations driven by uncorrelated white noise. Equation 3.1 was derived from the random forcing model presented by Constantinescu et al. (2007).

$$K(x, y) \left(\frac{\partial^2 Z}{\partial x^2} + \frac{\partial^2 Z}{\partial y^2} \right) + \left(\frac{\partial}{\partial x} (u_x \cdot Z) + \frac{\partial}{\partial y} (u_y \cdot Z) \right) + L \cdot Z = \sigma \cdot \xi(x, y) \quad (3.1)$$

The terrain height is represented by the variable Z , the model coefficients are represented by K , u , L , and σ , and the random variable is $\xi(x, y)$. The variables x and y represent the distances in the lateral and longitudinal directions of the surface map. To simplify the equation, the following notation is used to approximate a particular point P .

$$P(x_i, y_j) = P_{ij} \quad (3.2)$$

The finite difference method (FDM) is a numerical method to approximate solutions for partial differential equations. It divides a function on an evenly spaced grid, in which each node is dependent on its surrounding nodes. For the methodology presented, the values of the nodes represent the terrain heights, variable Z , on the surface map. Using the FDM, the second derivatives can be approximated with the following equations. Equation 3.3 presents approximations in the x direction, while Equation 3.4 presents the approximations in the y direction.

$$\left(\frac{\partial^2 Z}{\partial x^2}\right)_P = \left(\frac{\partial^2 Z}{\partial x^2}\right)_{ij} \approx \frac{Z_{i+1,j} - 2Z_{ij} + Z_{i-1,j}}{\Delta x^2} \quad (3.3)$$

$$\left(\frac{\partial^2 Z}{\partial y^2}\right)_P = \left(\frac{\partial^2 Z}{\partial y^2}\right)_{ij} \approx \frac{Z_{i,j+1} - 2Z_{ij} + Z_{i,j-1}}{\Delta y^2} \quad (3.4)$$

As for the first derivative values, Equation 3.5 and Equation 3.6 approximate the central difference value for the x and y directions, respectively.

$$\left(\frac{\partial u}{\partial x}\right)_P = \left(\frac{\partial u}{\partial x}\right)_{ij} \approx \frac{u_{i+1,j} - u_{i-1,j}}{2\Delta x} \quad (3.5)$$

$$\left(\frac{\partial u}{\partial y}\right)_P = \left(\frac{\partial u}{\partial y}\right)_{ij} \approx \frac{u_{i,j+1} - u_{i,j-1}}{2\Delta y} \quad (3.6)$$

Using the second derivative and first derivative equations for FDM (Equations 3.3 - 3.6), the second order stochastic partial differential equation, which is modeled by Equation 3.1, can be solved to produce Equation 3.7.

$$\begin{aligned} K_{ij} & \left(\frac{Z_{i+1,j} - 2Z_{ij} + Z_{i-1,j}}{\Delta x^2} + \frac{Z_{i,j+1} - 2Z_{ij} + Z_{i,j-1}}{\Delta y^2} \right) \\ & + \left(\frac{u_{i+1,j}Z_{i+1,j} - u_{i-1,j}Z_{i-1,j}}{2\Delta x} + \frac{u_{i,j+1}Z_{i,j+1} - u_{i,j-1}Z_{i,j-1}}{2\Delta y} \right) \\ & + L_{ij} \cdot Z_{ij} = \sigma_{ij} \cdot \xi_{ij} \end{aligned} \quad (3.7)$$

Equation 3.7 can be further simplified in terms of terrain height, Z . This is shown in Equation 3.8, whereas the coefficients A - E are shown by Equations 3.9 - 3.13, respectively.

$$A Z_{ij} + B Z_{i,j+1} + C Z_{i+1,j} + D Z_{i,j-1} + E Z_{i-1,j} = \sigma_{ij} \cdot \xi_{ij} \quad (3.8)$$

$$A = \left[-2K_{ij} \left(\frac{1}{\Delta x^2} + \frac{1}{\Delta y^2} \right) + L_{ij} \right] \quad (3.9)$$

$$B = \left[\frac{K_{ij}}{\Delta y^2} + \frac{u_{i,j+1}}{2\Delta y} \right] \quad (3.10)$$

$$C = \left[\frac{K_{ij}}{\Delta x^2} + \frac{u_{i+1,j}}{2\Delta x} \right] \quad (3.11)$$

$$D = \left[\frac{K_{ij}}{\Delta y^2} - \frac{u_{i,j-1}}{2\Delta y} \right] \quad (3.12)$$

$$E = \left[\frac{K_{ij}}{\Delta x^2} - \frac{u_{i-1,j}}{2\Delta x} \right] \quad (3.13)$$

Coefficient A corresponds to the parameters related to a particular point on the surface map. Coefficients B - E correspond to the parameters related to the four surrounding nodes of that particular point, starting from the top node and rotating clockwise, respectively. Figure 3-1 illustrates a point with corresponding coefficient A and the coefficients relating to the four surrounding nodes.

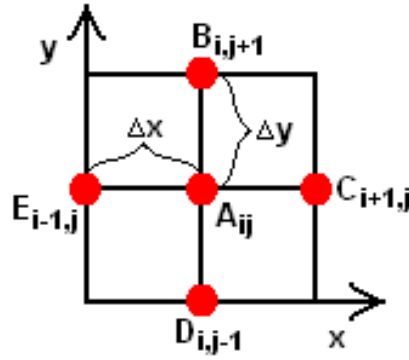


Figure 3-1 Coefficients A - E corresponding to their relative points.

An assumption made in our version of the finite difference approach concerns the boundary conditions imposed. The finite difference method is usually applied in models dealing with heat transfer where the boundary conditions are well defined. In the case of stochastic terrain profile modeling, there are no imposed boundary conditions. Therefore, we used a “wrap around” approach where the boundary point is equal to the last point at the opposite end of a specific row or column in the grid. This assumption is also shown in Figure 3-2, where the first value of the height on the bottom border, x_1 , is equal to the value of the right, bottom boundary condition, x_{N+1} , and the last value of the height on the bottom border, x_N , is equal to the value of the left, bottom boundary condition, x_0 . This figure only displays two boundary condition values on the bottom border in the x -direction. This idea is the same for the other border nodes. Although for

many practical purposes and applications of interest we consider that this assumption is acceptable (depending also on the correlation length), its implications and the limitations it imposes on the terrain model should be further investigated. Figure 3-2 also illustrates the notation that is used to simplify a point, P_{ij} , on the surface map for the equations (e.g., Equation 3.2).

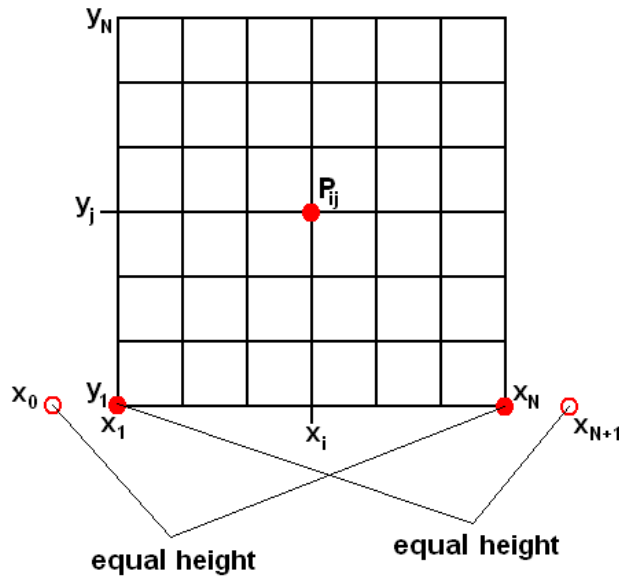


Figure 3-2 Illustration of boundary condition assumption and simplified notations.

With the boundary conditions thus defined, a terrain profile can be divided into nine different sections, in which each section has different boundary nodes. Figure 3-3 is an illustration with the nine different sections on an example of a 6 points by 6 points surface map. Sections one, three, seven, and nine always contain one node. They are the top left corner, top right corner, bottom left corner, and bottom right corner of a surface map, respectively. However, the number of nodes within sections two, four, five, six, and eight are dependent on the size of the terrain profile. Sections two, four, six, and eight are the top boundary, left boundary, right boundary, and bottom boundary, respectively. Section five includes all of the interior nodes of the surface map.

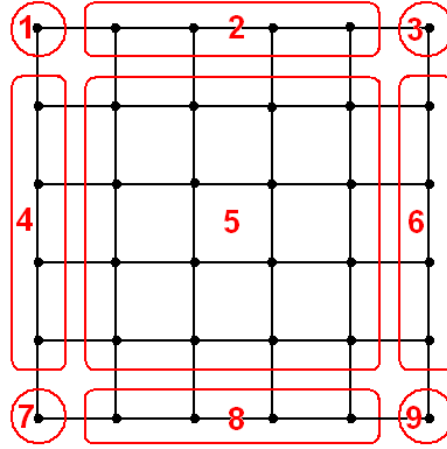


Figure 3-3 Illustration of nine different sections with different surrounding nodes.

There are two different approaches to solve for the nodes using FDM: implicit method and explicit method. In solving the FDM explicitly, it requires the values of the surrounding nodes, which means there is only one unknown value which we can solve directly. When all the values for the surrounding nodes are unknown, the FDM will have to be solved implicitly. A system of equations will be created in which all of the values will be solved simultaneously.

Equation 3.8 will be followed by the implicit method because the terrain heights are unknown on the surface map. Figure 3-4 shows an example of the system of equations on a 4 point by 4 point surface map written in matrix form. Every point on the surface map has an equation that is dependent on its surrounding nodes. In computational aspects, another assumption is made that the surface map can only have an equal number of points in both the x and y directions (e.g., square surface map). The left hand side will consists of the sparse matrix of coefficients A - E and a vector of the unknown height Z_{ij} , while the right hand side will equal to a vector of $\sigma_{ij} * \zeta_{ij}$. The empty cells in the sparse matrix are equal to zero. This notation is also used in Figures 3-5 and 3-6. Depending on the number of points on the axis of the surface map, k , this matrix form is written so that every consecutive set of k equations will be equal to a column on the surface map (e.g., Figure 3-4 is a 4 points by 4 points map, so first four equations equal to column 1, next four equations equal to column 2, etc).

A	B		D	C							E				
D	A	B			C							E			
	D	A	B			C							E		
B		D	A				C							E	
E				A	B		D	C							
	E			D	A	B			C						
		E			D	A	B			C					
			E	B		D	A				C				
				E				A	B		D	C			
					E			D	A	B			C		
						E			D	A	B			C	
							E	B		D	A			C	
C								E				A	B	D	
	C								E			D	A	B	
		C								E			D	A	B
			C								E	B		D	A

Z ₁₁
Z ₁₂
Z ₁₃
Z ₁₄
Z ₂₁
Z ₂₂
Z ₂₃
Z ₂₄
Z ₃₁
Z ₃₂
Z ₃₃
Z ₃₄
Z ₄₁
Z ₄₂
Z ₄₃
Z ₄₄

=

$\sigma_{11} \zeta_{11}$
$\sigma_{12} \zeta_{12}$
$\sigma_{13} \zeta_{13}$
$\sigma_{14} \zeta_{14}$
$\sigma_{21} \zeta_{21}$
$\sigma_{22} \zeta_{22}$
$\sigma_{23} \zeta_{23}$
$\sigma_{24} \zeta_{24}$
$\sigma_{31} \zeta_{31}$
$\sigma_{32} \zeta_{32}$
$\sigma_{33} \zeta_{33}$
$\sigma_{34} \zeta_{34}$
$\sigma_{41} \zeta_{41}$
$\sigma_{42} \zeta_{42}$
$\sigma_{43} \zeta_{43}$
$\sigma_{44} \zeta_{44}$

Figure 3-4 System of equations of a 4 points by 4 points surface map in matrix form.

The matrix of coefficients $A-E$ is sparse. There is a particular pattern for the sparse matrix in this methodology due to the assumptions imposed on the boundary conditions. To create the sparse matrix, the following steps are taken. In Figures 3-5a, 3-5b, and 3-5c are example submatrices of a 5 point by 5 point surface map. The size of these matrices is equal to the number of points on a side of a surface map (e.g., for a 5 point by 5 point surface map, the dimensions of the matrix is 5x5). Figure 3-5a is a matrix containing coefficients A , B , and D . Coefficient A will always fill the main diagonal. Coefficient B will always fill the diagonal above the main diagonal and the bottom left cell of the matrix. Coefficient D will always fill the top right cell of the matrix and the diagonal below the main diagonal. Figure 3-5b is a matrix containing the coefficient C on the main diagonal. Lastly, Figure 3-5c is a diagonal matrix of coefficient E .

A	B			D
D	A	B		
	D	A	B	
		D	A	B
B			D	A

C				
	C			
		C		
			C	
				C

E				
	E			
		E		
			E	
				E

a Matrix with coefficients A, B, D **b** Matrix with coefficient C **c** Matrix with coefficient E

Figure 3-5 Matrices within a sparse matrix of a 5 points by 5 points surface map.

The next step in creating a sparse matrix is to input Figures 3-5a, 3-5b, and 3-5c. Figure 3-6 shows an example of the entire sparse matrix for a 5 point by 5 point surface map. The dimensions of the sparse matrix is equal to the entire number of points on the surface map (e.g., shown is an example of a 5 points by 5 points surface map, which has a total of 25 points; therefore, the dimensions of the sparse matrix will be 25 by 25). To better visualize the procedures, imagine taking the square root of the dimensions of the sparse matrix, and each cell also contains a grid with the same dimensions (e.g., in a 25 by 25 sparse matrix, a 5 by 5 matrix can be reduced, which is drawn by a thicker line in Figure 3-6, and within each cell, a 5 by 5 matrix is inserted). When this step is completed, insert Figure 3-5a into the main diagonal. Figure 3-5b will fill the diagonal above the main diagonal and the bottom left cell. Finally, Figure 3-5c will fill the top right cell and the diagonal below the main diagonal. This method in creating the sparse matrix can be applied to any size surface map greater than 2 by 2. The sparse matrix in Figure 3-4 can be used to validate the procedures.

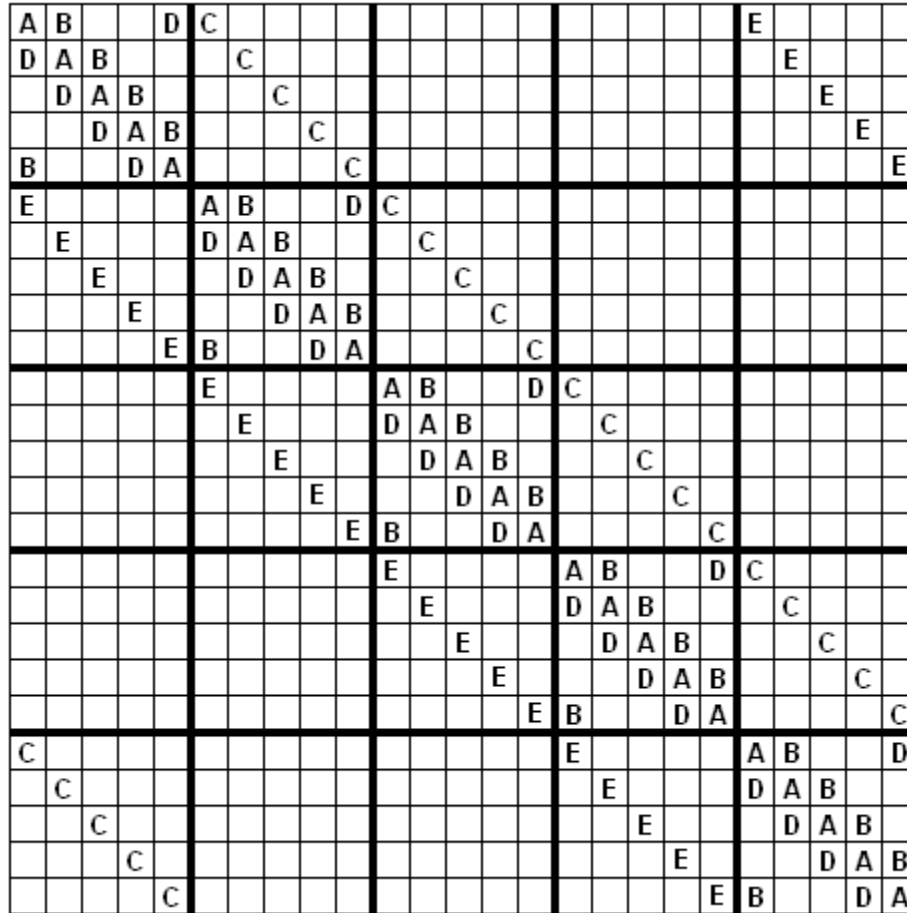


Figure 3-6 Sparse matrix of a 5 points by 5 points surface map.

Figure 3-7 is a realization of a two-dimensional terrain profile using the stochastic PDEs method developed in this study, and was built on an 80 points by 80 points x - y grid. This surface map was created using MATLAB^{®1}. Sparse matrices were used in efforts to implicitly solve the system of equations. For this particular case, the lateral and longitudinal directions extend from 0 units to 3 units. Therefore, the spatial domain for both the lateral and longitudinal directions is equal to 0.0375 units. All of the model coefficients were set to a value of 1 for the simulation illustrated in Figure 3-7. Appendix A.1 displays the MATLAB m-file used to create this surface.

¹ MATLAB is a registered trademark of The MathWorks

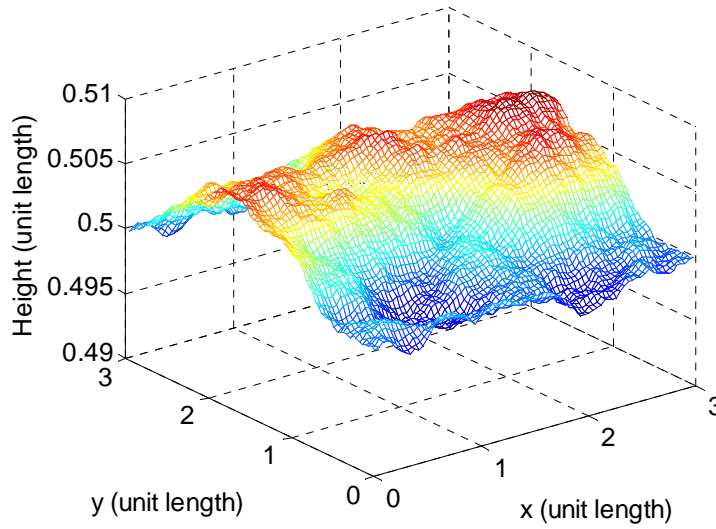


Figure 3-7 Realization of a 2-D terrain profile using stochastic PDEs.

The methodology introduced is not only limited to modeling stochastic terrain profiles. The second-order stochastic partial differential equation is a mathematical tool that can also model other stochastic systems and processes.

3.2 Experimental analysis of model coefficients

An analysis was conducted to analyze the influence of the model coefficients in the stochastic PDE on the topology of the terrain created. Two-dimensional terrain profile data (obtained experimentally) was used to approximate the model coefficients K , u , L , and σ of a stochastic system of partial differential equations. The model parameters are space dependent. Our study shows that the characteristic correlation length is equal to $\sqrt{K/L}$ and the value of σ influences the amplitude of the terrain height. The results of the study conducted to investigate the significance of the model parameter u and its impact on the terrain profile variation are inconclusive. Further analysis of this parameter is needed.

It has been noticed that, as the value of K increases while the value of L remains constant, the difference between the height of the terrain profile decrease. An experiment was performed to analyze the parameter K , which is an indirect method of understanding the correlation length. The parameters L , u , and σ were held constant at 1, while the value of K was varied. The

maximum and minimum values were taken from a terrain profile on a grid of 10 points by 10 points. The difference between the maximum heights and the minimum heights were recorded. This procedure was repeated 100 times and the average of the difference of heights were recorded. The same procedures were performed for three different experiments where the value for σ varied from 0.1, 1, and 10.

Figure 3-8 shows the results on a log-log plot for the parameter analysis of the K value. One can notice the similarity in the shape, as well as in the values for peaks and slopes, when σ changes with one or two orders of magnitude. While the average difference in height converges to values close to σ in all cases presented for a K value less than 0.02, for values of K larger than 0.1, the height difference decreases with an abrupt slope. Also, the general trend is for K to decrease for σ between 0.02 and 0.1, but there is a noticeable local maximum at 0.1. The results for the three experiments were very consistent.

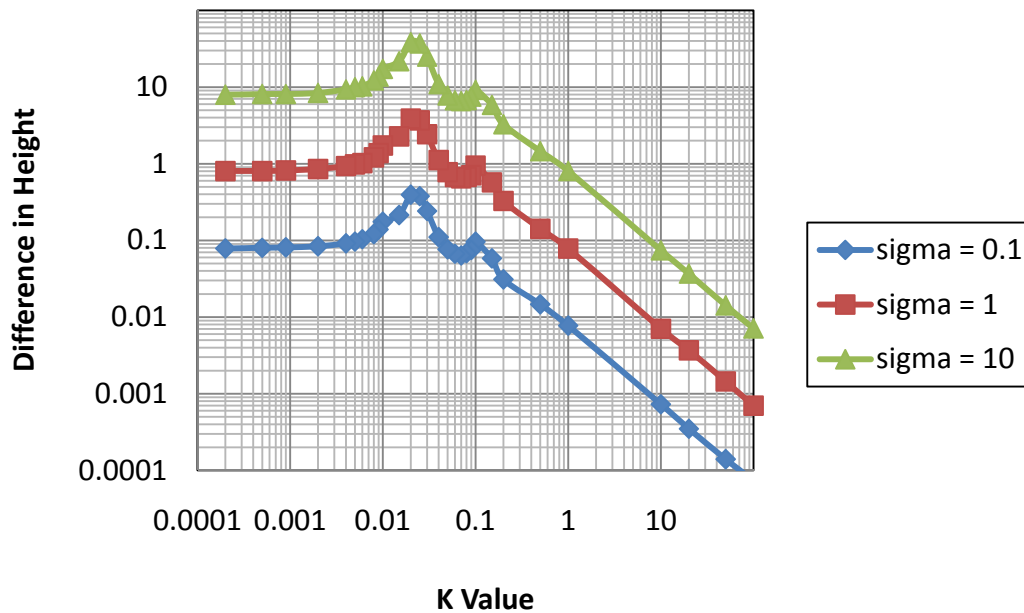


Figure 3-8 Parameter analysis of K value.

Figure 3-9 shows more detailed experiments (i.e., a finer grid for K) performed in the region of the K value less than 0.1. The y axis is presented on a log scale while the x axis is presented on a linear scale. Further analysis in this region shows a complicated pattern for the difference in heights of the terrain profile. Looking at the figure, there seems to be “spikes”, or local maxima,

at particular values of K . The pattern is consistent for all three cases of σ . This shows that K is indirectly affected by the value of σ . The reasons behind the pattern of the graphs in Figure 3-9 are unknown. Further experiments by defining a finer grid for K will have to be performed to investigate the relationship in this region in more details.

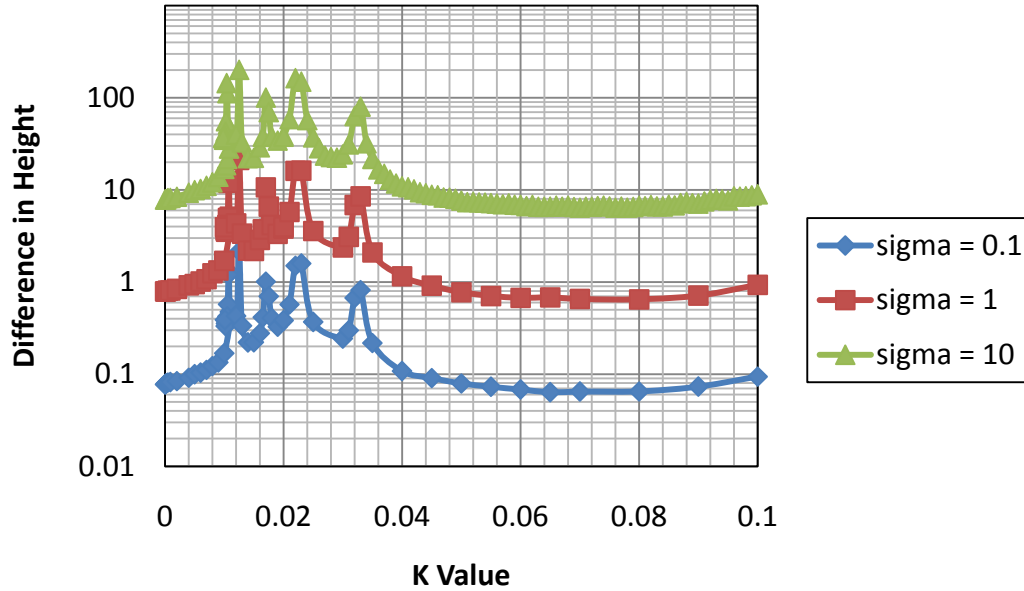


Figure 3-9 Parameter analysis for K values less than 0.1.

So far, five “spikes” have been recorded for the three different σ values, which are shown in Table 3-1. All of the local maxima values in the difference of heights were at the same values of K , which validates the conclusion that the graphs are consistent for different values of σ and share the same pattern.

Figure 3-10 shows a plot for the region of the K values greater than 0.1 with σ values of 0.1, 1, 3, 5, 8, and 10. Unlike the region for the K values less than 0.1, the graphs for the region of K values greater than 0.1 are very consistent in the defined range. The lines plotted do not have unexpected peaks, and carry the same pattern throughout the entire graph. By using a variety of σ values, the conclusion that the σ value indirectly affects K is supported.

Table 3-1 Local maxima values for the region of the K values less than 0.1.

σ	K	Local Maxima Values
0.1	0.0108	1.291
0.1	0.0125	2.1568
0.1	0.017	1.0137
0.1	0.022	1.5061
0.1	0.033	0.8202
1	0.0108	12.5386
1	0.0125	21.2149
1	0.017	10.6772
1	0.022	16.1323
1	0.033	8.5196
10	0.0108	143.8502
10	0.0125	200.4067
10	0.017	100.6133
10	0.022	163.0471
10	0.033	80.155

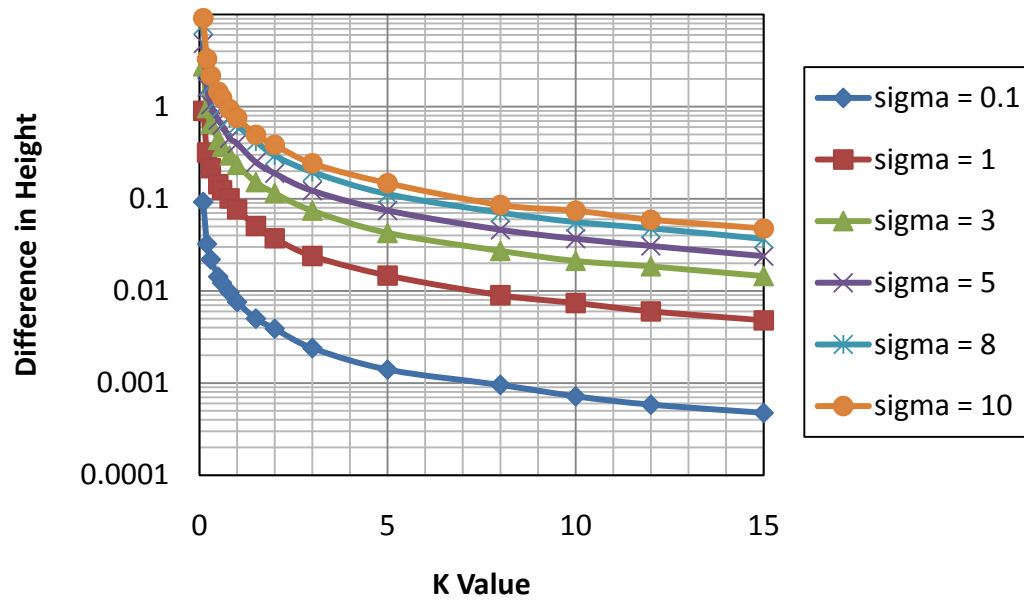


Figure 3-10 Parameter analysis for K values greater than 0.1.

The “best fit” line for the plots shown in Figure 3-10 are calculated and shown in Table 3-2. These equations are functions of the difference in terrain heights and the K value, and are correspondent to a single σ value. The “best fit” equations are modeled with a power function.

Table 3-2 “Best fit” line for graphs in regions of K values greater than 0.1.

σ	“Best fit” line
0.1	$\Delta Height = 0.007 K^{-1.01}$
1	$\Delta Height = 0.074 K^{-1}$
3	$\Delta Height = 0.222 K^{-1}$
5	$\Delta Height = 0.372 K^{-1}$
8	$\Delta Height = 0.594 K^{-1.02}$
10	$\Delta Height = 0.738 K^{-1.01}$

Moreover, a standard equation is developed for the K value. First, a linear relationship is assumed between the σ value and the coefficient of the best fit line. This relationship is shown through Equation 3.14. The exponent of the power function is assumed to always have a constant value of -1. This is a reasonable assumption since it is rounded to the nearest integer.

$$coefficient = 0.074 \sigma \quad (3.14)$$

Inserting Equation 3.14 into the “best fit” line equation will lead to Equation 3.15.

$$\Delta Height = 0.074 (\sigma) K^{-1} \quad (3.15)$$

Rearranging Equation 3.15 in terms of the K will lead to a standardized equation for the model coefficient K . As shown in Equation 3.16, K is dependent on σ and the difference in heights.

$$K = \frac{0.074 (\sigma)}{\Delta Height} \quad (3.16)$$

To further support our conclusions of K , Figures 3-11a, 3-11b, 3-11c, and 3-11d represents 4 realizations (e.g., 80 points by 80 points grid) with K values of 1, 2, 4, and 10, respectively, while the other parameters, L , u , and σ , were held constant at 1. The maximum height, minimum height, and the difference in heights are recorded from the subplots in Figure 3-11 and are shown

in Table 3-3. The data shows that as the value of K (e.g., correlation length) increases, the difference in terrain height decreases.

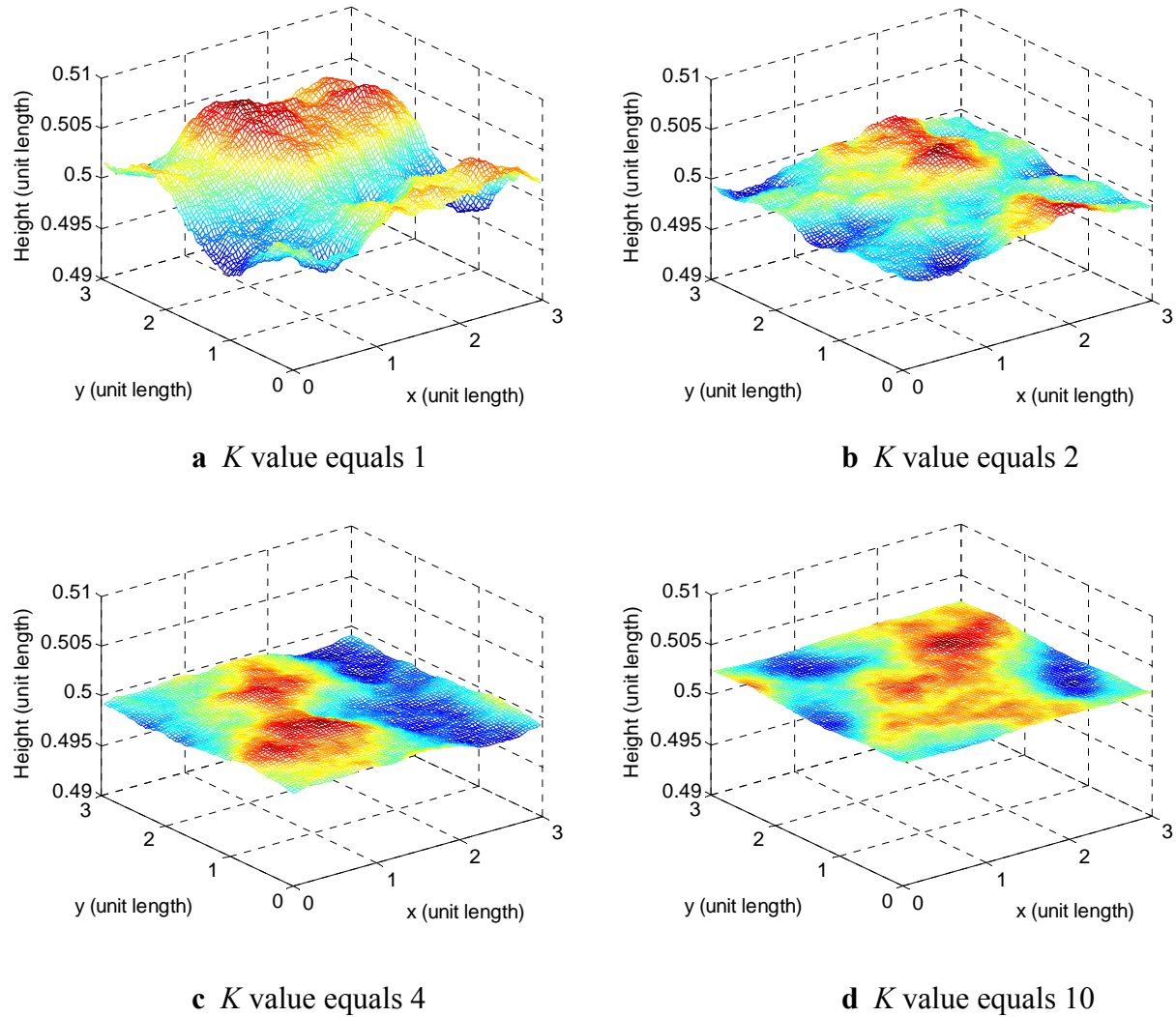


Figure 3-11 Realizations for parameter analysis of model coefficient K .

Table 3-3 Numerical values recorded from subplots in Figure 3-11.

Subplot	K Value	Maximum Height (unit length)	Minimum Height (unit length)	Difference in Heights (unit length)
a	1	0.50619	0.49573	0.01046
b	2	0.50837	0.5047	0.00367
c	4	0.50063	0.4983	0.00233
d	10	0.50272	0.50176	0.00096

Further analysis on the σ value shows that as the value of σ increases, the amplitude of the terrain profile also increases. Another experiment was performed to analyze the parameter σ . The parameters L and u were held constant at 1, while the value of K was held constant at 10,000. From our previous experiment, the results showed that as K increased, the difference in terrain height decreased. By setting the value of K at a large number, the variability of the terrain height will be minimized. As shown in Figure 3-12, the values of the average maximum height and values of the average minimum heights overlap each other. This experiment was also based on a terrain profile created on a 10 points by 10 points grid. The maximum and minimum values were recorded from the entire surface map after 100 simulations, and the values of the terrain heights were averaged to obtain the points plotted in Figure 3-12. The terrain height as a function of σ with L , u , and K constant is presented in Figure 3-12.

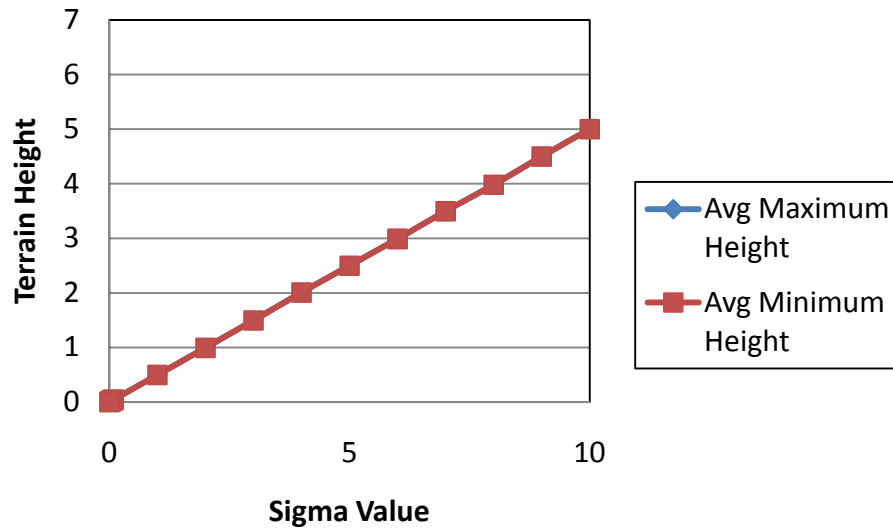


Figure 3-12 Parameter analysis of σ value.

The results from Figure 3-12 support the conclusions from the previous experiment, since there was almost no error between the averaged maximum and averaged minimum terrain heights while the value of K is a large number. Figure 3-12 shows that the lines are identical. From the plot, the “best fitted” line was derived and the equation is shown below.

$$Z = 0.5 \sigma \quad (3.17)$$

This equation shows the relationship between the terrain height, Z , and one of the model coefficients, σ .

Figure 3-13a, 3-13b, 3-13c, and 3-13d are realizations (e.g., 80 points by 80 points grid) that have different σ values of 1, 10, 25, and 100, respectively. All of the other model parameters, K , L , and u , are held constant at 1. The purpose of the subplots is to show that the amplitude of the terrain height is close to half of the value of σ (e.g., Equation 3.17).

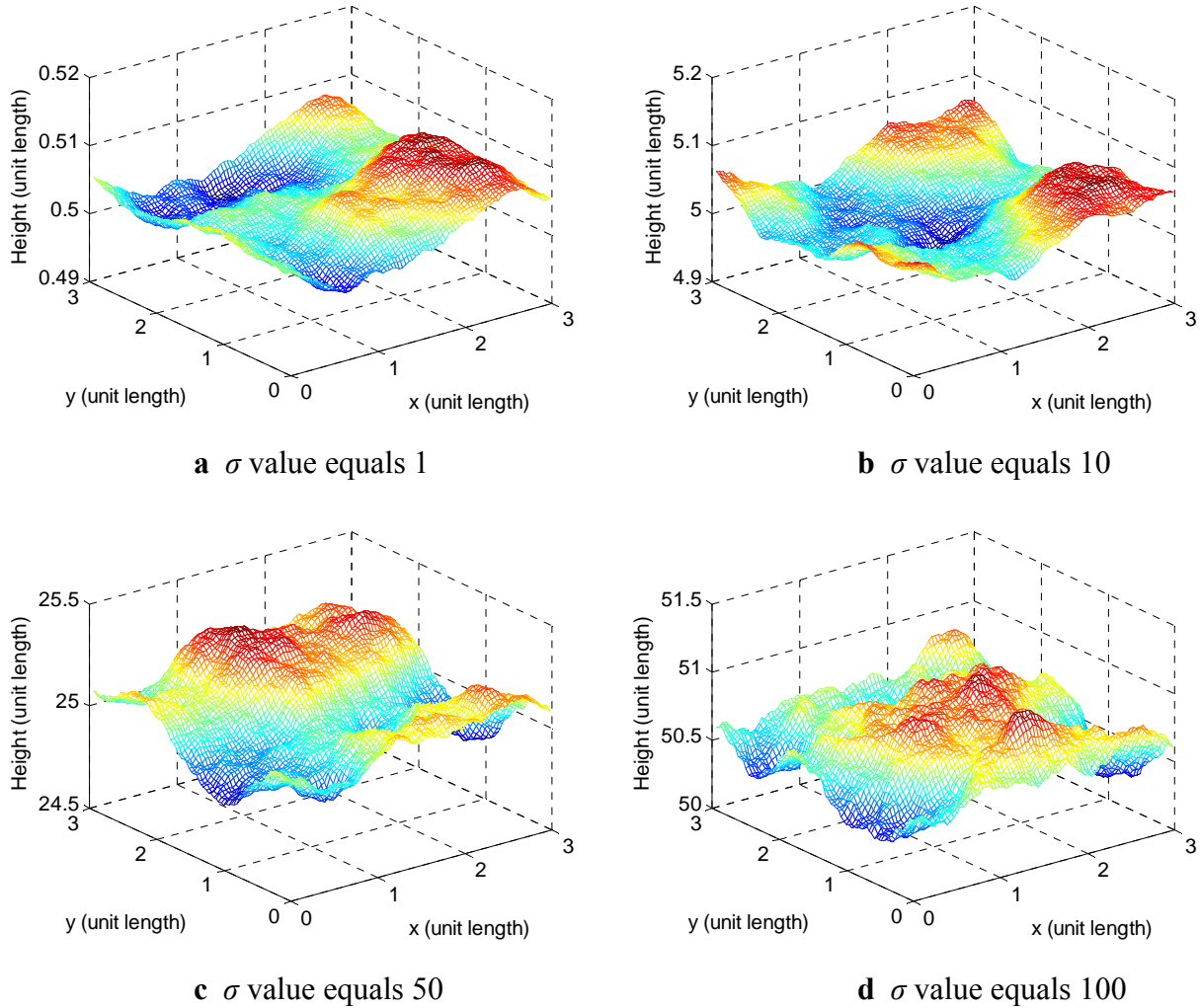


Figure 3-13 Realizations for parameter analysis of model coefficient σ .

From the experimental analysis of the model coefficients K and σ , relationships can be obtained to model the terrain profiles. In particular, Equations 3.16 and 3.17 can be used to derive the

correlation lengths and amplitudes of the stochastic terrain topologies. The next sections show procedures to extract and process raw terrain data to validate the methodology and the experimental analysis for the model coefficients. Appendix A.2 contains more tabulated values collected from the experimental runs.

3.3 Processing raw terrain data with Surfer

Terrain data was obtained from Virginia Tech's Vehicle Terrain Performance Laboratory (VTPL), directed by Dr. John Ferris. The raw terrain data was taken over a gravel road with a DGPS base station antenna, and it consisted of 32,934,540 points. The width of the terrain profile was taken to be around 4.2 meters. Within that range, the technology at VTPL has the capability of capturing 940 data points. The output of the data consists of three tab delimited columns (x position, y position, and z position). The positive x coordinate corresponds to East, the positive y coordinate corresponds to North, and the z coordinate corresponds to the ellipsoidal height.

Since the raw data file has a large amount of data points, it would require long computational times and memory to process the entire data set. Therefore, an m-file is written using the programming software MATLAB to parse the raw data. This m-file was obtained from Trey Smith, a current graduate student at VTPL, and is displayed in Appendix A.3. The m-file parses the raw data into separate data files with .dat extensions, with each file containing a maximum of 4,000,000 points. Therefore, the data was converted into 9 different sections, which are shown in Figure 3-14. The vehicle carrying the DGPS base station antenna recorded data from section 1 to section 9. One can notice that the terrain data is not taken parallel to the Cartesian coordinate system, and the raw data is not uniformly spaced on the grid. The red square in section 5 is the processed data that will be used for the analysis of the stochastic terrain profiles. This will be explained in the next section.

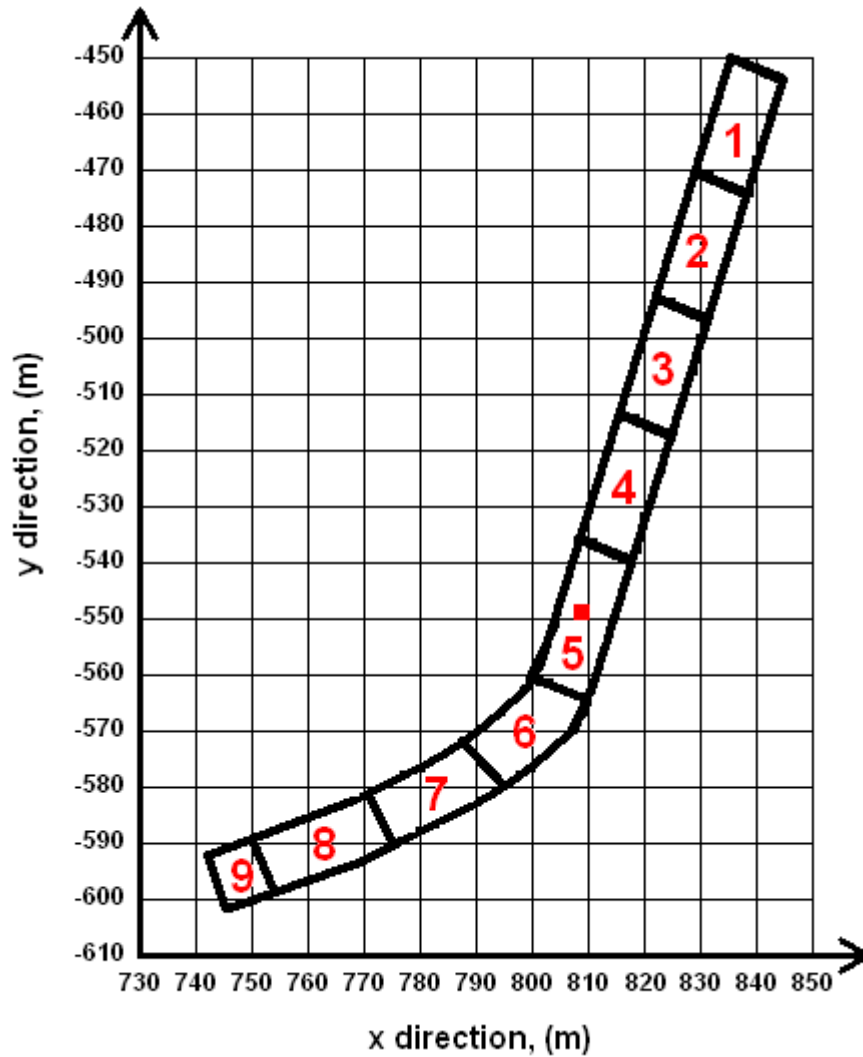
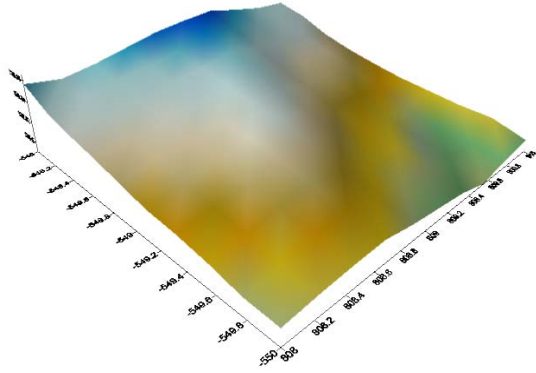


Figure 3-14 Map of the parsed raw terrain data obtained from VTPL.

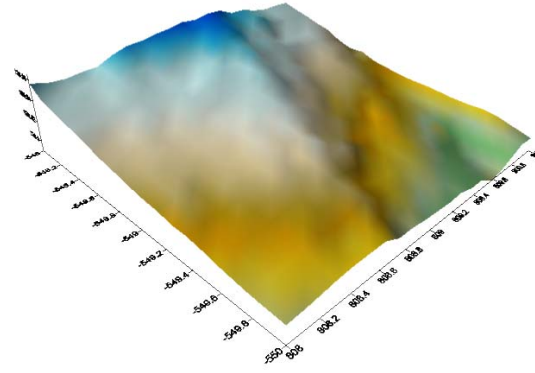
After the data is parsed, the commercial visualization tool named Surfer^{®2} was used to further process and visualize the data. Surfer has a gridding method feature in which the raw data can be gridded on a uniformly spaced x - y plane. Other features also include defining the exact dimensions of a piece of the terrain in the raw data. Appendix A displays step by step instructions to obtain the processed data from Surfer. A square piece of terrain in section 5 (shaded in red on Figure 3-14) with the x coordinates of 808 to 810 and y coordinates of -550 to -548 was selected. Figures 3-15a, 3-15b, 3-15c, and 3-15d illustrate another feature of Surfer, in which it can read and apply a certain number of points to the defined surface map. The terrain

² Surfer is a registered trademark of the Golden Software

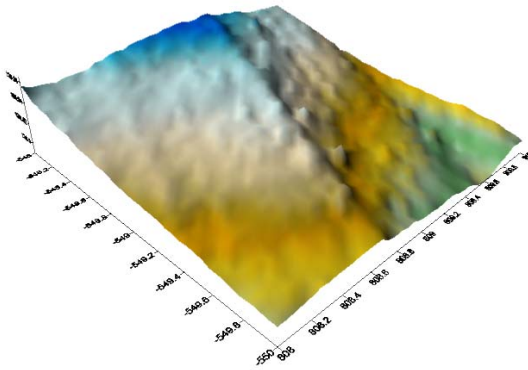
profile is more detailed as the total number of points on the grid increases from a 100 point surface, a 400 point surface, a 1600 point surface, and a 6400 point surface, respectively.



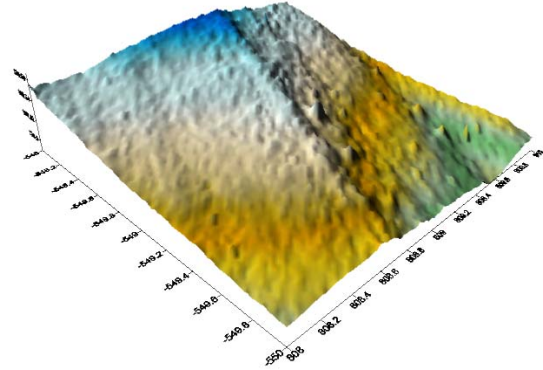
a 10 points by 10 points



b 20 points by 20 points



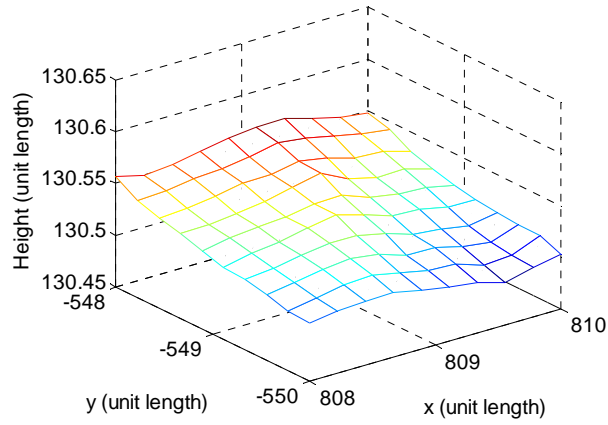
c 40 points by 40 points



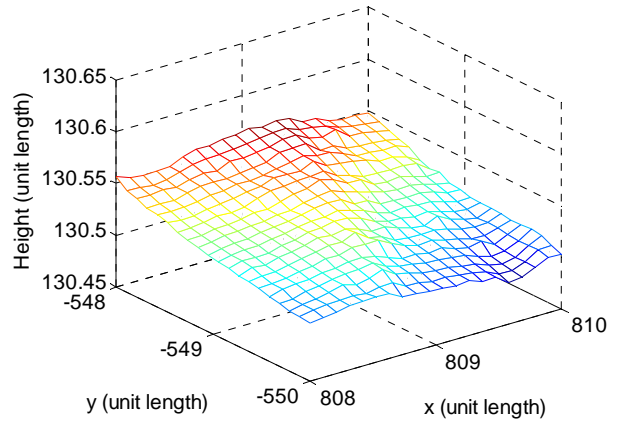
d 80 points by 80 points

Figure 3-15 Processed terrain profile from raw data set in Surfer.

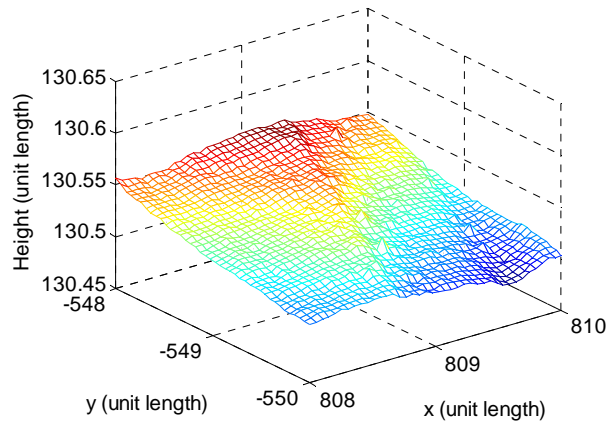
The coordinates and the terrain heights of the processed data are then extracted into a separate file, which also has a .dat extension. Since MATLAB is used to solve the stochastic PDE model, it will also be used to read and mesh the terrain files for further validation of the methodology. Figures 3-16a, 3-16b, 3-16c, and 3-16d are representations of the respective subplots in Figure 3-15 that are produced through MATLAB. Appendix A.3 also contains the m-file used to open and recreate the terrain file from Surfer.



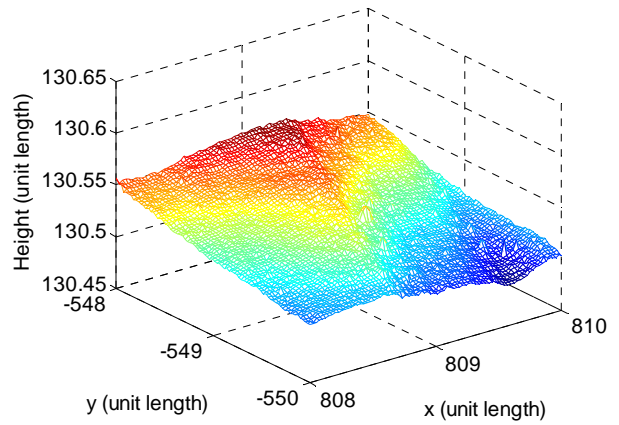
a 10 points by 10 points



b 20 points by 20 points



c 40 points by 40 points



d 80 points by 80 points

Figure 3-16 Processed terrain profile from raw data set read in MATLAB.

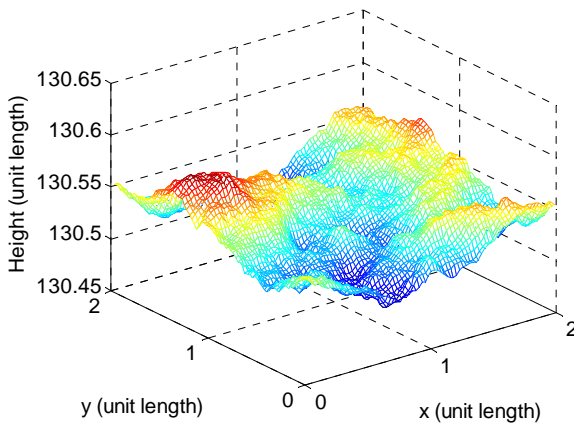
From MATLAB, the average height of the entire surface map, maximum height, and minimum height are equal to 130.53 m, 130.57 m, and 130.49 m, respectively. These values are used to obtain the model parameters for the stochastic PDEs. This procedure is described in the next section.

3.4 Validating the stochastic PDE method

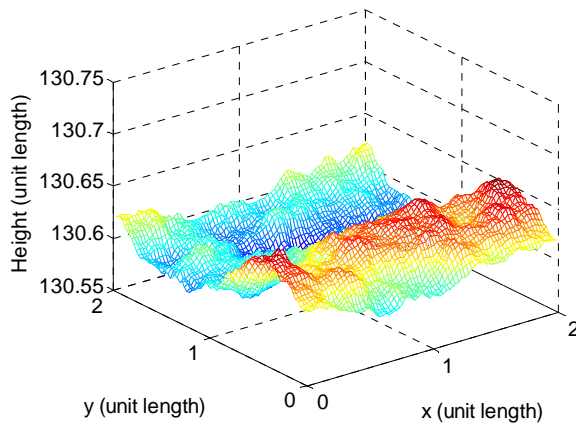
By processing and extracting the key parameters from the 2 meter by 2 meter surface map, the stochastic PDE method can be validated. In particular, the average terrain height of all the points on the surface map and the difference between the terrain heights and the average terrain height of the entire surface map is collected from the raw data. Procedures similar to the experimental

analysis of the model parameters were taken to achieve a terrain profile with similar stochastic properties. All the stochastic terrain profiles were averaged for 100 runs in a 80 point by 80 point surface map. The stochastic properties were calculated to match those of Figure 3-16d.

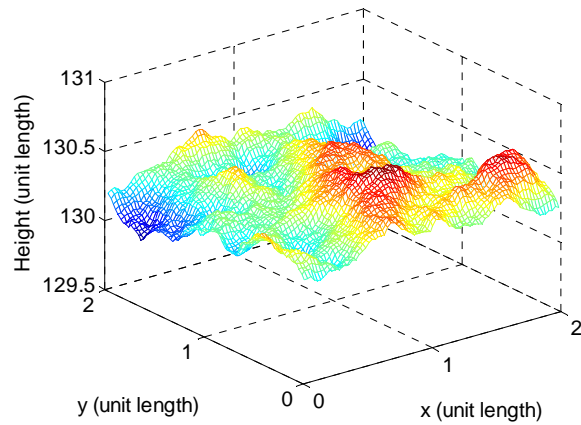
From Equation 3.17, the value of σ is equal to twice the value of the terrain height. Therefore, the mean terrain height of the entire surface of the raw data (130.53 m) can be considered to be the terrain height term in Equation 3.17, which leads to a σ value of 261.06 m. The four subplots in Figure 3-17 display four different trials for a σ value equal to 261.06 m, while the other model parameters are held constant at 1. The average terrain height of the entire surface, the maximum height of the entire surface, and the minimum height of the entire surface are recorded and displayed in Table 3-4. The average values for the four trials of the stochastic terrains are also displayed in Table 3-4 to compare with the values of the original deterministic terrain. The results are promising, in that the average terrain heights for the stochastic surfaces are close to the original terrain height average.



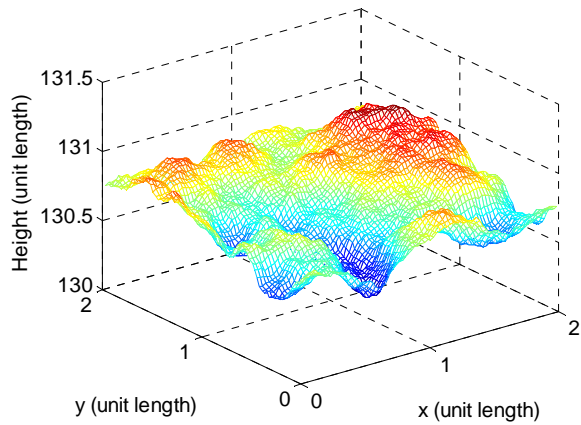
a Trial 1



b Trial 2



c Trial 3



d Trial 4

Figure 3-17 Trial runs for input of σ while model parameters remain at 1.

Table 3-4 Recorded values for subplots of Figure 3-17.

Trial	Terrain Mean (m)	Terrain Max (m)	Terrain Min (m)
1	130.54	130.587	130.497
2	130.61	130.657	130.558
3	130.312	130.64	129.95
4	130.76	130.083	130.39
Average	130.5554	130.4917	130.3487
Det. Terrain	130.53	130.57	130.49

Next, the correlation length, which is also related to the K value, of the original surface map is extracted and implemented into the stochastic model. The correlation length is defined in this methodology as the vertical distance between the terrain height and the average height of the entire surface. The correlation length is calculated and recorded for each point on the original surface map, which will present a 80 by 80 matrix of K values (e.g., equal to the number of points on the surface map). Now, the correlation length for each point on the surface map and the σ value are known, which allows the calculation of the K value through Equation 3.16. Figure 3-18 shows four trials with the σ value equal to 261.06 m, the calculated K value for each point on the surface, and the other model parameters equal to 1. Table 3-5 displays the average of the terrain height for the entire stochastic surface, the maximum terrain point on the entire surface, the minimum terrain point on the entire surface, the average of these values for the four trials,

and the corresponding values for the original terrain. Compared to the subplots in Figure 3-17, the correlation between the neighboring points (not the same as the correlation length) were better correlated to the original terrain data in the subplots of Figure 3-18. Unfortunately, the amplitude of the terrain topology increased drastically. The assumption of the “wrap around” boundary condition are displayed through the subplots shown in Figure 3-18. The original terrain did not have an upward curve on the x axis. The stochastic surfaces have the curve because the boundary condition of the nodes on the x axis correlates to the points defined on the top of the terrain, which is also sloping downwards because of the points on the x axis.

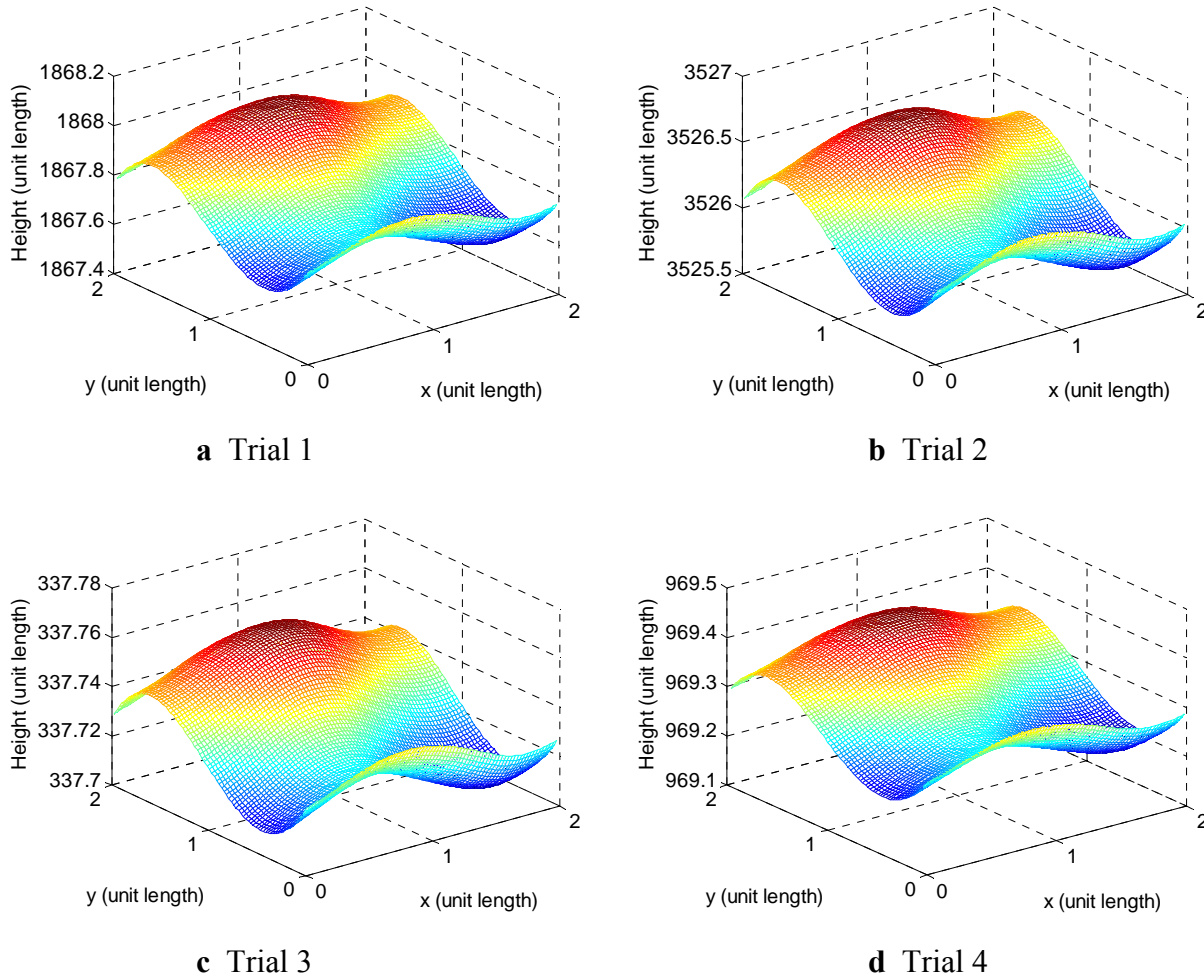


Figure 3-18 Trial runs for input of σ and K values.

Table 3-5 Recorded values for subplots of Figure 3-18.

Trial	Terrain Mean (m)	Terrain Max (m)	Terrain Min (m)
1	1867.8	1868	1867.6
2	3526.1	3526.6	3525.6
3	337.732	337.7583	337.7044
4	969.3079	969.4142	969.1961
Average	1675.235	1675.443	1675.025
Det. Terrain	130.53	130.57	130.49

Further analysis showed that the absolute values of K for the original data were calculated to be in the range from 489.67 (minimum value) to 42766 (maximum value) with Equation 3.16. The analysis for the K value was conducted in the range between 0.1 and 15. We decided to scale the K values from the experimental data to bring them in this range. Thus, all K values are scaled to obtain a minimum K value of 0.2. The points in the matrix of K values are all divided by 2448.35, which is equal to the minimum value of K (489.67) divided by the scaled K value (0.2). Figure 3-19 displays four trials with the σ value equal to 261.06 m, the scaled K value for each point on the original surface, and the other model parameters (equal to 1). The average height of the entire stochastic terrain, the value of the maximum terrain height in the entire surface map, and value of the minimum terrain height in the entire surface map, the average of these values for the four trials, and the corresponding values for the deterministic terrain are recorded in Table 3-6. The subplots in Figure 3-19 show improved results, in which the amplitude of the stochastic terrain and the correlation between neighboring points are both similar to those of the original surface map.

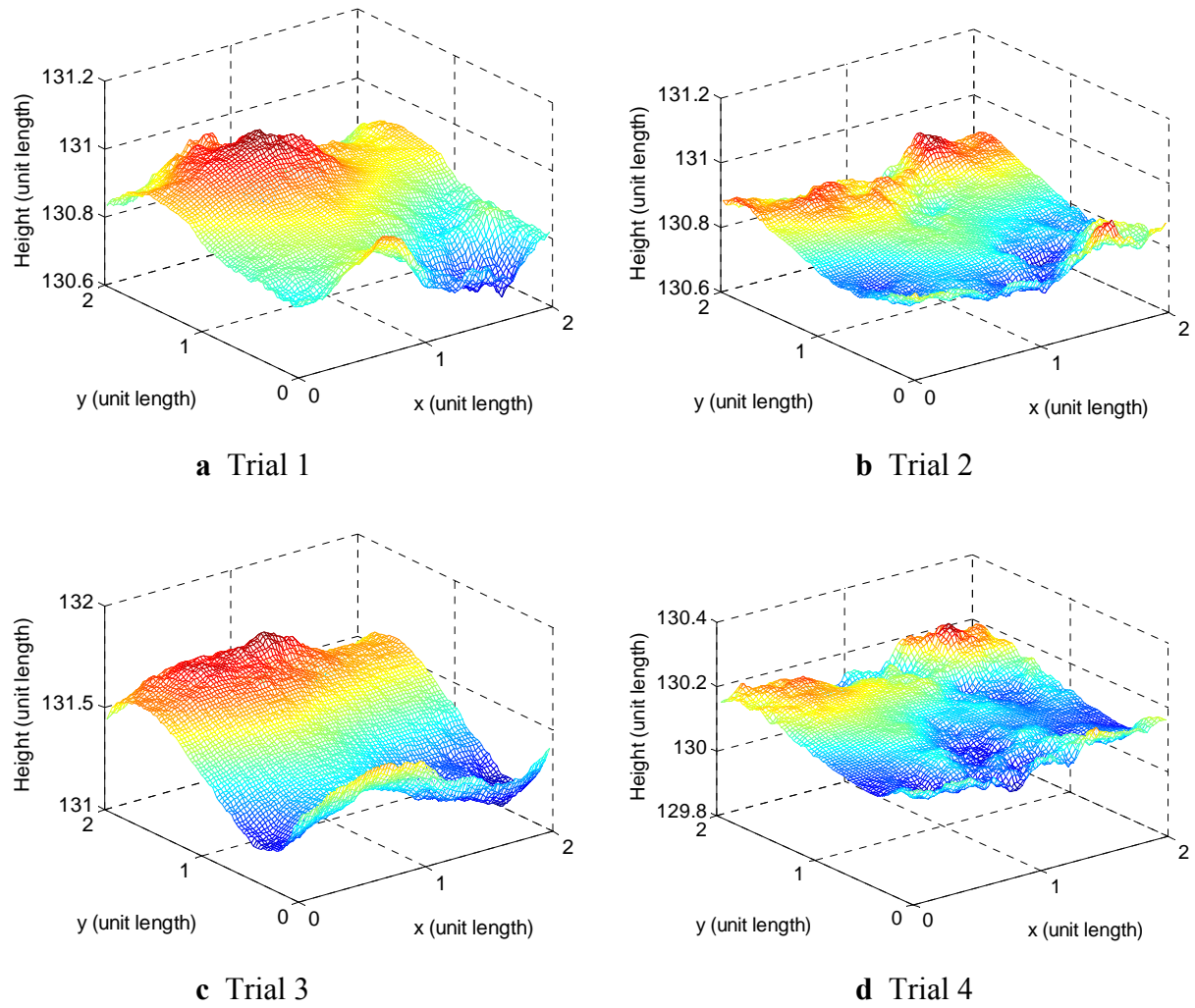


Figure 3-19 Trial runs for input of σ and reduced K values.

Table 3-6 Recorded values for subplots of Figure 3-19.

Trial	Terrain Mean (m)	Terrain Max (m)	Terrain Min (m)
1	130.87	131.0413	130.6424
2	130.8249	130.9401	130.7248
3	130.2278	130.3801	130.0314
4	131.1293	130.2454	131.0569
Average	130.763	130.6517	130.6139
Det. Terrain	130.53	130.57	130.49

Results from Tables 3-4 and 3-6 show that the first case and the third case present the stochastic terrains that are close representations of the average terrain height in the original terrain. As the

correlation length (also the K value) decreases, the variability in the terrain height increases. Therefore, the K value can be reduced to better present the numerical values for the correlation between the neighboring nodes. Figure 3-20 shows an updated simulation with the σ value equal to 261.06 and a constant K value equal to 0.2 (e.g., the same parameters used for case 1 with the exception of the K value which is now 0.2 instead of 1). Since the K value of 1 was arbitrarily selected for the first case, it is reasonable to also investigate the output when another value, such as 0.2 is used.

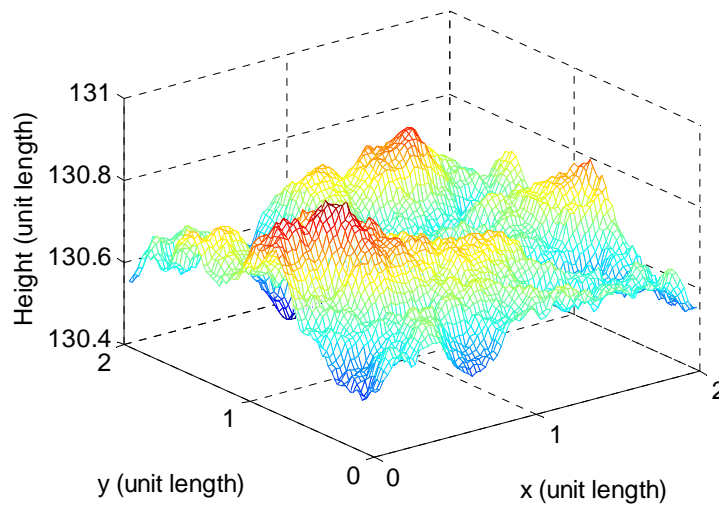


Figure 3-20 Simulation with σ value and K value equal to 0.2.

The main purpose of Table 3-7 is to compare the correlation between the neighboring nodes in the first case and the third case. The second case is not analyzed in this table because it is considered to be irrelevant since the average height of the stochastic terrain is drastically higher than the average height of the original terrain. One specific point on the surface map is used to examine the correlation between the neighboring nodes. The value of the center point is taken at point (40,40) in the 80 point by 80 point surface map. The values of the left point, the right point, the top point, and the bottom point are taken 10 points (0.125 m) away from the center point (e.g., left point is (30,40) on the 80 point by 80 point surface map). Since the grid is very fine (spatial domain of 0.025 m), it will be difficult to realistically show the correlation between two consecutive neighboring nodes.

Several experimental and simulation parameters are included in Table 3-7 and used to compute those metrics based on which we judged the accuracy of the terrain model created. These metrics are visually illustrated in Figure 3-21. The variable Δh_{exp} is computed as the difference between the average value of the entire deterministic terrain and the deterministic value of the terrain height at a particular point (e.g., correlation length in the deterministic surface). The variable Δh_{cd} is computed as the difference between the deterministic value of the neighboring nodes and the deterministic value of the center point. The variable Δh_{st} is computed as the difference between the average value of the entire stochastic terrain and the stochastic value of the terrain height at each point (e.g., correlation length in the stochastic surface). The variable Δh_{cst} is computed as the difference between the average value of the stochastic neighboring points and the average value of the center point. The numbers in the subscripts for variables Δh_{st} and Δh_{cst} correspond to the respective case number (e.g., 1 and 3). The terrain height for each case was obtained as an average of the values for the four different trials. As the number of trials increase, the average values should become closer to the original terrain profile, which in turn will improve the correlations between the neighboring nodes.

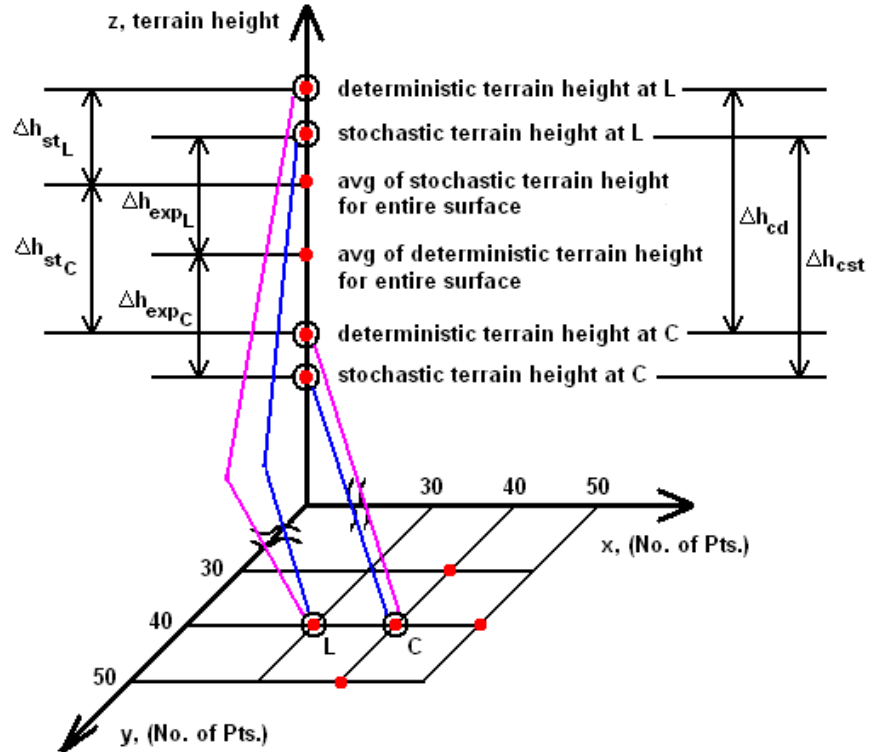


Figure 3-21 Definition of variables used in Table 3-7.

From the values in Table 3-7, both cases show that the mean value of the terrain height over the entire stochastic surface map is close to the average value of the terrain height over the entire deterministic surface map. However, the correlation between the neighboring nodes in case 3 is better than the correlation between the neighboring nodes in case 1 compared to the deterministic terrain. This is shown by the values of Δh_{cd} , Δh_{cst1} , and Δh_{cst3} (highlighted in red). The value of Δh_{cst3} is closer to the value of Δh_{cd} than the value of Δh_{cst1} is to the value of Δh_{cd} . By inserting both the value σ (average of the original terrain height over the entire surface) and the matrix of K values (correlation length of the original terrain height for each point), the simulations obtained from case 3 best represents the correlation and the amplitude of the original terrain.

Table 3-7 Comparison between correlation of boundary nodes.

		Center Point	Left Point	Right Point	Top Point	Bottom Point
Deterministic terrain	Value of terrain	130.539	130.527	130.545	131	131
	Avg value of entire terrain	130.53				
	Δh_{exp}	-0.009	0.003	-0.015	-0.01	0
	Δh_{cd}		-0.012	0.006	-0	-0.01
Updated Case 1 (K=0.2)	Value of terrain	130.6456	130.7053	130.608047	131	131
	Avg value of entire terrain	130.6566				
	Δh_{st1}	0.010983	-0.048672	0.04855317	-0.06	0.08
	Δh_{cst1}		-0.059655	0.03757066	-0.07	0.07
Case 3	Trial 1	130.93	130.93	130.9	131	131
	Trial 2	130.8318	130.8313	130.815836	131	131
	Trial 3	131.44	131.47	131.41	131	132
	Trial 4	130.1071	130.1373	130.117473	130	130
	Avg of trial values	130.8272	130.8422	130.810827	131	131
	Avg value of entire terrain for four trials	130.513				
	Δh_{st3}	-0.314209	-0.32916	-0.2978271	-0.27	-0.36
	Δh_{cst3}		-0.014952	0.0163814	0.04	-0.05

Chapter 4 Stochastic Soil Model

This chapter presents both an experimental approach, and a computational approach to develop stochastic soil models. It is organized in the following manner. Section 4.1 shows the creation of stochastic soil models using experimental procedures. Section 4.2 explains the methodology in creating stochastic soil models using the polynomial chaos approach on Bekker's pressure-sinkage equation. Section 4.3 presents simulations and comparisons between the experimental approach and the computational approach.

4.1 Experimental tests to develop empirical soil models

To analyze off-road mobility of wheeled vehicles, soil models have to be integrated with the terrain profile models. Different techniques could be used to create soil models. One technique involves experiments to manually measure the pressure-sinkage relationship for different types of soil. Devices such as bevameters and cone penetrometers are used to measure the compaction level of the soil (also used to verify the density of the soil or the soil moisture). Due to the design of the device, experimental data recorded from different devices will show different results. Therefore, when experimental tests are performed, the pressure-sinkage parameters of the soil models are affected by many factors, some of which are: the type of soil, the compaction level of the soil, and the device used to collect the data.

Virginia Tech collaborated with NASA Glenn Research Center in the summer of 2008 to undertake some soil studies on GRC-1, which is a lunar soil simulant (Oravec, Asnani, and Zeng, 2008). As shown in Figure 4-1, the soil studies were performed on Virginia Tech's terramechanics rig (Taylor, 2008). The rig allows us to perform experiments indoor, thus eliminating the impact of weather conditions and unwanted factors on the soil properties. A procedure with high repeatability was developed at Virginia Tech and used to prepare the soil to obtain consistent compaction levels. The procedure was verified by comparing it with data obtained from the facilities at NASA GRC.

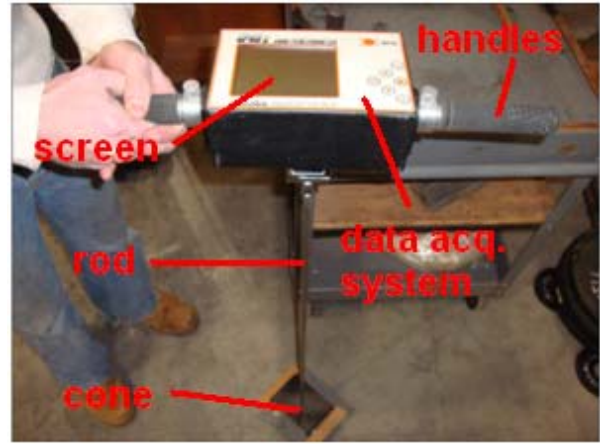


Figure 4-1 Cone penetrometer experiments performed on Virginia Tech's terramechanics rig.

The pressure-sinkage data was then obtained with a cone penetrometer CP40 II using a cone diameter of 20.27 mm. This device measures the compaction of the soil by pushing a rod into the surface of the terrain. As the cone on the tip of the rod inserts into the ground, the CP40 II collects the pressure data at different depth levels. The size of the cone (either 12.83 mm or 20.27 mm) and the maximum depth (up to 750 mm) can be defined by the user. To accurately collect the data points, the CP40 II monitors the rate at which the rod is being inserted into the ground to make sure that the user does not exceed the maximum speed of 2 m/min. Figure 4-2a and Figure 4-2b shows an image of the cone penetrometer CP40 II disassembled and assembled, respectively.



a Disassembled view



b Assembled View

Figure 4-2 Image of the cone penetrometer CP40 II.

Figure 4-3 shows the pressure-sinkage relationship for GRC-1 obtained experimentally at AVDL. The GRC-1 lunar soil simulant was prepared to be at 50% relative density, and has less than 1% moisture content (considered to be 100% dry). The soil compaction gradient, which is also the slope of the line in Figure 4-3, is calculated to be 5.0 kPa/mm (± 0.3 kPa/mm). In this figure, the “error” bars represent the distribution of the experimentally collected soil data, while the continuous line was obtained as the average value over the entire set of data.

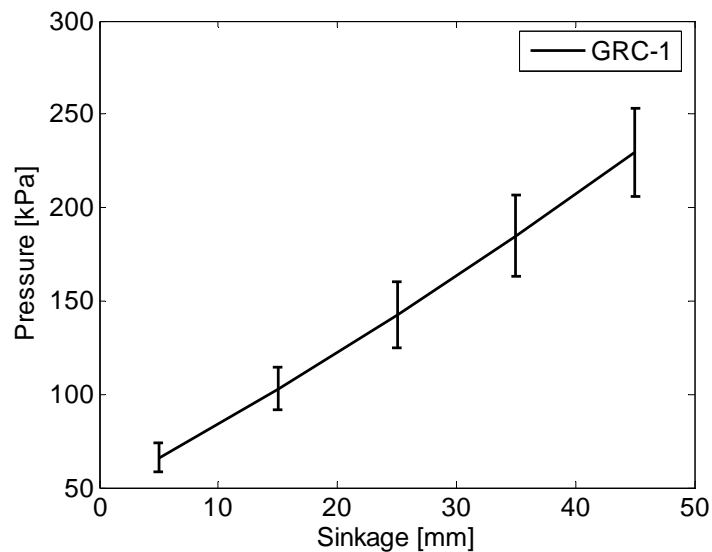


Figure 4-3 Pressure-sinkage relationship for GRC-1.

The best fit line for the cone penetrometer test data was modeled as a second order polynomial function, as shown in Equation 4.1, where P is the pressure (kPa) and s is the sinkage (mm). The standard deviations at the different sinkage locations are shown in Table 4-1. Appendix B contains the entire set of numerical values that are used to obtain Equation 4.1 and the line for Figure 4-3.

$$P = 0.013 s^2 + 3.437 s + 48.55 \quad (4.1)$$

Table 4-1 Standard deviations of GRC-1 at specific depths.

Depth (mm)	Standard Deviation
5	7.5763
15	11.7258
25	17.9796
35	21.9345
45	23.4638

4.2 Simulating stochastic soil models using the polynomial chaos approach

Soil models can also be obtained using a semi-empirical approach. Classic examples of semi-empirical techniques developed to quantify the soil conditions are Bekker's equation and Reece's equation (Wong, 2001). These equations are characterized for homogeneous terrains, and contain different soil parameters that relate to different types of soil and moisture contents. Bekker's pressure-sinkage relationship is represented by Equation 4.2,

$$p = \left(\frac{k_c}{b} + k_\phi \right) z^n \quad (4.2)$$

where p is pressure, z is sinkage, b is the width of the rectangular contact area, and n , k_c , and k_ϕ are pressure-sinkage parameters. The pressure-sinkage parameters vary with different soil types. Unlike the experimental tests that were performed at AVDL, the parameters for Bekker's equation are collected through bevameter plate-sinkage tests.

In prior studies, Li and Sandu (2007) used the polynomial chaos approach to quantify the effect of the uncertainties in the soil properties on the pressure-sinkage relation. The moisture content

was the uncertain parameter and it was assumed to have a linear relationship with the pressure-sinkage parameters. Therefore, the moisture content affected the pressure-sinkage relationship indirectly. A particular case study was shown using the collocation method to obtain pressure-sinkage relations of Michigan sandy loam. The moisture content had uncertainties between 0% and 30%, and was assumed to have a uniform distribution and a normal (Gaussian) distribution (Sandu, Sandu, and Li, 2005).

For the methodology presented in this thesis, the polynomial chaos approach was used on Bekker's equation to create stochastic soil models in which the random variable was one of the pressure-sinkage parameters k_ϕ . This analysis shows a direct affect on Bekker's equation, and it also eliminates the assumption of a linear relationship between the pressure-sinkage parameters. Another reason for creating such soil models is to make comparisons between the experimental tests of GRC-1, which will be further described in the next section. The moisture content of the lunar soil simulant was not an uncertain value. Therefore, the methodology in this thesis is more applicable to the experimental results of GRC-1.

Using the Karhunen-Loeve expansion, the uncertain parameter k_ϕ can be expressed as

$$k = \sum k_\phi^j \psi^j(\xi(\theta)) \quad (4.3)$$

where $\psi^j(\xi_{i1} \dots \xi_{in})$ are the generalized Askey-Wiener polynomial chaoses and $\xi = (\xi_{i1} \dots \xi_{in})$ are the multi-dimensional random variables (Sandu, Sandu, and Ahmadian, 2006a). The assumption was made that the random variables are uniformly distributed. Therefore, the Legendre polynomials of order 3 were used for the basis function (Equation 4.4) in the polynomials chaos method,

$$\int_{-1}^{+1} L_i(\xi) L_j(\xi) \frac{1}{2} d\xi = 0 \quad \text{for } i \neq j \quad (4.4)$$

where $L_i(\xi) L_j(\xi)$ are orthogonal polynomials and ξ is an independent random variable (Sandu, Sandu, and Ahmadian, 2006a). Other distributions may include the normal distribution (Hermite polynomials as basis function) and the beta distribution (Jacobi polynomials as basis function).

The uncertainty in the k_ϕ value was then propagated through Bekker's equation using the collocation method. For this particular case study, the four collocation roots were developed to be ± 0.8611 and ± 0.34 . These collocation roots were applied to the Legendre polynomials to obtain the collocation matrix to calculate the uncertain pressure-sinkage relation. Appendix B.2 reveals detailed calculations for the methodology presented in this section.

The Karhunen-Loeve expansion is not limited to being applied to only the pressure-sinkage parameter k_ϕ . Similar case studies can be simulated with n or k_c being the random parameter to analyze how the uncertainties within those parameters affect Bekker's equation.

4.3 Comparison of results for stochastic soil models

In this section we compare the stochastic soil model against the experimental data. The pressure-sinkage parameters for the two soil model techniques were taken with different devices. Data obtained from a cone penetrometer test is different from data obtained from a bevameter (plate-sinkage) test. The main difference is the zone of influence that is taken from each device. When measuring with a cone penetrometer, the zone of influence is much less than that of a bevameter test since the diameter of the plate is at least 5 times larger than the diameter of the cone. The cone penetrometer has more influence on the soil to the side of the cone, whereas the bevameter tests influences the soil directly below the plate. Therefore, the soil tested by a bevameter is usually stronger compared to a cone penetrometer test since the plate compacts the soil more than the cone. The results are not expected to completely match. However, the characteristics of the plots should be similar.

The numerical simulations are based on the parameters shown in Table 4-2. Heather Oravec (2009) obtained the pressure-sinkage parameters in Bekker's equation for GRC-1 by following the procedures for a bevameter plate-sinkage test in Wong (1980). Separate bevameter tests were performed on GRC-1 with different densities and different plate diameters. A simulation for dry sand is also shown in which the pressure-sinkage parameters are obtained from Wong (1980). Dry sand is chosen because the moisture content of GRC-1 is close to 0%. For all of the cases shown in Figure 4-2, there is 100% uncertainty in the randomization of k_ϕ .

Table 4-2 Pressure-sinkage parameters for numerical simulations.

Terrain	Moisture Content	Density (g/cc)	n	k_c (kN/m ⁿ⁺¹)	k_ϕ (kN/m ⁿ⁺²)	b (m)
GRC-1	< 1%	1.64	0.9	119.1	2186.2	0.076
GRC-1	< 1%	1.67	1.05	813.8	-1629.9	0.102
GRC-1	< 1%	1.75	1.09	1232.3	-2349.5	0.19
Dry Sand	0%	-	1.1	0.99	1528.43	0.1

Figure 4-4 shows the simulated stochastic soil properties of GRC-1 with 1.64 g/cc density and measured with a 0.076 plate diameter. Figure 4-5 shows the simulated stochastic soil properties of GRC-1 with 1.67 g/cc density and measured with a 0.102 plate diameter. Figure 4-6 shows the simulated stochastic soil properties of GRC-1 with 1.75 g/cc density and measured with a 0.19 plate diameter. All of the simulations were modeled using the polynomial chaos approach. A 1000-run Monte Carlo simulation and the probability density function are also displayed to verify the polynomial chaos method. From Figures 4-4a, 4-5a and 4-6a, the correlation between the Monte Carlo results and the polynomial chaos results looks very promising. The probability density functions are shown in subplot b for all of the figures. As the sinkage and pressure increase, the value of the PDF decreases for all cases. Comparing the analytical method with the experimental test, the graphs do not completely match since different devices were used to obtain the soil parameters, but the slope of the lines are very similar for all three cases.

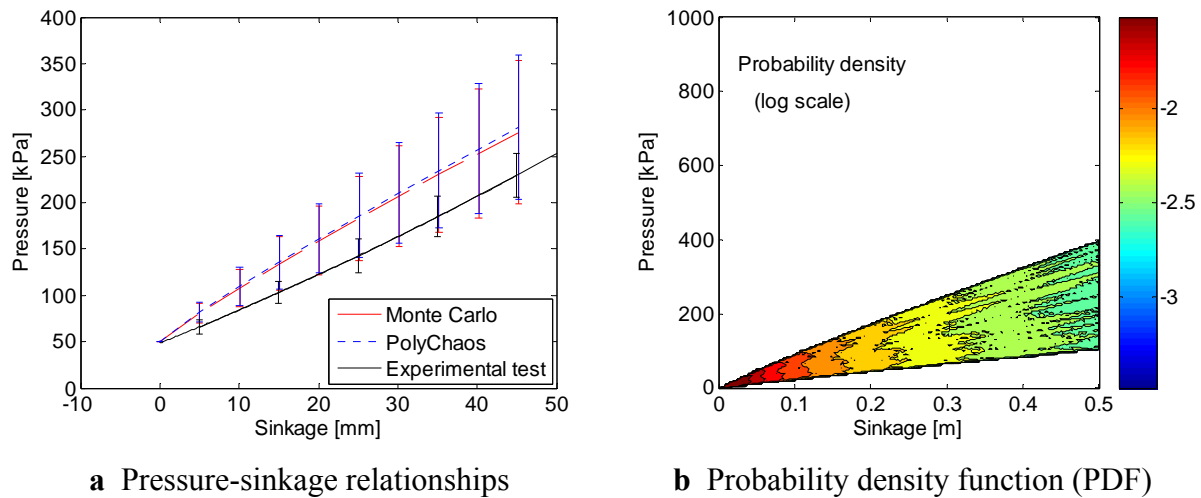
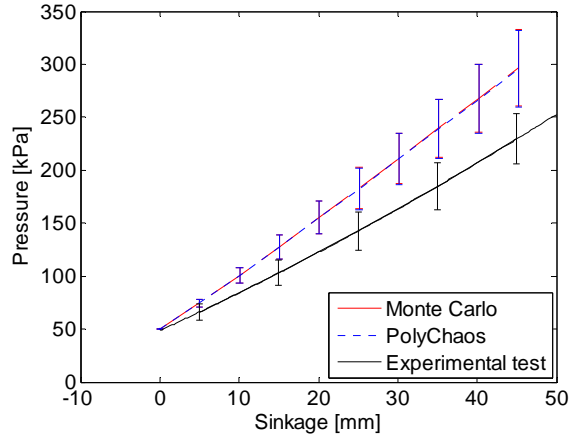
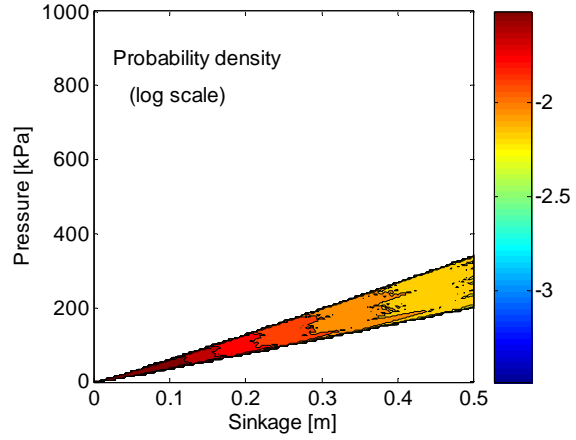


Figure 4-4 Stochastic simulation of GRC-1 with $b = 0.076$ m and density = 1.64 g/cc.

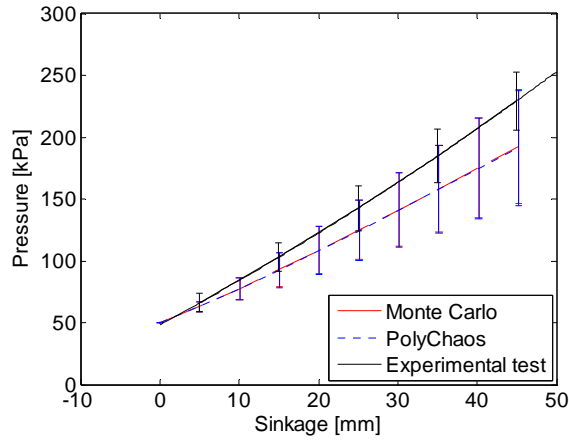


a Pressure-sinkage relationships

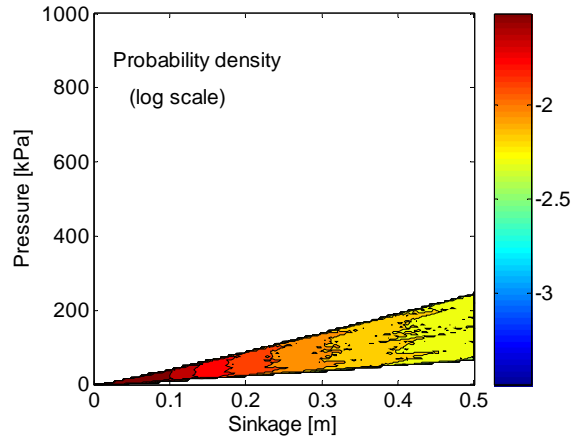


b Probability density function (PDF)

Figure 4-5 Stochastic simulation of GRC-1 with $b = 0.102$ m and density = 1.67 g/cc.



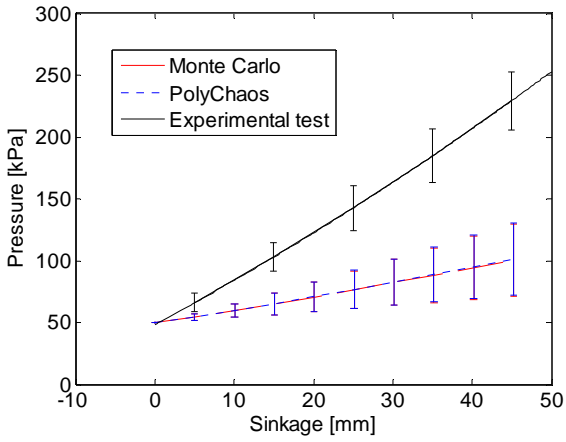
a Pressure-sinkage relationships



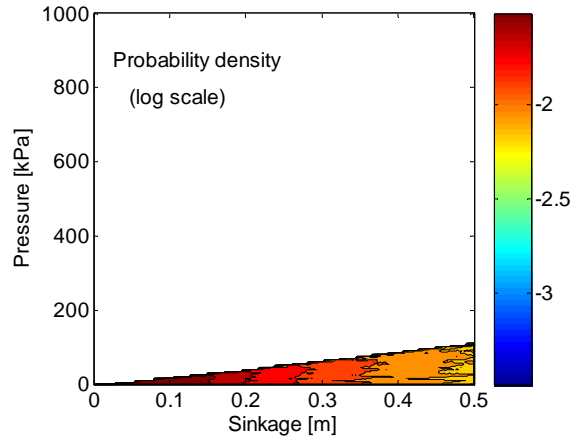
b Probability density function (PDF)

Figure 4-6 Stochastic simulation of GRC-1 with $b = 0.19$ m and density = 1.75 g/cc.

Figure 4-7 illustrates the stochastic simulation of dry sand (0% moisture) with the polynomial chaos method. Similar to Figures 4-4 to 4-6, a Monte Carlo simulation and a PDF is used to verify the polynomial chaos approach, and the results are promising. The PDF shows that as the pressure and sinkage increase, the value of the PDF decreases in the range of -1.5 to -2.25. The characteristics of the dry sand is also similar to that of GRC-1 with the exception of the slope of the graph.



a Pressure-sinkage relationships



b Probability density function (PDF)

Figure 4-7 Stochastic simulation of dry sand (0% moisture).

Chapter 5 Integrated Terrain-Soil Simulation Environment

To further analyze off-road mobility studies, the stochastic terrain model and the stochastic soil model will be incorporated into the simulation framework. This chapter presents an integrated terrain and soil simulation environment. To illustrate the capabilities of the simulation environment developed, several case studies are presented. Section 5.1 introduces the soil parameters and the tire parameters used for the simulations. Sections 5.2 to 5.4 present case studies of a rigid plate, rigid wheel, and flexible wheel “stepping” over a deterministic surface, respectively. Section 5.5 and 5.6 present case studies of a rigid wheel and flexible wheel rolling over deterministic surfaces, respectively. Section 5.7 presents case studies of a rigid wheel and flexible wheel rolling over a deterministic terrain with stochastic soil properties. Section 5.8 presents case studies of a rigid wheel and flexible wheel rolling over a stochastic terrain with deterministic soil properties. Section 5.9 presents case studies for a rigid wheel and flexible wheel rolling over stochastic terrain with stochastic soil properties. Appendix C contains all MATLAB m-files used to create the simulations shown in this chapter. Figure 5-1 shows a chart of all of the case studies presented in this chapter.

5.1 Parameters used for the simulation environment

In a virtual proving ground, the wheel and soil interaction has to be simulated in order to analyze the mobility of vehicles over different soil types. The simulations in this chapter are all created on a 2 m by 2 m (40 points by 40 points) surface map and the technique developed can be easily applied to the terrain profiles and soil characteristics modeled in the previous chapters. For the simulations including the deterministic terrain profiles, the terrain height is initially set to 1 m. One advantage of the modeling technique developed in this study is its capability to run such simulations in real time. To illustrate the capabilities of the simulation framework developed, all of the case studies discussed here have been simulated on a homogeneous soil terrain (Sandy Loam). The pressure-sinkage parameters are displayed in Table 5-1 (Wong, 2001). Table 5-2 consists of the parameters for the tire that is being simulated on the terrain (Wulfsohn and Upadhyaya, 1992).

			Plate	Rigid Wheel	Flexible Wheel
Stepping	Deterministic soil	Deterministic flat terrain	X	X	X
Rolling	Stochastic soil	Stochastic terrain		X	X
		Deterministic flat terrain		X	X
	Deterministic soil	Stochastic terrain		X	X
		Deterministic semi-oval bump terrain		X	X
		Deterministic flat terrain		X	X

Figure 5-1 Chart of all the case studies presented in this chapter.

Table 5-1 Pressure-sinkage parameters for Sandy Loam.

Soil	Moisture content (%)	n	k_c (kN/m ²)	k_ϕ (kN/m ³)	c (kPa)	ϕ (deg)
Sandy loam (LLL)	15	0.7	5.27	1515.04	1.72	29°

Table 5-2 Parameters for tire model.

Tire	Dynamic Load (kN)	Average slip (%)	Contact width (mm)	Contact length (mm)
Tire Model 1	18.67	27.72	590	595

5.2 “Stepping” with a rigid plate on a flat terrain profile

The first case scenario is a rigid plate “stepping” on a flat terrain profile. The motivation behind implementing this case study is the fact that Bekker’s pressure-sinkage relation was developed based on experiments performed with rigid plates on soft soil. Stepping is defined here as one contact patch being stepped on right in front of the previous one. (The contact patches do not overlay each other). For the “stepping” cases, all of the contact patches are assumed to be rectangular, which, for the purpose of this thesis, is considered to be a reasonable assumption. From Bekker’s pressure-sinkage relationship, the sinkage of the terrain can be calculated with the parameters shown in Table 5-1 and Table 5-2. The contact patch is assumed to have an evenly distributed pressure distribution of 51.9 kPa (e.g., vertical force of 18.67 kN). It can be seen from Figure 5-2 that the terrain topology is updated upon the “stepping” with the rigid plate. Although not graphically shown, the soil parameters are also changed and updated since the plate will compact the soil underneath.

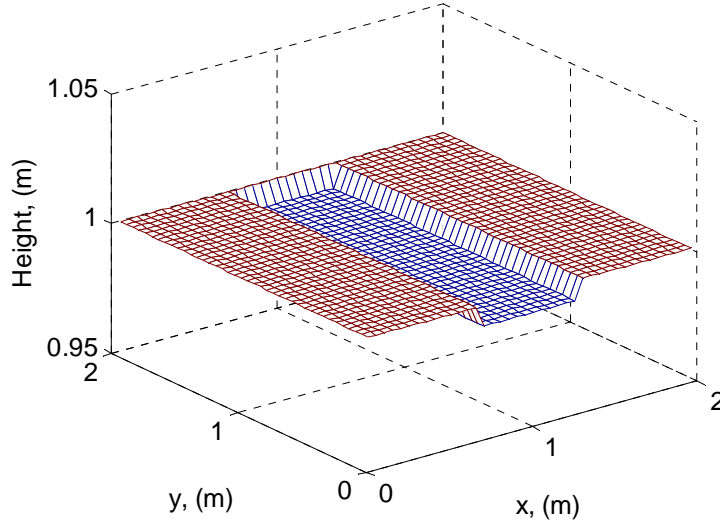


Figure 5-2 Rigid plate “stepping” on a deterministic flat surface.

5.3 “Stepping” with a rigid wheel on a flat terrain profile

As shown in Figure 5-4, the second case study is a rigid wheel “stepping” on a two-dimensional terrain profile (40 points by 40 points). Instead of having a uniformly distributed contact area, the pressure distribution is modeled here as

$$p_z(\xi) = P_{max} \left(1 + A_1 s \left(\xi - \frac{l_p}{2} \right) \right) \sqrt{1 - \frac{\left(\xi - \frac{l_p}{2} \right)^2}{\left(\frac{l_p}{2} \right)^2}} \quad (5.1)$$

where A_1 is the shape change factor, s is the longitudinal slip ratio, l_p is the length of the contact patch, and ξ is the exact location in the contact patch. Therefore, ξ can only be a value between 0 and l_p , which is shown in Figure 5-3. This figure was taken from Chan (2008, p. 35).

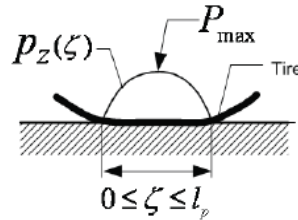


Figure 5-3 Elliptic pressure distribution of contact patch.

The variable P_{max} is the maximum pressure of the contact patch and it is modeled below

$$P_{max} = \frac{4}{\pi b l_p} F_z \quad (5.2)$$

where F_z is the vertical load, and b is the width of the contact patch (Chan, 2008). This simulation assumed uniform pressure distribution in the lateral direction of the contact patch. By using the pressure distribution equation in Bekker's pressure-sinkage relationship, the values for the sinkage at each distance of the contact patch can be calculated. Figure 5-4 incorporates the pressure distribution in the contact patch of a rigid wheel "stepping" on a flat surface.

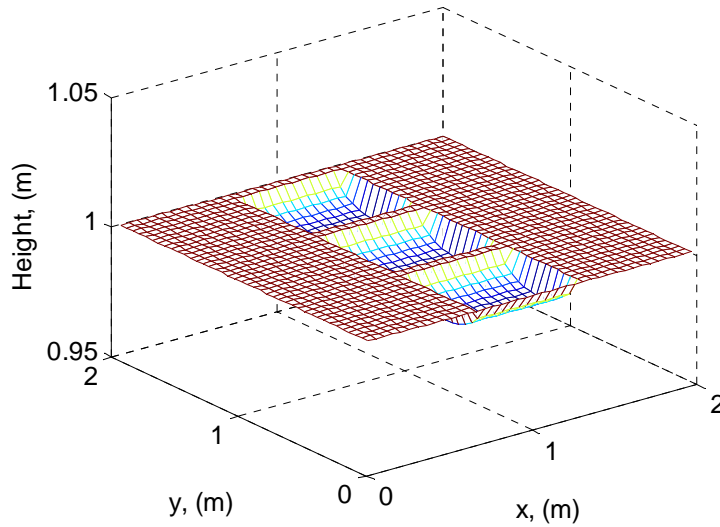


Figure 5-4 Rigid wheel "stepping" on a deterministic flat surface.

5.4 "Stepping" with a flexible wheel on a flat terrain profile

The third case study is for a flexible wheel "stepping" on a two-dimensional flat terrain profile (40 points by 40 points), as shown in Figure 5-5. The model accounts for the pressure distribution, the sinkage, and the deflection of the flexible wheel. The deflection is derived from the following formula for the length of the contact patch

$$l_p = \sqrt{r^2 - (r - z - \delta)^2} + \sqrt{r^2 - (r - \delta)^2} \quad (5.3)$$

where r is the radius of the wheel, z is the sinkage of the terrain, and δ is the deflection of the wheel (Schwanghart, 1991). The radius of the wheel for this case study is assumed to be half of the length of the contact patch. This equation can be modified to the following.

$$-2\delta^2 + (4r - 2z)\delta - l_p^2 + 2rz - z^2 = 0 \quad (5.4)$$

The quadratic equation is then used to solve for the values of tire deflection, which is shown in Equation 5.5.

$$\delta = \frac{2z - 4r \pm \sqrt{(16r^2 - 8z^2)}}{-4} \quad (5.5)$$

The flexible wheel sinkage in this case study is calculated by subtracting from the original terrain height the deflected wheel radius. Therefore, to simulate Figure 5-5, the sinkage values in the contact patch of a flexible wheel are calculated by adding the deflection of the flexible wheel to the sinkage of the rigid wheel (e.g., calculation of the sinkage of the rigid wheel is the same as that shown in the previous case study). The calculation of the deflection of the wheel is not limited to Equation 5.5. There are many other equations to calculate the deflection of the wheel in which the formulations can be dependent on parameters other than the sinkage and radius of the wheel. Equation 5.5 was best suited for the case studies in this thesis since it was dependent on parameters to which we had access.

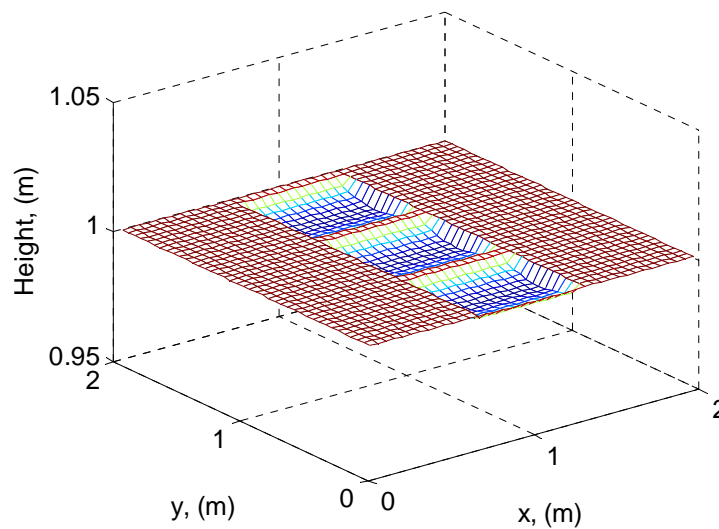


Figure 5-5 Flexible wheel “stepping” on a deterministic flat surface.

5.5 Rolling with a rigid wheel on a deterministic terrain profile

The next case studies are for a rigid wheel rolling on a two-dimensional flat terrain profile and on a two-dimensional terrain profile with an obstacle (the grid was 40 points by 40 points). Compared with the rigid wheel “stepping” case, for the rolling simulation the geometry of the contact patch is no longer assumed to be a rectangle. The slip ratio in the contact patch is also accounted for in this case, being incorporated in the description of the pressure distribution (Equation 5.1). As the rigid wheel is rolling, the contact patch creates a superellipse (Hallonborg, 1996), as shown in Figure 5-6. A superellipse is modeled with the following equation

$$\frac{(x - h)^n}{a^n} + \frac{(y - k)^n}{b^n} = 1 \quad (5.6)$$

where a is the width of the contact patch, b is the length of the contact patch, x and y are the coordinates of the contact patch, and h and k are the coordinates of the center of the contact patch. The value of n influences the curve of the superellipse. For all of the rolling case studies presented in this thesis, the geometry of the contact patch is presented by Equation 5.6 where the value of n is equal to 1 (ellipse).

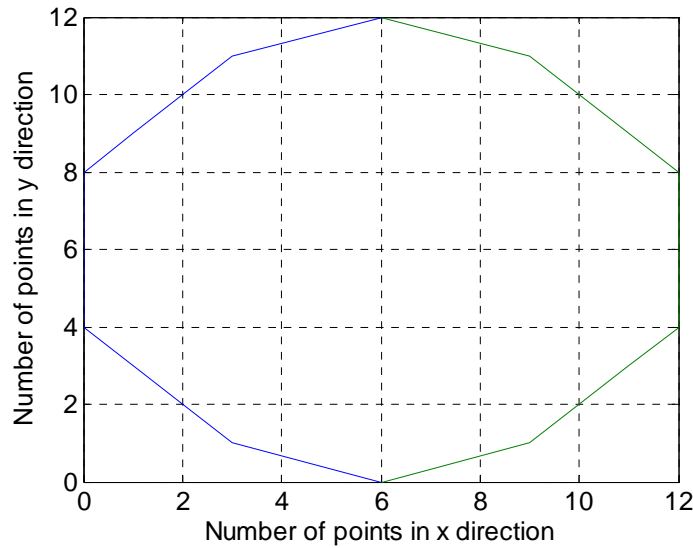


Figure 5-6 Geometry of contact patch of rolling wheel.

Snapshot from the simulations of the rigid wheel rolling on sandy loam are presented in Figures 5-7 and 5-9. Figure 5-7 shows the rigid wheel rolling on a deterministic flat surface of terrain height equal to 1 m. One can notice the elliptical shape of the contact patch contour.

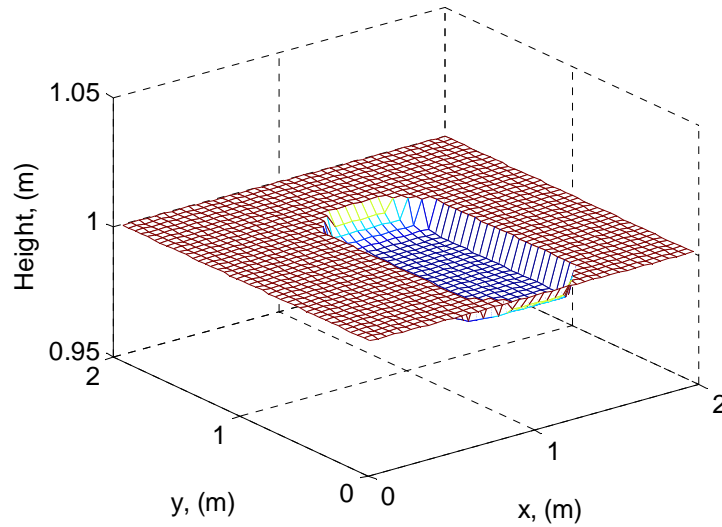


Figure 5-7 Rigid wheel rolling on deterministic flat surface.

Figure 5-8 shows a deterministic terrain surface with a semi-oval bump. The length of the bump is 0.5 m while the height of the bump is equal to 1.012 m. Figure 5-9 shows a rigid wheel rolling over the semi-oval bump that was created on the deterministic surface. When the rigid wheel is analyzed on the stochastic terrain, there will be many bumps and obstacles. Therefore, this case study was implemented to see the initial affects of a deterministic obstacle.

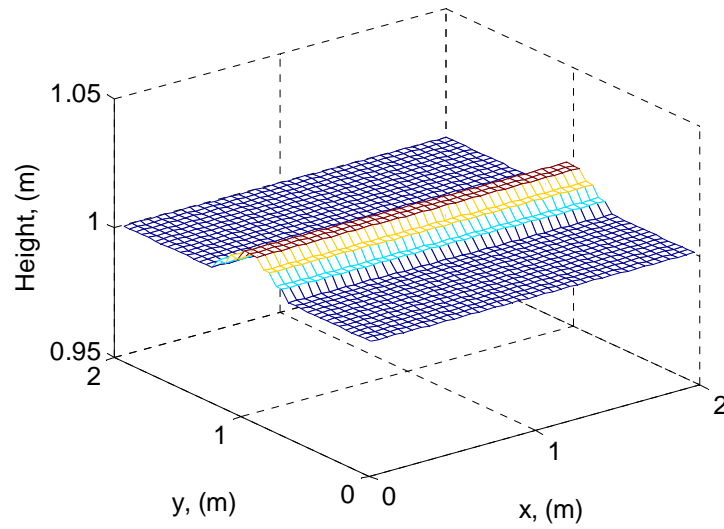


Figure 5-8 Deterministic terrain surface with semi-oval bump.

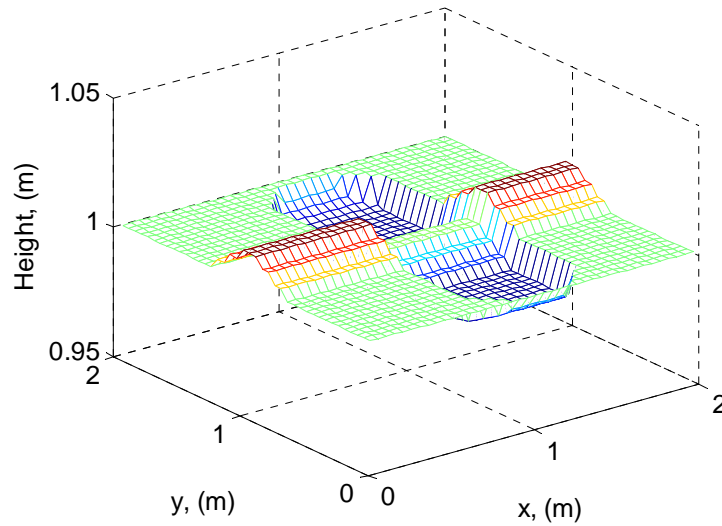


Figure 5-9 Rigid wheel rolling on a surface with a semi-oval bump.

5.6 Rolling with a flexible wheel on a deterministic terrain profile

The case studies shown in this section are for a flexible wheel rolling on a two-dimensional flat terrain profile and on a two-dimensional terrain profile with an obstacle. The simulation was performed in a similar manner with the case studies of a rigid wheel rolling on a deterministic

terrain profile, the only difference being in the deflection of the wheel. The calculation for the deflection of the wheel is the same as that shown section 5.4.

Snapshot from the simulation of the flexible wheel rolling on sandy loam are presented in Figures 5-10 and 5-11. Figure 5-10 shows a flexible wheel rolling on a deterministic flat surface of 1 m terrain height. Figure 5-11 shows a flexible wheel rolling on a deterministic surface with a semi-oval bump, as shown in Figure 5-8. The main differences between Figures 5-10 and 5-11 and Figures 5-7 and 5-9, respectively, are the value of the sinkage and the curvature of the bottom of the contact patch.

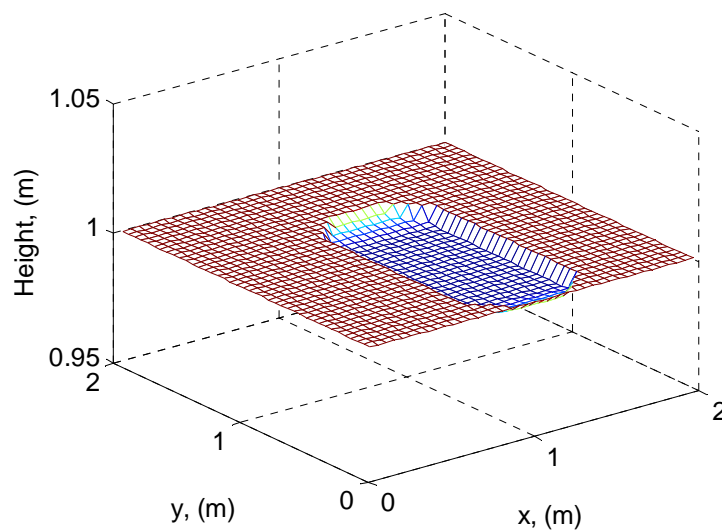


Figure 5-10 Flexible wheel rolling on deterministic flat surface.

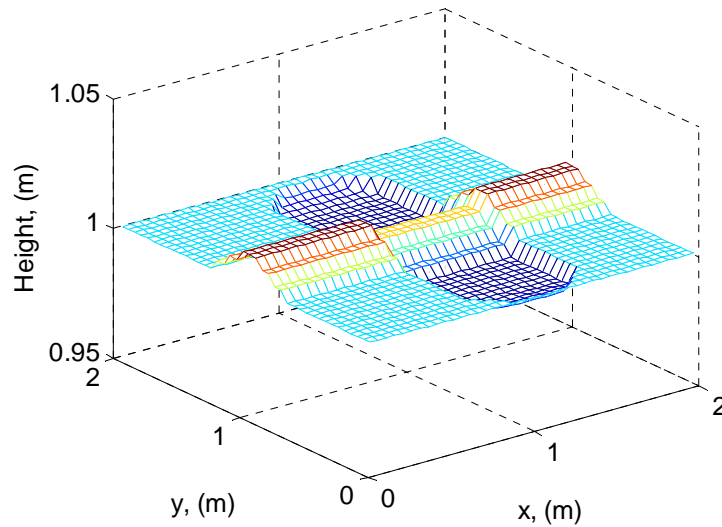


Figure 5-11 Flexible wheel rolling on a surface with a semi-oval bump.

To better visualize the “stepping” and rolling cases on a deterministic flat terrain profile with a height of 1 m, a side view of all of the case studies are shown in Figure 5-12. The solid gray line represents the stepping of the rigid plate. The solid purple line and the dashed green line represent the rolling and “stepping” of the rigid wheel, respectively. The solid red line and the dashed blue line represent the rolling and “stepping” of the flexible wheel, respectively.

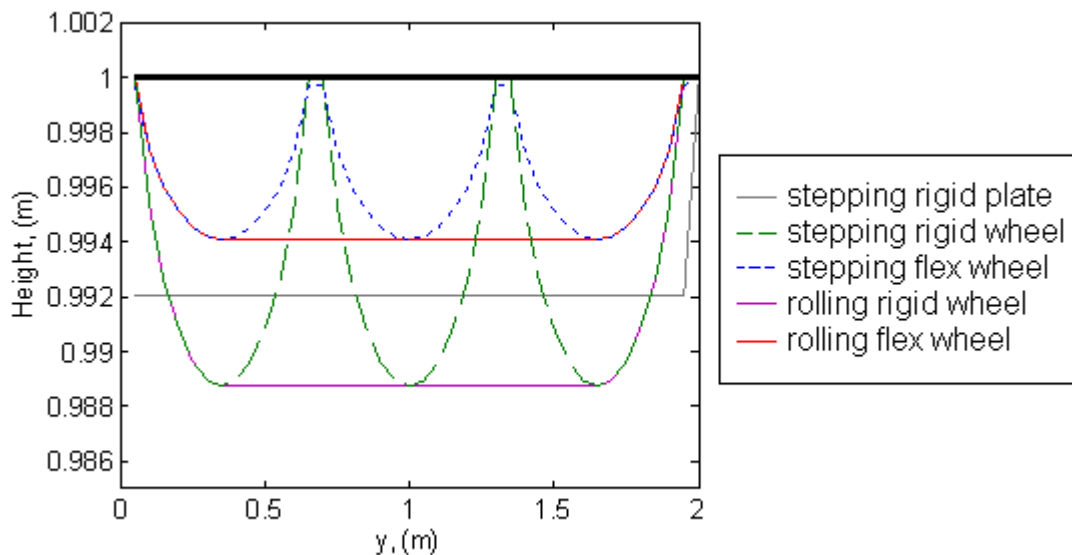


Figure 5-12 Side view of all case studies on flat deterministic terrain profiles.

5.7 Rolling on deterministic terrain profile with stochastic soil properties

The case studies shown in this section are the rolling of a rigid and flexible wheel over a flat deterministic terrain profile with stochastic soil properties. Similar to the model represented in Chapter 4 of this thesis, the uncertain parameter in Bekker's pressure-sinkage equation is k_ϕ . For the simulations provided, the value of k_ϕ is assumed to have a uniform distribution, and has a 20% uncertain amplitude (the soil model in Chapter 4 has 100% uncertainty). The uncertain parameter is applied to every point on the surface map. Figure 5-13 shows the simulation of a rigid wheel rolling over a deterministic profile with stochastic soil parameter k_ϕ . Figure 5-14 shows the side view of the simulation. As the rigid wheel rolls over the terrain, the profile under the contact patch is not uniform since the sinkage at each point has a stochastic value.

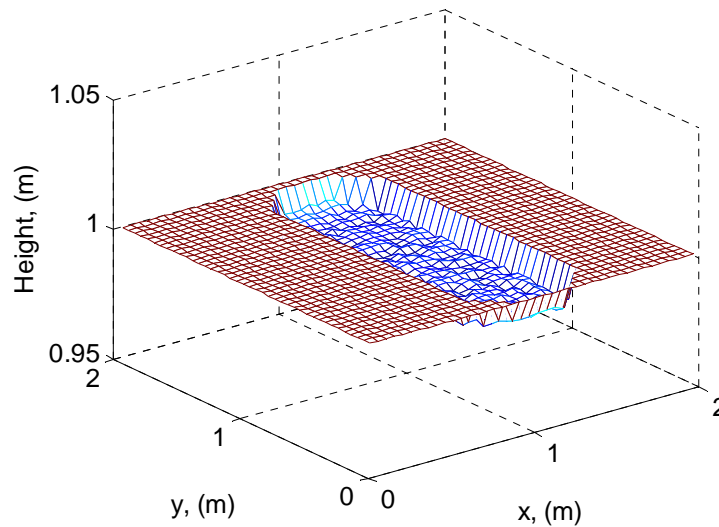


Figure 5-13 Rigid wheel rolling over terrain with stochastic soil parameter.

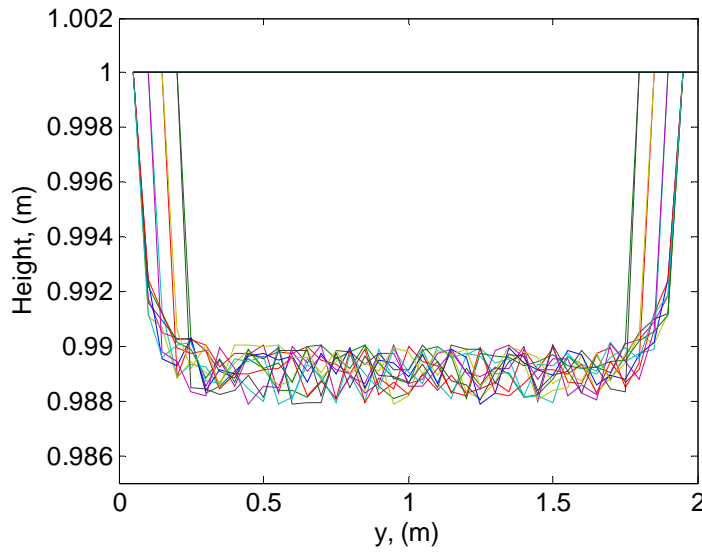


Figure 5-14 Side view of Figure 5-13.

The next case study is the flexible wheel rolling over a deterministic terrain profile with stochastic soil properties. Similar to the case study shown above, the uncertain parameter is k_ϕ in Bekker's equation, and the uncertainty is assumed to have a uniform distribution. Figure 5-15 shows the flexible wheel over stochastic soil, while Figure 5-16 shows the side view of the simulation. The calculations for the sinkage of the flexible wheel are the same as that shown in section 5-4.

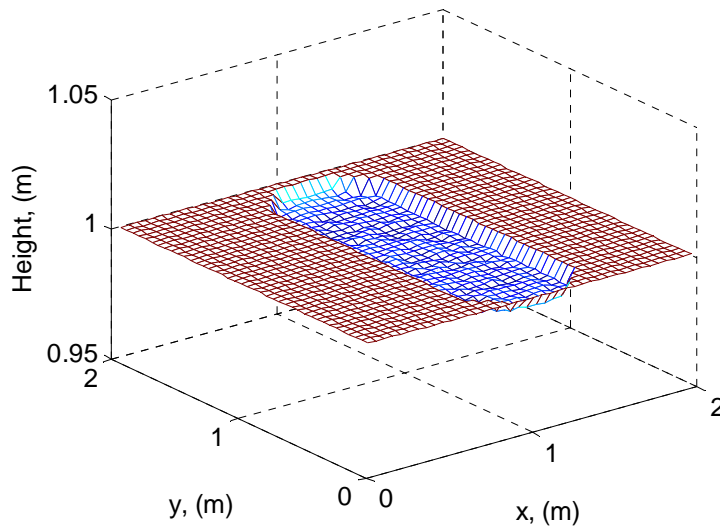


Figure 5-15 Flexible wheel rolling over terrain with stochastic soil parameter.

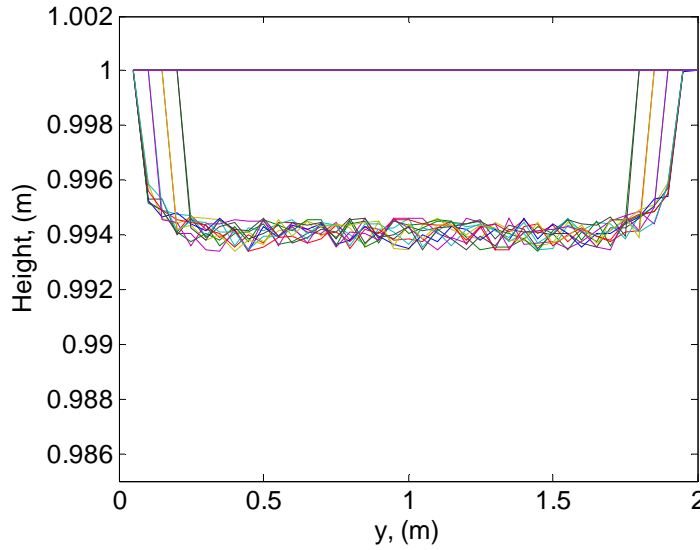


Figure 5-16 Side view of Figure 5-15.

5.8 Rolling on stochastic terrain profile with deterministic soil properties

This study shows the rolling of a flexible and rigid wheel over a stochastic terrain profile, which is developed in Chapter 3. For the simulations, all of the model parameters, K , L , u , and σ , were set to 1. Unlike the case studies shown in the previous section, the parameter k_ϕ is deterministic and held at a constant value throughout the surface map for these simulations. Figure 5-17 shows a rigid wheel rolling over a stochastic terrain with deterministic soil properties. Figure 5-18 shows the side view of the simulation. As the rigid wheel rolls over the terrain, the pattern in the terrain underneath the contact patch is the same as the original terrain height pattern, with the exception of the sinkage.

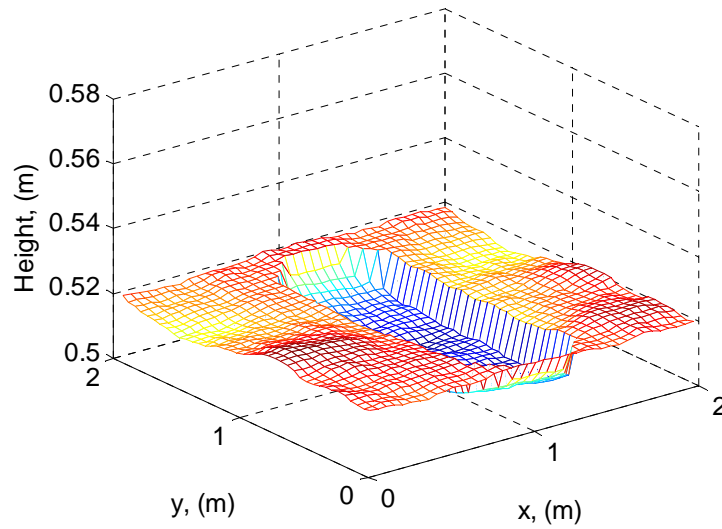


Figure 5-17 Rigid wheel rolling over stochastic terrain with deterministic soil.

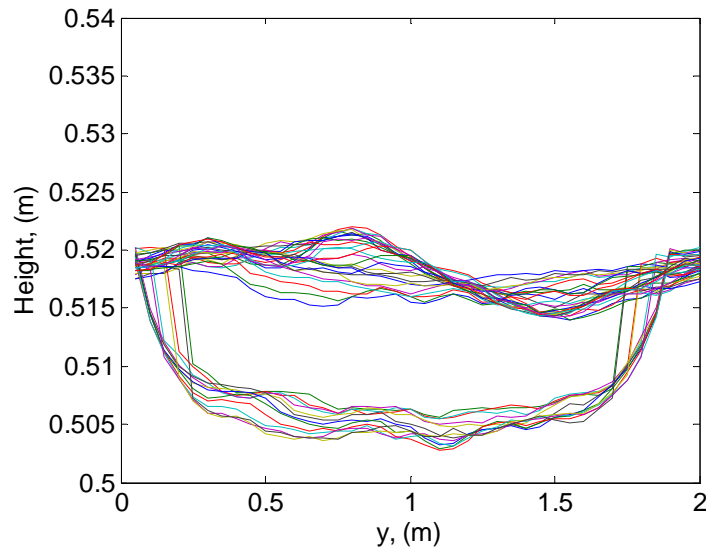


Figure 5-18 Side view of Figure 5-17.

Figure 5-19 and Figure 5-20 shows the simulation of the flexible wheel rolling over the stochastic terrain with deterministic soil parameters and the side view of the simulation environment, respectively. Similar to the case studies shown above, all of the model parameters for the stochastic terrain profile were set to a value of 1. The calculations for the sinkage of the flexible wheel are the same as that shown in section 5-4.

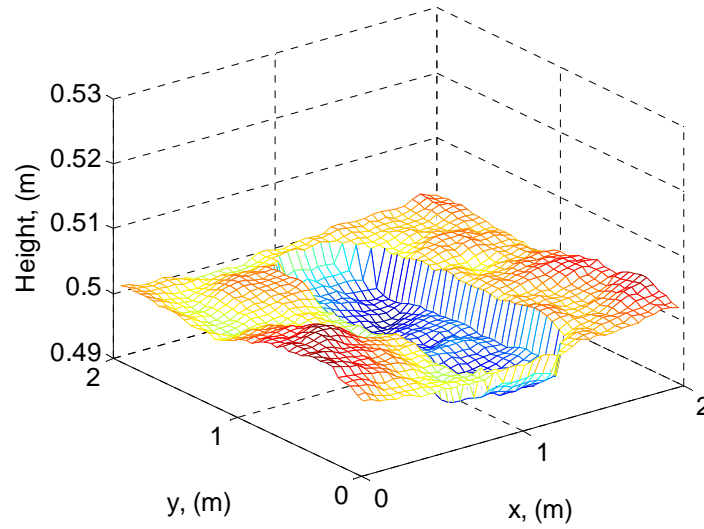


Figure 5-19 Flexible wheel rolling over stochastic terrain with deterministic soil.

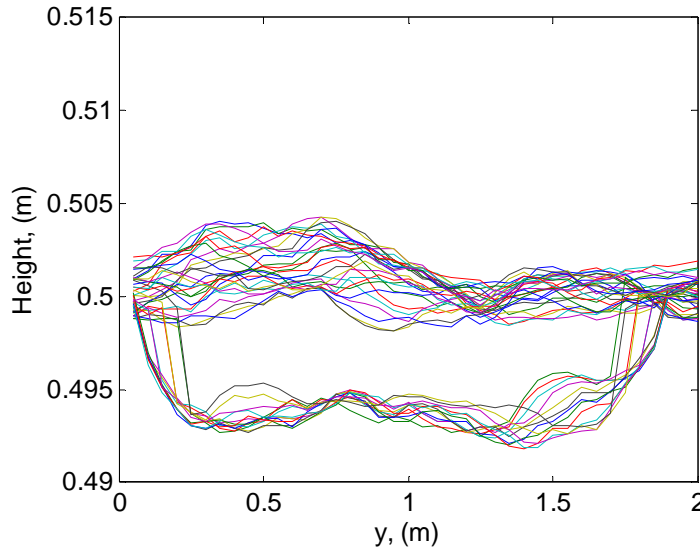


Figure 5-20 Side view of Figure 5-19.

5.9 Rolling on stochastic terrain profile with stochastic soil properties

The studies shown in this section includes a flexible and rigid wheel rolling over the developed model of the stochastic terrain profile and incorporates the effects of stochastic soil parameters. Similar to section 5.8, the model parameters for the stochastic terrain profile is all set to a value of 1. As for the stochastic soil properties, the uncertain parameter is k_ϕ with uncertain amplitude of 20%. The distribution is also assumed to be uniform. Figure 5-21 presents a snapshot of the

simulation of the rigid wheel while Figure 5-22 shows the side view of the simulation. Since the simulation incorporates stochastic soil parameters, the terrain underneath the contact patch is not uniform with the pattern of the original stochastic terrain height.

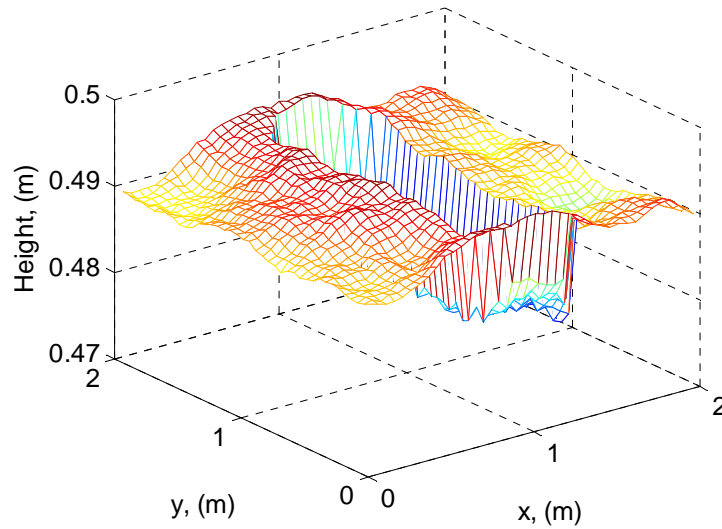


Figure 5-21 Rigid wheel rolling over stochastic terrain with stochastic soil.

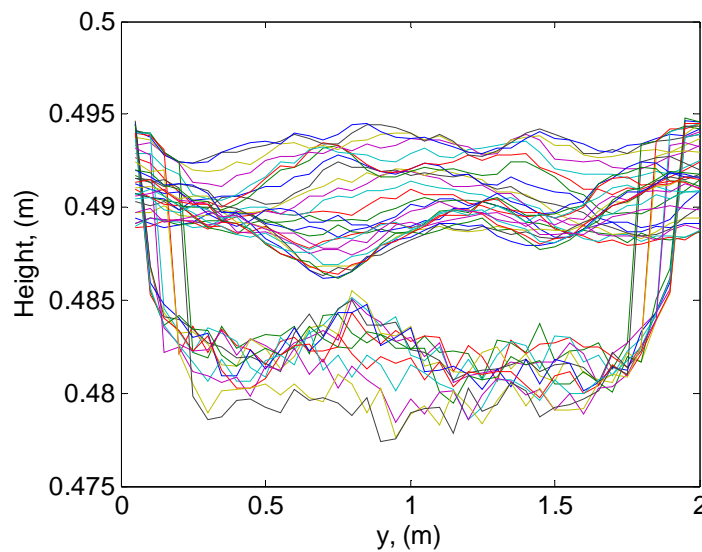


Figure 5-22 Side view of Figure 5-21.

Another case study is shown in Figure 5-23 where the flexible wheel is rolling over a stochastic terrain profile with stochastic soil parameters. The parameters are the same as the case study

shown above. The only difference is that the simulation includes a flexible wheel instead of a rigid wheel. Figure 5-24 shows the side view of the simulation of the flexible wheel.

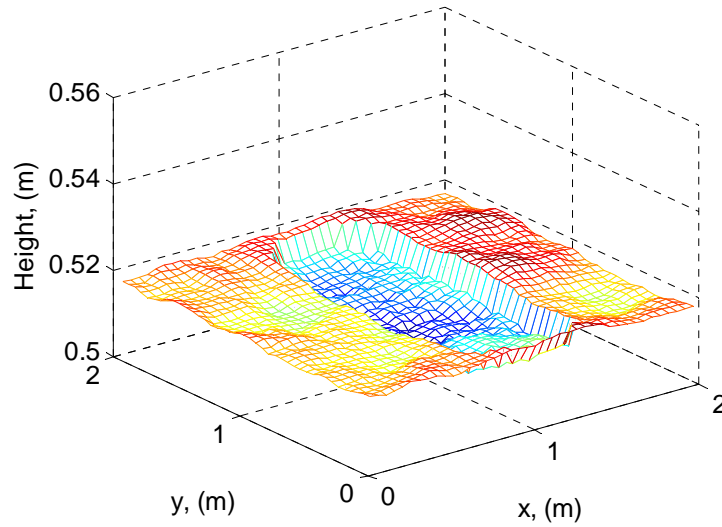


Figure 5-23 Flexible wheel rolling over stochastic terrain with stochastic soil.

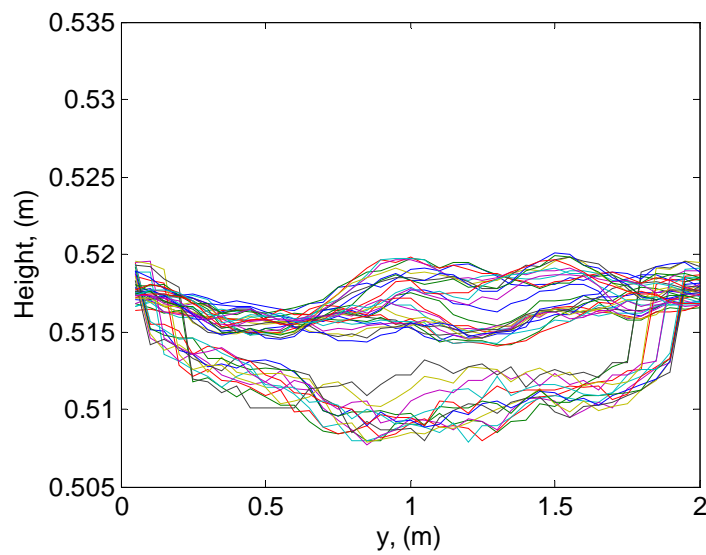


Figure 5-24 Side view of Figure 5-23.

Chapter 6 Conclusions

Terrain profile modeling is critical in the analysis of off-road mobility studies. An approach to model the non-stationary two-dimensional (terrain height along both x and y directions) terrain profiles is developed in this thesis. The methodology includes solving stochastic partial differential equations using the finite difference method. Note that, although in this study this methodology was used to create stochastic terrain profiles, the treatment of the stochastic PDEs presented is general, and may be used for other applications. The “wrap around” method was used as an assumption for the boundary conditions. One advantage of this methodology is the ability to easily change the model coefficients to efficiently and realistically create a model of terrain profile with the desired stochastic properties.

The model coefficients for the stochastic PDE are K , u , L , and σ . These coefficients are considered to be space-dependent. From further analysis of the model coefficients, the characteristic correlation length is calculated to be $\sqrt{K/L}$ and the uncorrelated white noise is represented by the variable σ . An experiment was performed to analyze the effects of the correlation length and the uncorrelated white noise. Results show that there is a specific relationship between the correlation length and the difference in terrain heights. The parameter analysis of K shows that there is a consistent relationship between K and σ values. Analysis of σ shows that there is a linear relationship between the uncorrelated white noise and the amplitude of the terrain height. The σ value affects the K value indirectly.

Raw terrain data was extracted from a gravel road measured by VTPL. With the program Surfer, the raw data was processed and key parameters were extracted to validate the stochastic PDE method to model terrain profiles. With the knowledge of the model coefficients K , L and σ , the average terrain height of all the points on the surface map (e.g., scalar value of σ) and the difference between the terrain height and the average terrain height of the entire surface map at each point (e.g., matrix of values for correlation length, $\sqrt{K/L}$) was recorded from the gravel road data. Applying these values to the model coefficients allowed the recreation of a stochastic

terrain profile with similar characteristics of terrain amplitude and correlation between neighboring nodes.

Results from different experiments were taken to illustrate the uncertainties in the soil parameters. The first experiment involved collecting data from the Virginia Tech's terramechanics rig. A cone penetrometer method was used to extract pressure-sinkage data from the lunar soil simulant GRC-1. The Karhunen-Loeve expansion and the polynomial chaos theory were also used to create a stochastic model for the soil parameters. Bekker's equation was used to model the soils, and the pressure-sinkage parameter k_ϕ is used as the uncertain parameter. The Monte Carlo simulation and the probability density function were used to validate the technique. The parameters in Bekker's equation were derived from bevameter plate-sinkage tests. Depending on the device used to collect the data, the pressure sinkage parameters will vary. Results show a comparison between the device used to obtain the soil parameters (cone penetrometer versus bevameter plate-sinkage test) and the method used to obtain the pressure-sinkage curves (experimental tests versus poly chaos model).

To analyze the mobility of wheeled vehicles in off-road conditions, simulations were created for the "stepping" and for the rolling of a rigid wheel and of a flexible wheel on two 2D terrain profiles (40 points by 40 points) with homogeneous soil (LLL sandy loam). Simulations include a combination of case studies with the implementation of the terrain profile methodology developed and the incorporation of stochastic soil properties. The stepping with a rigid plate has also been investigated since the parameters in Bekker's equation were collected through plate-sinkage tests. The simulations were all created on surface maps, similar to the procedures used for the terrain profile modeling. Several case studies were run, as follows:

- "Stepping" with rigid plate on deterministic flat surface
- "Stepping" with rigid wheel on deterministic flat surface
- "Stepping" with flexible wheel on deterministic flat surface
- Rolling with rigid wheel on deterministic flat surface
- Rolling with rigid wheel over deterministic semi-oval bump
- Rolling with flexible wheel on deterministic flat surface
- Rolling with flexible wheel over deterministic semi-oval bump

- Rolling with rigid wheel on deterministic flat surface with stochastic soil
- Rolling with flexible wheel on deterministic flat surface with stochastic soil
- Rolling with rigid wheel on stochastic surface with deterministic soil
- Rolling with flexible wheel on stochastic surface with deterministic soil
- Rolling with rigid wheel on stochastic surface with stochastic soil
- Rolling with flexible wheel on stochastic surface with stochastic soil

All simulations were created in real time. There were also consistent tire parameters that were used for the wheel in every simulation (e.g., the length and the width of the contact patch and the vertical load of the wheel). The slip ratio was only applied to the rolling simulations. To realistically represent the simulation of a tire rolling, the contact patch was also modeled as a superellipse. The simulations mainly focused on the effect of the vertical force on the terrain. The lateral dynamics were assumed to be uniform.

Chapter 7 Future Work

The main focus of this thesis was to illustrate a proposed methodology to create virtual proving grounds by modeling the terrain profile (surface map) using stochastic partial differential equations. This method has the advantage of allowing the researcher to create as much terrain profile as needed for the off-road vehicle dynamics simulation using a limited amount of data, while preserving the stochastic properties of the original terrain profile (from which the experimental data was collected). Moreover, creating such terrain profile is efficient, and can be done in real time. However, further analysis will be needed to accurately represent the surface of the terrain.

To efficiently and realistically recreate stochastic terrain profiles, the model coefficients (particularly u) will have to be further analyzed. Additional techniques are being explored to continue to refine the estimation of the model coefficients in order to realistically model the terrain profile. Experiments have been performed on the model coefficient u , but there has been no final conclusion on the effect of this variable on the terrain profile. Another challenge was to extract the model coefficients from experimental data to realistically represent the terrain measured. Further studies could investigate extracting the model coefficient from terrain data. Also, certain assumptions were made for the technique of solving the stochastic partial differential equation. The boundary condition assumption will have to be further reviewed and verified. Further analysis of the relationship between K and σ for the K values less than 0.1 will be aimed at explaining the peaks observed.

Another goal of this thesis was to incorporate the terrain model, soil model, and the wheel-terrain contact model into a simulation framework. Steps could be taken to enhance the simulations for the tire and soil interactions. As for now, the only parameters shown in the simulations are the pressure distribution in the contact patch of a wheel and the sinkage, which focuses on the forces in the vertical direction. Steps were also taken to realistically show the geometry of the contact patch as being a superellipse. Although this may be a good foundation for the simulation environment of off-road mobility studies, there are many other factors that need to be shown for realistic simulations of the tire and soil interaction, such as shear stress and shear displacement.

For off-road vehicles, there is also a bulldozing effect where some of the soil displaces around the wheel, effect currently not shown in the simulation. The lateral dynamics of the contact patch will have to be analyzed and implemented into the models. The current scenarios only consist of one run of a single wheel over the terrain. Repetitive loading can also be implemented into the simulations.

References

- Alexander, F.J., Garcia, A.L. and Tartakovsky, D.M. (2005) 'Algorithm refinement for stochastic partial differential equations: II. Correlated systems', *Journal of Computational Physics*, Vol. 207, Issue 2, pp. 769-787.
- Andr  n, P. (2006) 'Power spectral density approximations of longitudinal road profiles', *International Journal of Vehicle Design*, Vol. 40, No. 1/2/3, pp. 2-14.
- Bauer, R., Leung, W. and Barfoot, T. (2005) 'Experimental and Simulation Results of Wheel-Soil Interaction for Planetary Rovers'. *Paper Presented at the International Conference on Intelligent Robots and Systems*. Aug. 2-5, 2005. Edmonton, Canada.
- Bin, C., Jian-qiao, L., Meng, Z., Yin-wu, L. and Wei-kui L. (2008) 'The Pressure-Sinkage Characteristics of the Simulant Lunar Soil'. *Paper Presented at the 16th International Conference of the International Society for Terrain-Vehicle Systems*. Nov. 25-28, 2008. Turin, Italy.
- Chaika, M., Gorsich, D., and Sun, T.C. (2004) 'Some statistical tests in the study of terrain modeling', *International Journal of Vehicle Design*, Vol. 36, No. 2/3, pp. 132-148.
- Chan, B.J. (2008) *Development of an off-road tire model for vehicle dynamics simulations*. PhD dissertation. Virginia Tech.
- Chantasiriwan, S. (2005) 'Solutions of partial differential equations with random Dirichlet boundary conditions by multiquadric collocation method', *Engineering Analysis with Boundary Elements*, Vol. 29, Iss. 12, pp. 1124-1129.
- Chung, T.J. and Lee, J.K. (1975) 'Dynamics of viscoelastoplastic soil under a moving wheel', *Journal of Terramechanics*, Vol. 12, No. 1, pp. 15-31.
- Constantinescu, E.M., Chai, T., Sandu, A., and Carmichael, G.R. (2007) 'Autoregressive models of background errors for chemical data assimilation', *Journal of Geophysical Research*, Vol. 112, Iss. D12309.
- Cyganowski, S. (1995) 'A MAPLE Package for Stochastic Differential Equations'. *Paper Presented at the 7th Biennial Conference of Computational Techniques and Applications*. July 3-5, 1995. Victoria, Australia.
- Day, T.D. (2005) 'Simulation of Tire Interaction with Curbs and Irregular Terrain', *Engineering Dynamics Corporation, HVE White Papers*, Library Ref. WP-2005-6.

- Debella-Gilo, M., Etzelmuller, B., and Klakegg O. (2007) 'Digital soil mapping using digital terrain analysis and statistical modeling integrated into GIS: Examples from Vestfold County Norway'. *Paper Presented at the 11th Scandinavian Research Conference on Geographical Information Sciences. Sept. 5-7, 2007. Ås, Norway.*
- Duncan, T.E., Pasik-Duncan, B. and Zimmer, P. (1996) 'Computational Methods for some Stochastic Partial Differential Equations'. *Paper Presented at the 35th Conference on Decision and Control, Dec. 11-13, 1996. Kobe, Japan.*
- Ellery, A., Patel, N., Richter, L., Bertrand, R., and Dalcomo, J. (2005) 'Exomars rover chassis analysis & design'. *Paper Presented at the 8th International Symposium on Artificial Intelligence, Robotics, and Automation in Space. Sept. 5-8, 2005. Munich, Germany.*
- Elmqvist, M., Jungert, E., Lantz, F., Persson, A., and Söderman, U. (2001) 'Terrain modeling and analysis using laser scanner data', *International Archives of Photogrammetry and Remote Sensing*, Vol. XXXIV-3/W4. pp. 219-226.
- El-Sayed, A.M.A. and Gaber, M. (2006) 'The Adomian decomposition method for solving partial differential equations of fractal order in finite domains', *Physics letters*, Vol. 359, No. 3, pp. 175-182.
- Fenton, G.A. (1999) 'Estimation for stochastic soil models', *Journal of Geotechnical and Geoenvironmental Engineering*, Vol. 125, No. 6, pp. 470-485.
- Ferretti, G. and Girelli, R. (1999) 'Modelling and simulation of an agricultural tracked vehicle', *Journal of Terramechanics*, Vol. 36, Iss. 3, pp. 139-158.
- Garber, M. and Wong, J.Y. (1981) 'Prediction of Ground Pressure Distribution under Tracked Vehicles – II. Effects of Design Parameters of the Track-Suspension System on Ground Pressure Distribution', *Journal of Terramechanics*, Vol. 18, No. 2, pp. 71-79.
- Gibson, W.E. (1967) 'An exact solution for a class of stochastic partial differential equations', *SIAM Journal on Applied Mathematics*, Vol. 15, Iss. 5, pp. 1357-1362.
- Hallonborg, U. (1996) 'Super ellipse as tyre-ground contact area', *Journal of Terramechanics*, Vol. 33, No. 3, pp. 125-132.
- Hatger, C. (2005) 'On the use of airborne laser scanning data to verify and enrich road network features'. *Paper Presented at the XXII International Cartographic Conference. July 11-16, 2005. A Coruña, Spain.*

- Hossain, F., Anagnostou, E.N., and Lee, K.H. (2004) 'A non-linear and stochastic response surface method for Bayesian estimation of uncertainty in soil moisture simulation from a land surface model', *Nonlinear Processes in Geophysics*, Vol. 11, No. 4, pp. 427-440.
- Howe, J.G., Chrstos, J.P., Allen, R.W., Myers, T.T., Lee, D., Liang, C.Y., Gorsich, D.J., and Reid, A.A. (2004) 'Quarter car model stress analysis for terrain/road profile rating', *International Journal of Vehicle Design*, Vol. 36, No. 2/3, pp. 248-269.
- Hyypä, J., Pyysalo, U., Hyypä, H. and Samberg, A. (2000) 'Elevation Accuracy of Laser Scanning-Derived Digital Terrain and Target Models in Forest Environment'. *Paper Presented at 4th EARSeL-SIG-Workshop LIDAR. June 16-17, 2000. Dresden, Germany.*
- Iagnemma, K., Kang, S., Shibly, H. and Dubowsky, S. (2004) 'Online Terrain Parameter Estimation for Wheeled Mobile Robots with Application to Planetary Rovers', *IEEE Transactions on Robotics*, Vol. 20, No. 5, pp. 921-927.
- Ishigami, G., Miwa, A., Nagatani, K. and Yoshida, K. (2007) 'Terramechanics-Based Model for Steering Maneuver of Planetary Exploration Rovers on Loose Soil', *Journal of Field Robotics*, Vol. 24, No. 3, pp. 233-250.
- Kamat, V.R. and Martinez J.C. (2003) 'Automated Generation of Large-Scale Dynamic Terrain in 3D Animation of Simulated Construction Processes'. *Paper Presented at Conference on Construction Applications of Virtual Reality, CONVR 2003. Sept. 24-26, 2003. Blacksburg, Virginia.*
- Kern, J.V. and Ferris, J.B. (2006) 'Preliminary results for model identification in characterizing 2-D topographic road profiles'. *Proceedings of the SPIE, Vol. 6228: Modeling and Simulation for Military Applications. April 18, 2006. Orlando, Florida.*
- Kern, J.V., Ferris, J.B., Gorsich, D., and Reid, A.A. (2007) 'Characterizing 2D road profiles using ARIMA modeling techniques'. *Proceedings of the SPIE, Vol. 6564: Modeling and Simulation for Military Operations II. April 10, 2007. Orlando, Florida.*
- Khot, L.R., Salokhe, V.M., Jayasuriya, H.P.W. and Nakashima, H. (2007) 'Experimental validation of distinct element simulation for dynamic wheel-soil interaction', *Journal of Terramechanics*, Vol. 44, Issue 6, pp. 429-437.
- Kim, C., Lee, E.K., Hänggi, P., and Talkner, P. (2007) 'Numerical method for solving stochastic differential equations with poissonian white shot noise', *Physical review. E*,

- Statistical, nonlinear, and soft matter physics*, Vol. 76 (1), No. 1, pp. 011109-1 – 011109-10.
- Kim, Y., Thompson, D. and Machiraju, R. (2003) ‘Rough Surface Modeling Using Surface Growth’. *Paper Presented at the International Conference on Shape Modeling and Applications. May 12-16, 2003. Seoul, Korea.*
- Kumar, P. and Dewangan, K.N. (2004) ‘Deflection and Contact Characterisitics of a Power Tiller Tyre’, *The CIGR Journal of Scientific Research*, Vol. VI, pp. 1-8.
- Larson, A.C., Voyles, R.M. and Demir G.K. (2004) ‘Terrain Classification Through Weakly-Structured Vehicle/Terrain Interaction’. *Paper Presented at the IEEE International Conference on Robotics and Automation, ICRA '04. April 26 – May 1, 2004. New Orleans, LA.*
- Li, L. (2008) *Treatment of Uncertainties in Vehicle and Terramechanics Systems Using a Polynomial Chaos Approach*. PhD dissertation. Virginia Tech.
- Li, L. and Sandu, C. (2007) ‘Modeling and simulation of 2D ARMA terrain models for vehicle dynamics applications’, *SAE 2007 Transactions Journal of Commercial Vehicles*, Vol. 116, Sect. 2, pp. 1-9.
- Li, L. and Sandu, C. (2007) ‘Stochastic Analysis of Tire-Force Equations’. *Paper Presented at the SAE 2007 Commercial Vehicle Engineering Congress. Oct. 30 – Nov. 1, 2007. Chicago, Illinois.*
- Li, L. and Sandu, C. (2008) ‘Stochastic modeling of 1-D and 2-D terrain profiles using a polynomial chaos approach’. *Paper Presented at the International Society for Terrain-Vehicle Systems (ISTVS) 2008 Conference. Nov. 25-28, 2008. Turin, Italy.*
- Li, L., Sandu, C. and Sandu, A. (2005) ‘Modeling and simulation of a full vehicle with parametric and external uncertainties’. *Paper Presented at the 2005 ASME International Mechanical Engineering Congress and RD&D Expo. Nov. 5-11, 2005. Orlando, Florida.*
- Lythe, G. (1998) ‘Stochastic PDEs: Domain Formation in Dynamic Transitions’, *Anales de Fisica*, Vol. 4, pp. 55-63.
- Maas, H.G. (2001) ‘The suitability of airborne laser scanner data for automatic 3D object reconstruction’. *Paper Presented at the 3rd International Workshop on Automatic Extraction of Man-Made Objects from Aerial and Space Images. June 10-15, 2001. Ascona, Switzerland.*

- Nguyen, V.N., Matsuo, T., Inaba, S. and Koumoto, T. (2008) 'Experimental analysis of vertical soil reaction and soil stress distribution under off-road tires', *Journal of Terramechanics*, Vol. 45, Issues 1-2, pp. 25-44.
- Nobile, F., Tempone, R., and Webster, C.G. (2008) 'A sparse grid stochastic collocation method for partial differential equations with random input data', *SIAM Journal on Numerical Analysis*, Vol. 46, Iss. 5, pp. 2309-2345.
- Okello, J.A. (1992) 'Prediction of the force distribution between the soil and a pneumatic wheel', *Journal of Agricultural Engineering Research*, Vol. 51, No. 4, pp. 249-262.
- Oravec, H.A. (2009) *Understanding Mechanical Behavior of Lunar Soils for the Study of Vehicle Mobility*. PhD dissertation. Case Western Reserve University.
- Oravec, H.A., Asnani, V.M., and Zeng, X. (2008) 'The development of a soil for lunar surface mobility testing in ambient conditions'. *Paper Presented at the Eleventh Biennial ASCE Aerospace Division International Conference on Engineering, Science, Construction, and Operations in Challenging Environments. March 3-5, 2008*. Long Beach, California.
- Park, S., Popov, A.A. and Cole, D.J. (2004) 'Influence of soil deformation on off-road heavy vehicle suspension vibration', *Journal of Terramechanics*, Vol. 41, Issue 1, pp. 41-68.
- Park, W.Y., Chang, Y.C., Lee, S.S., Hong, J.H., Park, J.G., and Lee, K.S. (2008) 'Prediction of the tractive performance of a flexible tracked vehicle', *Journal of Terramechanics*, Vol. 45, Iss. 1-2, pp. 13-23.
- Patel, N., Scott, G.P. and Ellery, A. (2005) 'Application of Bekker Theory for Planetary Exploration through Wheeled, Tracked and Legged Vehicle Locomotion'. *Paper Presented at the 2005 American Institute of Aeronautics and Astronautics. Aug. 30 – Sept. 1, 2005*. Long Beach, California.
- Ramji, K., Gupta, A., Saran, V.H., Goel, V.K., and Kumar, V. (2004) 'Road roughness measurements using PSD approach', *Journal of the Institution of Engineers*, Vol. 85, No. Nov, pp. 193-201.
- Rashidi, M. and Gholami, M. (2008) 'Multiplate Penetration Tests to Predict Soil Pressure-Sinkage Behaviour', *World Applied Sciences Journal*, Vol. 3, No. 5, pp. 705-710.
- Rößler, A., Seaïd, M., and Zahri, M. (2008) 'Method of lines for stochastic boundary-value problems with additive noise', *Applied Mathematics and Computation*, Vol. 199, Iss. 1, pp. 301-314.

- Sadow, S. and Trimper, S. (1993) 'Gaussian white noise as a many-particle process: the Kardar-Parisi-Zhang equation', *Journal of Physics: Mathematical and Theoretical*, Vol. 26, No. 13, pp. 3079-3084.
- Sandu, A., Sandu, C., Ahmadian, M. (2006a) 'Modeling multibody systems with uncertainties. Part I: theoretical and computational aspects', *Multibody System Dynamics*, Vol. 15, Iss. 4, pp. 369-391.
- Sandu, A., Sandu, C., Ahmadian, M. (2006b) 'Modeling multibody systems with uncertainties. Part II: numerical applications', *Multibody System Dynamics*, Vol. 15, No. 3, pp. 241-262.
- Sandu, C., Sandu, A., and Li, L. (2005) 'Stochastic modeling of terrain profiles and soil parameters', *SAE 2005 Transactions Journal of Commercial Vehicles*, Vol. 114, Sect. 2, pp. 211-220.
- Schurz, H. (2006) 'An Axiomatic Approach to Numerical Approximations of Stochastic Processes', *International Journal of Numerical Analysis and Modeling*, Vol. 3, No. 2, pp. 459-480.
- Schwanghart, H. (1991) 'Measurement of contact area, contact pressure and compaction under tires in soft soil', *Journal of Terramechanics*, Vol. 28, No. 4, pp. 309-318.
- Sharma, A.K. and Pandey, K.P. (1996a) 'A Review on Contact Area Measurement of Pneumatic Tyre on Rigid and Deformable Surfaces', *Journal of Terramechanics*, Vol. 33, No. 5, pp. 253-264.
- Sharma, A.K. and Pandey, K.P. (1996b) 'The deflection and contact characteristics of some agricultural tyres with zero sinkage', *Journal of Terramechanics*, Vol. 33, No. 6, pp. 293-299.
- Shen, J. (1996) 'A Block Finite Difference Scheme for Second-Order Elliptic Problems with Discontinuous Coefficients', *SIAM Journal of Numerical Analysis*, Vol. 33, No. 2, pp. 686-706.
- Shibly, H., Iagnemma, K., and Dubowsky, S. (2005) 'An equivalent soil mechanics formulation for rigid wheels in deformable terrain, with application to planetary exploration rovers', *Journal of Terramechanics*, Vol. 42, No. 1, pp. 1-13.
- Shoop, S.A., Richmond, P.W. and Lacombe, J. (2006) 'Overview of cold regions mobility modeling at CRREL', *Journal of Terramechanics*, Vol. 43, Issue 1, pp. 1-26.

- Taylor, B., Sandu, C., Biggans, J.S., and Ahmadian, M. (2008) 'Building an infrastructure for indoor terramechanics studies: the development of a terramechanics rig at Virginia Tech'. *Paper Presented at the International Society for Terrain-Vehicle Systems (ISTVS) 2008 Conference. Nov. 25-28, 2008. Turin, Italy.*
- Van, N.N., Matsuo, T., Koumoto, T., and Inaba, S. (2008a) 'Experimental device for measuring sandy soil sinkage parameters', *Saga Bulletin of the Faculty of Agriculture, Saga University*, Vol. 93, pp. 91-99.
- Van, N.N., Matsuo, T., Koumoto, T., and Inaba, S. (2008b) 'Effects of Tire Inflation Pressure on Soil Contact Pressure and Rolling Resistance of Farm Tractors', *Saga Bulletin of the Faculty of Agriculture, Saga University*, Vol. 93, pp. 101-108.
- Wang, Z. and Reece, A.R. (1984) 'The Performance of Free Rolling Rigid and Flexible Wheels on Sand', *Journal of Terramechanics*, Vol. 21, No. 4, pp. 347-360.
- Williams, S.B. and Mahon I. (2004) 'Design of an Unmanned Underwater Vehicle for Reef Surveying'. *Paper Presented at the 3rd IFAC Symposium on Mechatronic Systems. Sept. 6-8, 2004. Manly NSW, Australia.*
- Wong, J.Y. (2001) *Theory of Ground Vehicles: 3rd ed.*, Canada: John Wiley & Sons, Inc.
- Wulfsohn, D. and Upadhyaya, S.K. (1992) 'Determination of dynamic three-dimensional soil -tyre contact profile', *Journal of Terramechanics*, Vol. 29, No. 4/5, pp. 433-464.
- Wyk, D.J., Spoelstra, J. and Klerk, J.H. (1996) 'Mathematical modeling of the interaction between a tracked vehicle and the terrain', *Applied Mathematical Modelling*, Vol. 20, No. 11, pp. 838-846.
- Yang, Y., Bao, J., Kin, Y., and Cheng, Y. (2008) 'A virtual simulation environment for lunar rover: framework and key technologies', *International Journal of Advanced Robotic Systems*, Vol. 5, No. 2, pp. 201-208.
- Yeh, K.C., Lin, K.H. and Wang, Y. (2001) 'Effects of Irregular Terrain on Waves - A Stochastic Approach', *IEEE Transactions on Antennas and Propagation*, Vol. 49, No. 2, February 2001.
- Yong, R.N., Fattah, E.A., and Boonsinsuk, P. (1978) 'Analysis and prediction of tyre-soil interaction and performance using finite elements', *Journal of Terramechanics*, Vol. 15, No. 1, pp. 43-63.

- Yoon, S. (2003) 'A study on terrain-surface modeling and searching algorithms for real-time simulation of off-road vehicles', *Vehicle System Dynamics*, Vol. 39, No. 5, pp. 353-363.
- Zhang, T., Lee, J.H. and Liu, Qing (2005) 'Finite Element Simulation of Tire-Snow Interaction under Combined Longitudinal and Lateral Slip Condition'. *Paper Presented at the 15th International Conference of the ISTVS. Sept. 25-29, 2005. Hayama, Japan.*

Appendix A

Shown in this Appendix A are MATLAB codes and the raw data used to validate and perform the methodology for the stochastic terrain profiles. Appendix A.1 shows the MATLAB m-file used to create the stochastic terrain profiles. Appendix A.2 shows all of the tabulated values for the experimental analysis of the model parameters K and σ . Appendix A.3 shows the MATLAB m-file obtained from VTPL to parse the raw data file. Appendix A.4 shows procedures to process the raw data files after they are parsed.

A.1 MATLAB m-file used to create stochastic terrain profiles

```
clear all

%%%%%%%%%SPARSE MATRIX METHOD%%%%%%%%%

X=3; %enter distance of x-axis
Y=3; %enter distance of y-axis
imax=81; %enter # of lines
jmax=81; %enter # of lines
imin=1;
jmin=1;
dx=X/(imax-1);
dy=Y/(jmax-1);

%%define K
K(imin:imax-1,jmin:jmax-1)=1;

%%define L
L(imin:imax-1,jmin:jmax-1)=1;

%%define u
u(imin:imax-1,jmin:jmax-1)=1;

%%define sigma
sigma(imin:imax-1,jmin:jmax-1)=1;

correlation=sqrt(K./abs(L));

NoPts=(imax-imin)*(jmax-jmin);
zeta=rand(NoPts,1);
random=reshape(zeta,(NoPts/(imax-imin))),(NoPts/(imax-imin)));

d=[(-NoPts+sqrt(NoPts)),(-sqrt(NoPts)),(-sqrt(NoPts)+1),...
    -1,0,1,(sqrt(NoPts)-1),...
    (sqrt(NoPts)),(NoPts-sqrt(NoPts))];

Q=zeros(NoPts,9);
```

```

%%Interior Nodes
for i = imin+1:imax-2;
    for j = jmin+1:jmax-2;
        A(i,j)=-2*K(i,j)*((1/dx^2)+(1/dy^2))+L(i,j);
        B(i,j)=(K(i,j)/dy^2)+(u(i-1,j)/(2*dy));
        C(i,j)=(K(i,j)/dx^2)+(u(i,j+1)/(2*dx));
        D(i,j)=(K(i,j)/dy^2)-(u(i+1,j)/(2*dy));
        E(i,j)=(K(i,j)/dx^2)-(u(i,j-1)/(2*dx));
        V=sigma(i,j)*zeta;
    end
end

%%Top Left Corner Node
for i = imin;
    for j = jmin;
        A(i,j)=-2*K(i,j)*((1/dx^2)+(1/dy^2))+L(i,j);
        B(i,j)=(K(i,j)/dy^2)+(u(imax-1,j)/(2*dy));
        C(i,j)=(K(i,j)/dx^2)+(u(i,j+1)/(2*dx));
        D(i,j)=(K(i,j)/dy^2)-(u(i+1,j)/(2*dy));
        E(i,j)=(K(i,j)/dx^2)-(u(i,jmax-1)/(2*dx));
        V=sigma(i,j)*zeta;
    end
end

%%Top Right Corner Node
for i = imin;
    for j = jmax-1;
        A(i,j)=-2*K(i,j)*((1/dx^2)+(1/dy^2))+L(i,j);
        B(i,j)=(K(i,j)/dy^2)+(u(imax-1,j)/(2*dy));
        C(i,j)=(K(i,j)/dx^2)+(u(i,jmin)/(2*dx));
        D(i,j)=(K(i,j)/dy^2)-(u(i+1,j)/(2*dy));
        E(i,j)=(K(i,j)/dx^2)-(u(i,j-1)/(2*dx));
        V=sigma(i,j)*zeta;
    end
end

%%Bottom Left Corner Node
for i = imax-1;
    for j = jmin;
        A(i,j)=-2*K(i,j)*((1/dx^2)+(1/dy^2))+L(i,j);
        B(i,j)=(K(i,j)/dy^2)+(u(imax-2,j)/(2*dy));
        C(i,j)=(K(i,j)/dx^2)+(u(i,j+1)/(2*dx));
        D(i,j)=(K(i,j)/dy^2)-(u(imin,j)/(2*dy));
        E(i,j)=(K(i,j)/dx^2)-(u(i,jmax-1)/(2*dx));
        V=sigma(i,j)*zeta;
    end
end

%%Bottom Right Corner Node
for i = imax-1;
    for j = jmax-1;
        A(i,j)=-2*K(i,j)*((1/dx^2)+(1/dy^2))+L(i,j);
        B(i,j)=(K(i,j)/dy^2)+(u(imax-2,j)/(2*dy));
        C(i,j)=(K(i,j)/dx^2)+(u(i,jmin)/(2*dx));
        D(i,j)=(K(i,j)/dy^2)-(u(imin,j)/(2*dy));
    end
end

```

```

        E(i,j)=(K(i,j)/dx^2)-(u(i,j-1)/(2*dx));
        V=sigma(i,j)*zeta;
    end
end

%%Top Boundary Nodes
for i = imin;
    for j = jmin+1:jmax-2;
        A(i,j)=-2*K(i,j)*((1/dx^2)+(1/dy^2))+L(i,j);
        B(i,j)=(K(i,j)/dy^2)+(u(imax-1,j)/(2*dy));
        C(i,j)=(K(i,j)/dx^2)+(u(i,j+1)/(2*dx));
        D(i,j)=(K(i,j)/dy^2)-(u(i+1,j)/(2*dy));
        E(i,j)=(K(i,j)/dx^2)-(u(i,j-1)/(2*dx));
        V=sigma(i,j)*zeta;
    end
end

%%Bottom Boundary Nodes
for i = imax-1;
    for j = jmin+1:jmax-2;
        A(i,j)=-2*K(i,j)*((1/dx^2)+(1/dy^2))+L(i,j);
        B(i,j)=(K(i,j)/dy^2)+(u(imax-2,j)/(2*dy));
        C(i,j)=(K(i,j)/dx^2)+(u(i,j+1)/(2*dx));
        D(i,j)=(K(i,j)/dy^2)-(u(imin,j)/(2*dy));
        E(i,j)=(K(i,j)/dx^2)-(u(i,j-1)/(2*dx));
        V=sigma(i,j)*zeta;
    end
end

%%Left Boundary Nodes
for i = imin+1:imax-2;
    for j = jmin;
        A(i,j)=-2*K(i,j)*((1/dx^2)+(1/dy^2))+L(i,j);
        B(i,j)=(K(i,j)/dy^2)+(u(i-1,j)/(2*dy));
        C(i,j)=(K(i,j)/dx^2)+(u(i,j+1)/(2*dx));
        D(i,j)=(K(i,j)/dy^2)-(u(i+1,j)/(2*dy));
        E(i,j)=(K(i,j)/dx^2)-(u(i,jmax-1)/(2*dx));
        V=sigma(i,j)*zeta;
    end
end

%%Right Boundary Nodes
for i = imin+1:imax-2;
    for j = jmax-1;
        A(i,j)=-2*K(i,j)*((1/dx^2)+(1/dy^2))+L(i,j);
        B(i,j)=(K(i,j)/dy^2)+(u(i-1,j)/(2*dy));
        C(i,j)=(K(i,j)/dx^2)+(u(i,jmin)/(2*dx));
        D(i,j)=(K(i,j)/dy^2)-(u(i+1,j)/(2*dy));
        E(i,j)=(K(i,j)/dx^2)-(u(i,jmax-2)/(2*dx));
        V=sigma(i,j)*zeta;
    end
end

%%% Q matrix
Avector = reshape(A,NoPts,1);
Bvector = reshape(B,NoPts,1);

```

```

Cvector = reshape(C,NoPts,1);
Dvector = reshape(D,NoPts,1);
Evector = reshape(E,NoPts,1);

for i = imin:imax-1;                                %column 1
    Q(i,1)=C(i,jmax-1);
end

for k=sqrt(NoPts)+1:NoPts;                            %column 2
    Q(k-sqrt(NoPts),2)=Evector(k);
end

for k=sqrt(NoPts):sqrt(NoPts):NoPts;                    %column 3
    Q(k-sqrt(NoPts)+1,3)=Dvector(k);
end

for k=2:NoPts;                                          %column 4
    Q(k-1,4)=Bvector(k);
    Q(sqrt(NoPts):sqrt(NoPts):NoPts,4)=0;
end

for k=1:NoPts;                                          %column 5
    Q(k,5)=Avector(k);
end

for k=1:NoPts-1;                                       %column 6
    Q(k+1,6)=Dvector(k);
    Q(1:sqrt(NoPts):NoPts,6)=0;
end

for k=1:sqrt(NoPts):NoPts;                            %column 7
    Q(k+sqrt(NoPts)-1,7)=Bvector(k);
end

for k=1:NoPts-sqrt(NoPts);                            %column 8
    Q(k+sqrt(NoPts),8)=Cvector(k);
end

for k = 1:sqrt(NoPts);                                %column 9
    Q(k+(NoPts-sqrt(NoPts)),9)=Evector(k);
end

S=spdiags(Q,d,NoPts,NoPts);
figure(1);
spy(S);

Z=inv(S)*V;
MinHeight = min(Z);
MaxHeight = max(Z);
Difference = MaxHeight-MinHeight

Vmat=reshape(V,(NoPts/(imax-imin))),(NoPts/(imax-imin)));
Zmat=reshape(Z,(NoPts/(imax-imin))),(NoPts/(imax-imin)));
Zetamat=reshape(zeta,(NoPts/(imax-imin))),(NoPts/(imax-imin)));

```

```

xgrid=dx:dx:X;
ygrid=dy:dy:Y;

figure(2)
mesh(xgrid,ygrid,Zmat)
xlabel('x (unit length)')
ylabel('y (unit length)')
zlabel('Height (unit length)')

```

A.2 Tabulated values from experimental analysis of σ and K

This appendix shows the tabulated values recorded from the experimental analysis for the σ and K values. Tables A-1, A-2, and A-3 are tables representing values in Figure 3-8. The directions to obtain these values are as follows.

1. Create a 10 points by 10 points matrix
2. Extract the max and min values from 10 point by 10 point matrix
3. Calculate the difference of MaxHeight and MinHeight for each matrix
4. Run 100 times and record the difference for each run
5. Calculate the average of differences

Table A-1 Tabulated values for Figure 3-8, for $\sigma = 0.1$.

K	Correlation Length (Lc)	Average of MaxHeight - MinHeight
1.00E+09	31623	7.2266E-12
10000	100	7.2884E-07
1000	31.623	0.000007049
100	10	0.000072245
50	7.0711	0.00014
20	4.4721	0.00035
10	3.1623	0.00073
1	1	0.00775
0.5	0.70711	0.01466
0.2	0.44721	0.03108
0.15	0.3873	0.0583
0.1	0.31623	0.09608
0.09	0.3	0.0753
0.08	0.28284	0.06822
0.07	0.26458	0.06372
0.06	0.24495	0.06715
0.05	0.22361	0.07663
0.04	0.2	0.11038
0.03	0.17321	0.24246
0.025	0.15811	0.37887
0.02	0.14142	0.39461
0.015	0.12247	0.21455
0.01	0.1	0.17544
0.009	0.094868	0.13906
0.008	0.089443	0.12091
0.006	0.07746	0.10409
0.005	0.070711	0.09678
0.004	0.063246	0.09161
0.002	0.044721	0.08396
0.0009	0.03	0.08121
0.0005	0.022361	0.08024
0.0002	0.014142	0.07841

Table A-2 Tabulated values for Figure 3-8, for $\sigma = 1$.

K	Correlation Length (Lc)	Average of MaxHeight - MinHeight
1.00E+09	31623	7.11E-11
10000	100	0.00000707
1000	31.623	0.0000695
100	10	0.0007
50	7.0711	0.00145
20	4.4721	0.0037
10	3.1623	0.00705
1	1	0.078404
0.5	0.70711	0.14171
0.2	0.44721	0.32804
0.15	0.3873	0.57249
0.1	0.31623	0.94901
0.09	0.3	0.70936
0.08	0.28284	0.67474
0.07	0.26458	0.64759
0.06	0.24495	0.67124
0.05	0.22361	0.77845
0.04	0.2	1.11829
0.03	0.17321	2.43378
0.025	0.15811	3.68906
0.02	0.14142	3.88836
0.015	0.12247	2.28018
0.01	0.1	1.73457
0.009	0.094868	1.38037
0.008	0.089443	1.217
0.006	0.07746	1.02231
0.005	0.070711	0.98296
0.004	0.063246	0.93577
0.002	0.044721	0.8554
0.0009	0.03	0.81983
0.0005	0.022361	0.80451
0.0002	0.014142	0.80389

Table A-3 Tabulated values for Figure 3-8, for $\sigma = 10$.

K	Correlation Length (Lc)	Average of MaxHeight - MinHeight
1.00E+09	31623	7.2619E-10
10000	100	0.000070227
1000	31.623	0.00071442
100	10	0.0071
50	7.0711	0.0142
20	4.4721	0.0369
10	3.1623	0.0743
1	1	0.8049
0.5	0.70711	1.4563
0.2	0.44721	3.2757
0.15	0.3873	5.8622
0.1	0.31623	9.1901
0.09	0.3	7.5201
0.08	0.28284	6.7522
0.07	0.26458	6.5658
0.06	0.24495	6.722
0.05	0.22361	7.782
0.04	0.2	10.9352
0.03	0.17321	24.981
0.025	0.15811	36.9885
0.02	0.14142	38.497
0.015	0.12247	21.7855
0.01	0.1	17.2963
0.009	0.094868	13.6959
0.008	0.089443	12.2074
0.006	0.07746	10.2215
0.005	0.070711	10.001
0.004	0.063246	9.3448
0.002	0.044721	8.3888
0.0009	0.03	8.128
0.0005	0.022361	8.1004
0.0002	0.014142	7.9532

Tables A-4, A-5, and A-6 are tables representing the data taken for Figure 3-9. The procedures used to record these data points are the same as the ones listed above.

Table A-4 Tabulated values for Figure 3-9, for $\sigma = 0.1$.

K	Correlation Length (Lc)	Average of MaxHeight - MinHeight	Average Max Height	Average Min Height
9E-06	0.003	0.0774	0.0883	0.0109
0.00009	0.009486833	0.0782	0.0887	0.0105
0.0002	0.014142136	0.0796	0.0888	0.0093
0.0005	0.02236068	0.0813	0.0898	0.0086
0.0009	0.03	0.0821	0.0912	0.0091
0.002	0.04472136	0.0843	0.0917	0.0074
0.004	0.063245553	0.0917	0.0955	0.0039
0.005	0.070710678	0.0998	0.1003	5.54E-04
0.006	0.077459667	0.104	0.1021	-0.0019
0.007	0.083666003	0.1115	0.1057	-0.0058
0.008	0.089442719	0.1228	0.1118	-0.011
0.009	0.09486833	0.1344	0.1179	-0.0165
0.01	0.1	0.1688	0.1347	-0.034
0.011	0.104880885	0.3725	0.2352	-0.1373
0.0109	0.104403065	0.4752	0.2878	-0.1874
0.0108	0.103923048	1.291	0.6927	-0.5983
0.0107	0.103440804	1.2091	0.6534	-0.5556
0.0106	0.102956301	0.5748	0.3349	-0.2399
0.0105	0.102469508	0.4231	0.2595	-0.1636
0.0104	0.10198039	0.3658	0.233	-0.1329
0.0103	0.101488916	0.3546	0.2262	-0.1283
0.0102	0.100995049	0.3325	0.214	-0.1184
0.0101	0.100498756	0.3896	0.2435	-0.1461
0.012	0.109544512	0.4282	0.2624	-0.1658
0.0125	0.111803399	2.1568	1.1217	-1.0351
0.013	0.114017543	0.3351	0.2168	-0.1183
0.014	0.118321596	0.2212	0.1607	-0.0606
0.015	0.122474487	0.2223	0.161	-0.0613
0.016	0.126491106	0.2786	0.1864	-0.0922
0.0165	0.128452326	0.4156	0.2581	-0.1574
0.017	0.130384048	1.0137	0.5558	-0.4579
0.0175	0.132287566	0.7008	0.4018	-0.2989
0.018	0.134164079	0.4061	0.2554	-0.1508
0.019	0.137840488	0.3277	0.2151	-0.1126
0.02	0.141421356	0.3811	0.2408	-0.1403
0.02	0.141421356	0.3866	0.2418	-0.1448
0.021	0.144913767	0.5721	0.3368	-0.2353

0.022	0.14832397	1.5061	0.8039	-0.7022
0.023	0.151657509	1.5897	0.8446	-0.745
0.025	0.158113883	0.3689	0.2349	-0.134
0.03	0.173205081	0.2437	0.1729	-0.0708
0.031	0.176068169	0.299	0.1993	-0.0997
0.032	0.178885438	0.6719	0.3861	-0.2857
0.033	0.181659021	0.8202	0.461	-0.3592
0.035	0.187082869	0.2183	0.1587	-0.0595
0.04	0.2	0.1081	0.1042	-0.0038
0.045	0.212132034	0.0909	0.0956	0.0047
0.05	0.223606798	0.0794	0.0904	0.011
0.055	0.234520788	0.0731	0.087	0.0139
0.06	0.244948974	0.0683	0.0833	0.015
0.065	0.254950976	0.0638	0.0822	0.0185
0.07	0.264575131	0.0648	0.0823	0.0175
0.08	0.282842712	0.065	0.0824	0.0174
0.09	0.3	0.0734	0.088	0.0147
0.1	0.316227766	0.0943	0.0962	0.0019

Table A-5 Tabulated values for Figure 3-9, for $\sigma = 1$.

K	Correlation Length (Lc)	Average of MaxHeight - MinHeight	Average Max Height	Average Min Height
9E-06	0.003	0.7945	0.8971	0.1026
0.00009	0.009486833	0.7874	0.8951	0.1077
0.0002	0.014142136	0.7978	0.8993	0.1015
0.0005	0.02236068	0.8092	0.8955	0.0862
0.0009	0.03	0.8113	0.9069	0.0957
0.002	0.04472136	0.8451	0.9228	0.0777
0.004	0.063245553	0.9236	0.9592	0.0356
0.005	0.070710678	0.9519	0.9725	0.0206
0.006	0.077459667	1.0148	0.9983	-0.0165
0.007	0.083666003	1.076	1.0443	-0.0318
0.008	0.089442719	1.247	1.1203	-0.1268
0.009	0.09486833	1.339	1.1829	-0.1561
0.01	0.1	1.6989	1.3441	-0.3548
0.011	0.104880885	3.8016	2.4037	-1.398
0.0109	0.104403065	5.1379	3.0653	-2.0727
0.0108	0.103923048	12.5386	6.7615	-5.7771
0.0107	0.103440804	11.9072	6.4548	-5.4524
0.0106	0.102956301	4.9737	2.9715	-2.0021

0.0105	0.102469508	4.1742	2.6086	-1.5656
0.0104	0.10198039	3.7501	2.3666	-1.3835
0.0103	0.101488916	3.5228	2.2594	-1.2634
0.0102	0.100995049	3.6411	2.3284	-1.3128
0.0101	0.100498756	3.9469	2.4895	-1.4574
0.012	0.109544512	4.3469	2.6755	-1.6715
0.0125	0.111803399	21.2149	11.2139	-10.0011
0.013	0.114017543	3.3546	2.1601	-1.1944
0.014	0.118321596	2.1926	1.5663	-0.6263
0.015	0.122474487	2.1777	1.5998	-0.5779
0.016	0.126491106	2.8715	1.9161	-0.9554
0.0165	0.128452326	3.7401	2.3772	-1.3629
0.017	0.130384048	10.6772	5.8262	-4.851
0.0175	0.132287566	6.5919	3.8015	-2.7904
0.018	0.134164079	4.17	2.5928	-1.5772
0.019	0.137840488	3.3374	2.1771	-1.1603
0.02	0.141421356	3.8133	2.4052	-1.4082
0.02	0.141421356	3.9685	2.4932	-1.4753
0.021	0.144913767	5.7671	3.3777	-2.3894
0.022	0.14832397	16.1323	8.5556	-7.5766
0.023	0.151657509	16.2085	8.5959	-7.6125
0.025	0.158113883	3.5853	2.3013	-1.284
0.03	0.173205081	2.379	1.689	-0.6901
0.031	0.176068169	3.098	2.053	-1.045
0.032	0.178885438	6.8715	3.9293	-2.9423
0.033	0.181659021	8.5196	4.7666	-3.753
0.035	0.187082869	2.0987	1.5356	-0.5631
0.04	0.2	1.1565	1.0676	-0.0889
0.045	0.212132034	0.9146	0.9626	0.048
0.05	0.223606798	0.7758	0.8911	0.1154
0.055	0.234520788	0.7067	0.8463	0.1396
0.06	0.244948974	0.6737	0.833	0.1593
0.065	0.254950976	0.6821	0.8407	0.1587
0.07	0.264575131	0.6562	0.8328	0.1767
0.08	0.282842712	0.6495	0.8276	0.178
0.09	0.3	0.7134	0.8511	0.1377
0.1	0.316227766	0.9339	0.9684	0.0345

Table A-6 Tabulated values for Figure 3-9, for $\sigma = 10$.

K	Correlation Length (Lc)	Average of MaxHeight - MinHeight	Average Max Height	Average Min Height
9E-06	0.003	7.863	8.8737	1.0107
0.00009	0.009486833	7.8605	8.8929	1.0324
0.0002	0.014142136	7.8674	8.9352	1.0679
0.0005	0.02236068	8.1682	9.1279	0.9597
0.0009	0.03	8.1452	8.97	0.8249
0.002	0.04472136	8.4403	9.2927	0.8524
0.004	0.063245553	9.3133	9.6849	0.3716
0.005	0.070710678	9.9227	10.0421	0.1194
0.006	0.077459667	10.2573	10.0671	-0.1902
0.007	0.083666003	11.0634	10.532	-0.5314
0.008	0.089442719	12.0824	10.9512	-1.1313
0.009	0.09486833	13.8713	11.8628	-2.0085
0.01	0.1	16.9249	13.5273	-3.3976
0.0103	0.101488916	18.5449	14.1459	-4.399
0.0105	0.102469508	21.6883	15.8128	-5.8754
0.0108	0.103923048	28.0983	19.0308	-9.0675
0.0107	0.103440804	36.3407	23.208	-13.1327
0.0106	0.102956301	51.2961	30.8195	-20.4766
0.0105	0.102469508	112.1559	61.1672	-50.9886
0.0104	0.10198039	143.8502	76.7682	-67.082
0.0103	0.101488916	55.6029	32.8467	-22.7562
0.0102	0.100995049	42.7646	26.3779	-16.3866
0.0101	0.100498756	38.786	24.4184	-14.3676
0.01	0.1	34.9947	22.6218	-12.3729
0.0099	0.099498744	36.1465	23.2394	-12.9071
0.0098	0.098994949	36.7511	23.1981	-13.553
0.012	0.109544512	39.9519	25.1334	-14.8185
0.0125	0.111803399	200.4067	104.1484	-96.2582
0.013	0.114017543	32.7589	21.4909	-11.268
0.014	0.118321596	22.1127	16.1552	-5.9575
0.015	0.122474487	22.2937	16.3358	-5.9579
0.016	0.126491106	28.9857	19.5522	-9.4335
0.0165	0.128452326	37.6601	23.9301	-13.73
0.017	0.130384048	100.6133	40.029	-29.7443
0.0175	0.132287566	69.7733	55.6712	-44.9421
0.018	0.134164079	37.9306	24.0425	-13.8881
0.019	0.137840488	34.3306	22.152	-12.1786

0.02	0.141421356	38.8522	24.5725	-14.2798
0.02	0.141421356	37.6924	23.802	-13.8904
0.021	0.144913767	58.6656	34.3628	-24.3027
0.022	0.14832397	163.0471	86.6138	-76.4333
0.023	0.151657509	149.1133	79.5668	-69.5465
0.024	0.154919334	57.1228	33.5523	-23.5705
0.025	0.158113883	37.0915	23.5207	-13.5708
0.026	0.161245155	28.3169	19.1118	-9.2051
0.027	0.164316767	23.5769	16.7134	-6.8635
0.028	0.167332005	22.7127	16.4147	-6.298
0.029	0.170293864	22.3424	16.2375	-6.1049
0.03	0.173205081	24.3445	17.1685	-7.1759
0.031	0.176068169	31.1469	20.6396	-10.5073
0.032	0.178885438	63.3121	36.7059	-26.6062
0.033	0.181659021	80.155	44.6519	-35.5032
0.034	0.184390889	32.0178	20.9029	-11.1149
0.035	0.187082869	21.6747	15.903	-5.7717
0.036	0.18973666	16.6876	13.4166	-3.2711
0.037	0.192353841	14.9139	12.4912	-2.4227
0.038	0.194935887	12.9226	11.4355	-1.4871
0.039	0.197484177	11.7637	10.8201	-0.9436
0.04	0.2	10.9276	10.4876	-0.4401
0.041	0.202484567	10.6733	10.3334	-0.3399
0.042	0.204939015	10.1238	10.0249	-0.0989
0.043	0.207364414	9.4159	9.6982	0.2823
0.044	0.20976177	9.1996	9.5835	0.384
0.045	0.212132034	8.841	9.4813	0.6404
0.046	0.214476106	8.7201	9.338	0.6179
0.047	0.216794834	8.2628	9.1388	0.876
0.048	0.219089023	8.2185	9.1356	0.9171
0.049	0.221359436	7.9955	9.0131	1.0176
0.05	0.223606798	7.6603	8.8873	1.2269
0.051	0.225831796	7.3502	8.704	1.3538
0.052	0.228035085	7.4133	8.6837	1.2704
0.053	0.230217289	7.3334	8.6518	1.3184
0.054	0.232379001	7.2634	8.7511	1.4877
0.055	0.234520788	7.1802	8.579	1.3989
0.056	0.236643191	7.0995	8.6146	1.5151
0.057	0.238746728	6.9947	8.5139	1.5191
0.058	0.240831892	7.118	8.5739	1.4558
0.059	0.242899156	6.9045	8.4238	1.5193

0.06	0.244948974	6.8603	8.4264	1.566
0.061	0.246981781	6.6548	8.3588	1.704
0.062	0.248997992	6.8671	8.3371	1.4701
0.063	0.250998008	6.5439	8.2079	1.6641
0.064	0.252982213	6.5368	8.2643	1.7274
0.065	0.254950976	6.5737	8.3091	1.7354
0.066	0.256904652	6.7238	8.3821	1.6583
0.067	0.258843582	6.5854	8.3251	1.7396
0.068	0.260768096	6.7429	8.3352	1.5924
0.069	0.262678511	6.5287	8.2544	1.7257
0.07	0.264575131	6.432	8.2496	1.8176
0.071	0.266458252	6.5808	8.3178	1.737
0.072	0.268328157	6.5472	8.3169	1.7697
0.073	0.270185122	6.6914	8.2987	1.6074
0.074	0.27202941	6.7343	8.3701	1.6358
0.075	0.273861279	6.5917	8.3449	1.7532
0.076	0.275680975	6.4307	8.2488	1.8181
0.077	0.277488739	6.5685	8.2761	1.7076
0.078	0.279284801	6.4252	8.2157	1.7905
0.079	0.281069386	6.5277	8.2746	1.7469
0.08	0.282842712	6.7427	8.3038	1.5611
0.081	0.284604989	6.6652	8.3177	1.6525
0.082	0.286356421	6.8388	8.412	1.5733
0.083	0.288097206	6.6354	8.3189	1.6835
0.084	0.289827535	6.5966	8.2596	1.6631
0.085	0.291547595	6.8942	8.4077	1.5136
0.086	0.293257566	6.7967	8.369	1.5724
0.087	0.294957624	7.2236	8.6461	1.4225
0.088	0.296647939	7.3429	8.6658	1.3229
0.089	0.298328678	7.1863	8.6396	1.4533
0.09	0.3	7.0977	8.526	1.4283
0.091	0.301662063	7.5118	8.7718	1.26
0.092	0.303315018	7.8078	8.9367	1.1289
0.093	0.304959014	7.9649	8.9363	0.9715
0.094	0.306594194	7.8578	8.992	1.1342
0.095	0.3082207	7.6808	8.7318	1.0511
0.096	0.309838668	8.5355	9.1999	0.6644
0.097	0.31144823	8.4724	9.2718	0.7993
0.098	0.313049517	8.5245	9.2345	0.7101
0.099	0.314642654	8.7434	9.4405	0.6971
0.1	0.316227766	8.9381	9.4923	0.5541

Tables A-7, A-8, A-9, A-10, A-11 and A-12 are tables representing the data taken for Figure 3-10. The procedures used to record these data points are the same as the ones listed above.

Table A-7 Tabulated values for Figure 3-10, for $\sigma = 0.1$.

K	Correlation Length (Lc)	Average of MaxHeight – MinHeight	Average Max Height	Average Min Height
0.1	0.316227766	0.0923	0.0963	0.0041
0.2	0.447213595	0.0324	0.0665	0.0341
0.3	0.547722558	0.022	0.0612	0.0392
0.5	0.707106781	0.0143	0.0572	0.0429
0.6	0.774596669	0.0122	0.0562	0.044
0.8	0.894427191	0.0097	0.0547	0.045
1	1	0.0076	0.0534	0.0458
1.5	1.224744871	0.005	0.0526	0.0476
2	1.414213562	0.0039	0.0518	0.0479
3	1.732050808	0.0024	0.0511	0.0487
5	2.236067977	0.0014	0.0509	0.0495
8	2.828427125	0.00095612	0.0506	0.0496
10	3.16227766	0.00071859	0.0503	0.0496
12	3.464101615	0.00058342	0.0505	0.05
15	3.872983346	0.0004757	0.0497	0.0492

Table A-8 Tabulated values for Figure 3-10, for $\sigma = 1$.

K	Correlation Length (Lc)	Average of MaxHeight – MinHeight	Average Max Height	Average Min Height
0.1	0.316227766	0.9019	0.9498	0.0479
0.2	0.447213595	0.3181	0.6586	0.3404
0.3	0.547722558	0.2157	0.6103	0.3946
0.5	0.707106781	0.1443	0.5741	0.4298
0.6	0.774596669	0.1238	0.566	0.4421
0.8	0.894427191	0.1011	0.5498	0.4488
1	1	0.077	0.5385	0.4615
1.5	1.224744871	0.0508	0.5246	0.4738
2	1.414213562	0.0373	0.5218	0.4845
3	1.732050808	0.024	0.5103	0.4863
5	2.236067977	0.0147	0.508	0.4932
8	2.828427125	0.009	0.5043	0.4953
10	3.16227766	0.0074	0.5061	0.4987
12	3.464101615	0.006	0.5028	0.4967
15	3.872983346	0.0048	0.5068	0.502

Table A-9 Tabulated values for Figure 3-10, for $\sigma = 3$.

K	Correlation Length (Lc)	Average of MaxHeight – MinHeight	Average Max Height	Average Min Height
0.1	0.316227766	2.738	2.8452	0.1072
0.2	0.447213595	0.9651	1.9826	1.0176
0.3	0.547722558	0.653	1.831	1.178
0.5	0.707106781	0.4355	1.7309	1.2954
0.6	0.774596669	0.3665	1.6924	1.3259
0.8	0.894427191	0.2962	1.6449	1.3487
1	1	0.2339	1.6161	1.3822
1.5	1.224744871	0.1514	1.5689	1.4175
2	1.414213562	0.1154	1.5506	1.4352
3	1.732050808	0.0744	1.5247	1.4504
5	2.236067977	0.0426	1.514	1.4714
8	2.828427125	0.0272	1.5392	1.512
10	3.16227766	0.0212	1.5205	1.4993
12	3.464101615	0.0185	1.5098	1.4913
15	3.872983346	0.0145	1.5071	1.4926

Table A-10 Tabulated values for Figure 3-10, for $\sigma = 5$.

K	Correlation Length (Lc)	Average of MaxHeight – MinHeight	Average Max Height	Average Min Height
0.1	0.316227766	4.8448	4.8872	0.0424
0.2	0.447213595	1.6313	3.3334	1.7021
0.3	0.547722558	1.0505	3.0181	1.9676
0.5	0.707106781	0.7144	2.88	2.1657
0.6	0.774596669	0.6325	2.8167	2.1841
0.8	0.894427191	0.4536	2.7462	2.2926
1	1	0.3979	2.6978	2.2999
1.5	1.224744871	0.2492	2.6024	2.3533
2	1.414213562	0.1894	2.612	2.4226
3	1.732050808	0.1225	2.5383	2.4158
5	2.236067977	0.0747	2.5239	2.4493
8	2.828427125	0.0461	2.5184	2.4722
10	3.16227766	0.0369	2.5144	2.4776
12	3.464101615	0.0308	2.4995	2.4687
15	3.872983346	0.0239	2.4914	2.4675

Table A-11 Tabulated values for Figure 3-10, for $\sigma = 8$.

K	Correlation Length (Lc)	Average of MaxHeight – MinHeight	Average Max Height	Average Min Height
0.1	0.316227766	7.6795	7.8283	0.1488
0.2	0.447213595	2.6107	5.3268	2.7161
0.3	0.547722558	1.7228	4.8632	4.5975
0.5	0.707106781	1.2171	3.1404	3.3803
0.6	0.774596669	0.9938	4.5553	3.5615
0.8	0.894427191	0.7464	4.3819	3.6355
1	1	0.6303	4.3407	3.7104
1.5	1.224744871	0.419	4.2059	3.7868
2	1.414213562	0.2958	4.1468	3.8511
3	1.732050808	0.1954	4.0975	3.9021
5	2.236067977	0.1126	4.1143	4.0017
8	2.828427125	0.0709	4.0082	3.9374
10	3.16227766	0.056	4.0424	3.9864
12	3.464101615	0.0479	4.0258	3.9779
15	3.872983346	0.0368	3.9922	3.9555

Table A-12 Tabulated values for Figure 3-10, for $\sigma = 10$.

K	Correlation Length (Lc)	Average of MaxHeight – MinHeight	Average Max Height	Average Min Height
0.1	0.316227766	9.1453	9.5458	0.4006
0.2	0.447213595	3.3046	6.7149	3.4104
0.3	0.547722558	2.1688	6.0725	3.9037
0.5	0.707106781	1.4496	5.7409	4.2913
0.6	0.774596669	1.2465	5.654	4.4075
0.8	0.894427191	0.9418	5.4999	4.5581
1	1	0.7599	5.3164	4.5565
1.5	1.224744871	0.4955	5.2738	4.7784
2	1.414213562	0.3865	5.1651	4.7786
3	1.732050808	0.243	5.0651	4.8221
5	2.236067977	0.1478	5.0558	4.9079
8	2.828427125	0.0858	5.0702	4.9844
10	3.16227766	0.0743	5.0316	4.9573
12	3.464101615	0.0593	5.0551	4.9957
15	3.872983346	0.0476	5.0255	4.9779

Tables A-13 is a table representing the data taken for Figure 3-12. The procedures used to record these data points are the same as the ones listed above with the exception of the average difference in maximum height and minimum height.

Table A-13 Tabulated values for Figure 3-12.

sigma	Average Max Height	Average Min Height
12	5.9692	5.9691
10	5.0006	5.0005
9	4.5	4.4999
8	3.9822	3.9822
7	3.4978	3.4978
6	2.9891	2.9891
6	2.9901	2.9901
5	2.4984	2.4984
4	2.0076	2.0076
3	1.4959	1.4959
2	0.9936	0.9936
1	0.4967	0.4967
0.09	0.0447	0.0447
0.08	0.0399	0.0399
0.07	0.0351	0.0351
0.06	0.03	0.03
0.05	0.025	0.025
0.04	0.0201	0.0201
0.03	0.0151	0.0151
0.02	0.01	0.01
0.01	0.005	0.005
0.001	5.01E-04	5.01E-04

A.3 MATLAB m-file used to parse the raw data

This appendix shows the MATLAB m-file used to parse the raw data into separate files with each file containing 4,000,000 points. This m-file was obtained from Trey Smith, a graduate student at VTPL.

MATLAB m-file:

```
function parseXYZfile_20080808(directory,nLines,read_fType, write_fType)
% units: x,y (meters), z (m)
% Reads in a directory of xyz files, rewrites data to smaller xyz files

global headerlines
headerlines = 24;

% Get directory, either as a passed parameter or through a GUI
if (nargin<1),
    %directory = 'C:\Documents and Settings\jbferris\Desktop\DATA\Test'; end
```

```

        [file, directory] = uigetfile('*..*', 'Pick any file in the directory',
'Multiselect','on');
end

% If no filetypes were given, use the default values below:
if (nargin<4),
    read_fType = '.xyz';
    write_fType = '.dat';
end

if (directory(length(directory))~='\'), directory(length(directory)+1) = '\';
end

% Open the xyz files in the directory
F = open_files_get_filenames(directory, 1, read_fType);    % returns a
structure of fids and corresponding names of files
num-files = length(F);

% Establish processing parameters here
if (nargin<2),
nLines = 4000000;                % specifies number of points per file
end
%precision = 2;                % number of digits to keep after the decimal
point (in meters)

block = 0;                % track block, determines number of lines to skip
at beginning of file
lastBlock = 0;            % flag, indicates when end of file is reached

for i = 1:num-files;
    editFlag = input(['Parse ', F(i).filename, '? (1 for Yes, 2 for No)
    ']);
    if editFlag==1,
        while ~lastBlock
            [F(i).header,data,lastBlock] =
get_XYZdata(nLines,block*nLines,F(i),read_fType);
            nRows=size(data,1);

            %           uncomment this section if you would like to round xy
            %           coordinates to cm
            %           for k=1:nRows
            %               data(k,1)=round(data(k,1)*100)/100;
            %               data(k,2)=round(data(k,2)*100)/100;
            %           end
            %data = round(data*(10^precision))/(10^precision);    % round
data to desired precision
            new_filename = write_header_new_file(F(i),block+1,write_fType);
% writes header, discards existing file!!!
            write_data(new_filename,data,0,0,'tab');                % appends
data to newly created '.dat' file
            block = block+1;
        end
        editFlag = 0;
    end
end
end

```

```

return

function F = open_files_get_filenames(directory, verb,type)
% S is an array of structures containing only xyz file info
% D is an array of structures of file info from the dir command

F=[]; % initialize F in case there are no xyz files
D = dir(directory); % get directory info
nFiles=0; % track the number of xyz files
for i = 3:length(D), % loop on all possible entries that could be xyz
files (not first two)

    if D(i).isdir == 0, % make sure it is
a file
        [token, fType] = strtok(D(i).name, '.'); % strip extension
from filename
        if strcmp(fType,type), % make sure it is
an xyz file
            nFiles = nFiles+1; % track the number of
xyz files
            F(nFiles).filename = token; % add filename
(without extension) to list
            F(nFiles).directory = directory; % add fid
to list
        end
    end

end % for i = 3:length(D)

if (verb==1), % Display files that were opened if in 'verbose' mode
    disp('xyz files being analyzed...');
    for i=1:length(F), disp([num2str(F(i).directory), ' ', F(i).filename]);
end
    %for i=1:length(F), disp(F(i).filename); end
end

return % open_files_get_filenames

function [header,data,lastBlock] = get_XYZdata(nLines,offset,F,type)
% lastBlock = 1 -- this is the last block that needs to be processed
% lastBlock = 2 -- this block is empty, do not process it
% FORMAT: load_data(filenamepath, headerlines, columns, lines, offset,
delimiter, fixed length)

lastBlock=0;
global headerlines
cols = 3; % 3 columns of XYZ data

[header, data, col] =
load_data(strcat(F.directory,F.filename,type),headerlines,cols,nLines,offset,
'tab','true');

if length(data(:,1))<nLines
    lastBlock=1;

```

```

        nLines = length(data(:,1));
end

if length(data(:,1)) == 0
    lastBlock=2;
    data = [];
end

return

function [filename] = write_header_new_file(F, block,type)

filename = strcat(F.directory, F.filename, '_', num2str(block), type);
fidWrite = fopen(filename, 'wt'); % write file for writing,
discards existing file!!

% headerlines = F.header(1,1:length(F.header)-288);
% fprintf(fidWrite, '%s\n', headerlines); % write each
header line from S.header
% fprintf(fidWrite, '%-9s\t%-9s\t%-9s\n', 'X (m)', 'Y (m)', 'Z(m)');
fclose(fidWrite);

return

function append_data_file(S,Laserfid,startI,endI)
% S is structure with x y z header filename

if(nargin<4), startI=1; endI=length(S.t); end
filename = fopen(Laserfid);
[token, fType] = strtok(filename, '.'); % strip extension from
filename

filepath = [token '.xyz'];
data = [S.x(startI:endI), S.y(startI:endI), S.z(startI:endI)];
write_data(filepath, data, 0, 0, 'tab');

smalldata = [S.x(startI:100:endI), S.y(startI:100:endI), S.z(startI:100:endI)];
filepathsmall = [token '_sm.xyz'];
write_data(filepathsmall, smalldata, 0, 0, 'tab');

return

```

A.4 Procedures to obtained processed raw data

This section of the Appendix A explains how the processed data was collected through Surfer and MATLAB. The following are step by step instructions to obtain the processed data from a free Demo Version Surfer. When Surfer is opened, it automatically creates a new Plot Document. Go to “Grid” on the top toolbar and select “Menu” from the scroll down menu.

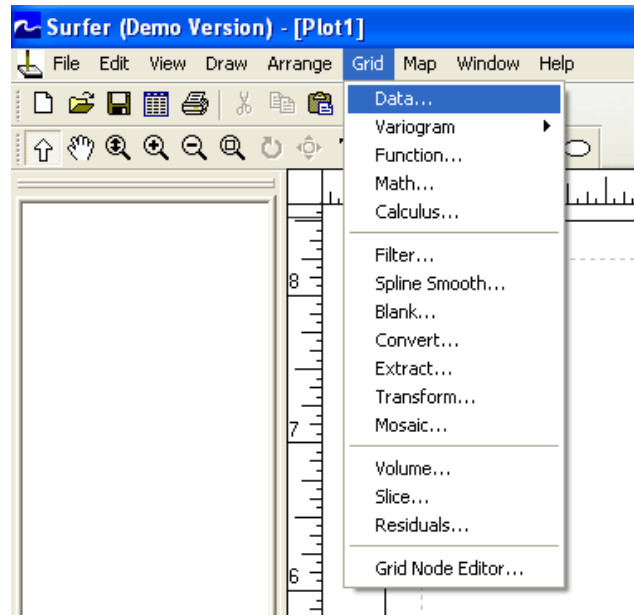


Figure A-1 Print screen of “Grid” on Surfer Toolbar.

Next, a pop up window will appear where you will have to select the file to be read by Surfer. In our case, it will be one of the 9 .dat extension files containing the terrain data that was parsed with the MATLAB m-file. For these procedures, the file containing section 5 was opened. Once the file is selected, another pop up window will appear as shown below. The “Gridding Method” option allows you to choose from several gridding types. For our case, the “Nearest Neighbor” method was chosen to obtain a uniformly spaced grid. The “Output Grid File” is the destination in which the output will be stored. The output will be in a file with a .grd extension, which can only be read with Surfer. The “Grid Line Geometry” displays the current dimensions, spacing, and number of lines of the current file by default. These variables can be changed according to the desire of the user.

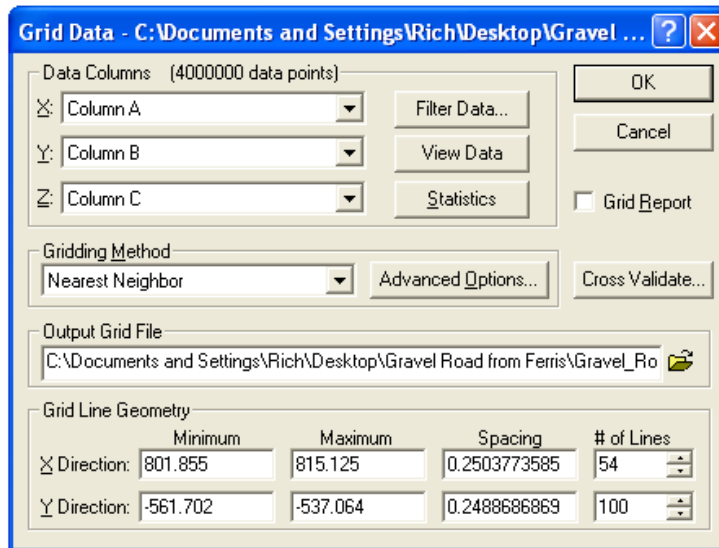


Figure A-2 Print screen of pop-up window in Surfer.

To obtain the 2 meter by 2 meter terrain profile that was used for our analysis (Figure 3-14), the following values were used and entered into their corresponding slots.

Table A-14 X and Y coordinates for processed data.

Direction	Minimum	Maximum
X	808	810
Y	-550	-548

To obtain the different subplots in Figures 3-14a, 3-14b, 3-14c, and 3-14d, the slot containing the “# of lines” will have to be adjusted accordingly. After all of the parameters are entered for the desired surface map, click “OK” and the file will be created. To recreate the subplots shown in Figure 3-14, go to “Map” on the top toolbar and select “Surface” from the scroll down menu, as shown below. Afterwards, a pop up window will appear and select the .grd extension file. This will create the subplots shown in Figure 3-14. With Surfer, there are numerous ways of representing the terrain surface. Described in these procedures are just one way of illustrating it. Surfer is a very powerful visualization tool, and there are many other features that can be used which are not described in these procedures.

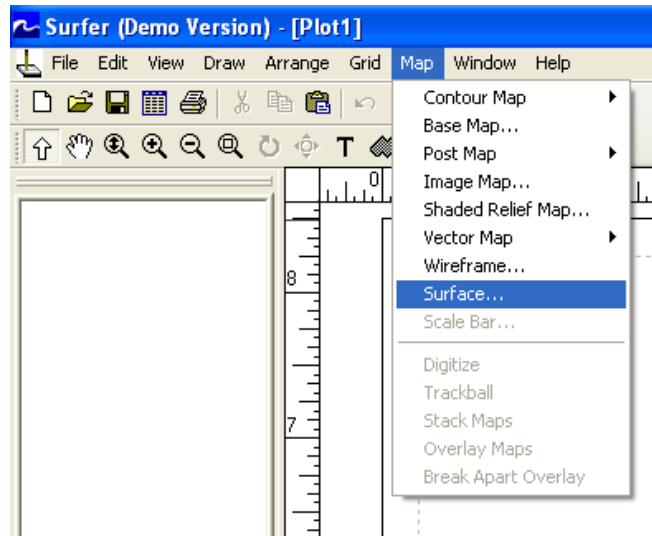


Figure A-3 Illustration of “Map” on Surfer Toolbar.

To recreate the image with MATLAB, the following m-file was created to open the .dat extension file from Surfer and mesh the points into the plot. Unfortunately, the Demo Version of Surfer did not allow the user to create the .dat extension file. I obtained this file through Trey Smith, who had the licensed version. The file that is opened in this m-file is named “Extract_80x80.dat”. This is the surface with 80 points by 80 points.

MATLAB m-file:

```
clear all

fid = fopen('Extract_80x80.dat','rt');
coursel=fscanf(fid,'%e');

%% Number of points on each axis; e.g., 3x3 grid, NoPts = 3
NoPts = 80;

for dim = 1:NoPts*NoPts
    x(dim) = coursel(dim*2+(dim-2));
    y(dim) = coursel(dim*2+(dim-2)+1);
    z(dim) = coursel(dim*2+(dim-2)+2);
end

xmesh = reshape(x,NoPts,NoPts);
ymesh = reshape(y,NoPts,NoPts);
zmesh = reshape(z,NoPts,NoPts);

figure(1)
mesh(xmesh,ymesh,zmesh)
xlabel('x (unit length)')
ylabel('y (unit length)')
zlabel('Height (unit length)')
```

Appendix B

Appendix B shows the procedures and raw data to complete the results shown for the stochastic soil model. Appendix B.1 shows the raw data that was collected from the cone penetrometer in Virginia Tech's terramechanics rig for the lunar soil simulant GRC-1. Appendix B.2 shows detailed procedures for the polynomial chaos approach to specifically create the stochastic soil models incorporated in this thesis. Appendix B.3 shows the MATLAB m-file to create the stochastic soil model.

B.1 Raw data for lunar soil simulant GRC-1

This section of Appendix B shows the raw data obtained from the cone penetrometer CP40 II for the lunar soil simulant GRC-1. For Tables B-1 and B-2, the values in the cells of the table are the pressure values (kPa) at the recorded depth.

Table B-1 Raw data obtained at depths of 5mm to 55mm for GRC-1.

Measurement	Depth (mm)					
	5	15	25	35	45	55
1	65	116	172	225	279	332
2	69	118	173	217	270	320
3	68	115	168	206	250	307
4	54	101	153	203	256	308
5	47	84	119	159	202	249
6	56	94	129	166	214	258
7	55	96	152	204	257	313
8	51	88	129	167	206	245
9	49	94	147	194	237	275
10	68	117	169	209	252	295
11	61	101	151	196	246	284
12	51	91	130	169	213	249
13	62	110	155	226	246	286
14	56	102	138	190	244	300
15	49	87	128	177	220	260

Table B-2 Raw data obtained at depths of 65mm to 115mm for GRC-1.

Measurement	Depth (mm)					
	65	75	85	95	105	115
1	382	423	466	518	587	684
2	362	421	476	539	614	688
3	357	411	465	522	582	674
4	368	437	498	559	618	735
5	284	340	397	467	538	654
6	300	347	401	465	538	654
7	369	420	478	530	581	669
8	288	327	379	445	526	630
9	308	347	425	466	531	622
10	335	376	423	481	548	634
11	326	374	420	474	533	626
12	297	336	388	443	549	605
13	329	366	394	431	476	565
14	352	407	465	519	581	664
15	299	346	395	447	502	569

Table B-3 shows the value of the slope for each of the corresponding measurements. The pressure is the y value while the depth is the x value. The overall average value of the slope for all 15 measurements is equal to 4.813 kPa/mm.

Table B-3 Slope of pressure and depth for each measurement.

Measurement	Slope (kPa/mm)
1	5.29965035
2	5.463286713
3	5.305944056
4	5.966433566
5	5.188111888
6	5.084615385
7	5.482517483
8	4.891258741
9	4.890559441
10	4.815034965
11	4.863636364
12	4.866783217
13	4.196503497
14	5.448251748
15	4.613636364

Table B-4 shows the calculated values of the mean and standard deviation for each depth.

Table B-4 Calculated mean and standard deviation for every depth interval.

Depth (mm)	Mean (mm)	Standard Deviation (mm)
5	57.4	7.57627877
15	100.9333333	11.72583635
25	147.5333333	17.97961809
35	193.8666667	21.93453463
45	239.4666667	23.46385265
55	285.4	28.28629148
65	330.4	33.01471533
75	378.5333333	37.76216297
85	431.3333333	39.41839068
95	487.0666667	40.45538401
105	553.6	39.76682034
115	644.8666667	45.05689525

B.2 Detailed procedures for the polynomial chaos approach

This section shows the detailed procedures in using the collocation approach to apply the polynomial chaos method to create stochastic soil models. The procedures listed are specified for the case study used in this thesis. Bekker's equation is used and the random parameter is k_ϕ . Using the Karhunen-Loeve expansion, the uncertain parameter can be displayed as

$$k = \sum_{j=1}^{\infty} k_{\phi}^j \psi^j(\xi(\theta)) \quad (B.1)$$

where $\psi^j(\xi_{i1} \dots \xi_{in})$ are the generalized Askey-Wiener polynomial chaoses and $\xi = (\xi_{i1} \dots \xi_{in})$ are the multi-dimensional random variables (Sandu, Sandu, and Ahmadian, 2006a). Plugging this expansion back into Bekker's equation will give

$$p = \left(\frac{k_c}{b} + \sum_{j=1}^{\infty} k_{\phi}^j \psi^j(\xi(\theta)) \right) z^n \quad (B.2)$$

The assumption was made that the random variables are uniformly distributed. Therefore, the Legendre polynomials were used for the basis function in the polynomials chaos method. Equation B.3 calculates the number of terms, S , used for the Legendre polynomials.

$$S = \frac{(n + q)!}{n! q!} \quad (B.3)$$

For our case study, the number of uncertainties in this system, q , is equal to 1 and the order of the polynomials, n , is equal to 3. Therefore, the number of terms used for the Legendre polynomials is equal to 4. Table B-5 shows the Legendre polynomials and the corresponding degree of the function.

Table B-5 Legendre polynomials to the 4th order.

Degree	Legendre polynomial
0	1
1	x
2	$\frac{1}{2}(3x^2 - 1)$
3	$\frac{1}{2}(5x^3 - 3x)$
4	$\frac{1}{8}(35x^4 - 30x^2 + 3)$

For this particular case study, the four collocation roots were chosen to be ± 0.8611 and ± 0.34 . Therefore, Equation B-1 can be expanded to the following.

$$k(\xi) = k_1\psi_0(\xi) + k_2\psi_1(\xi) + k_3\psi_2(\xi) + k_4\psi_3(\xi) \quad (B.4)$$

The value of ξ is equal to one of the four collocation roots while ψ_0 , ψ_1 , ψ_2 , and ψ_3 corresponds to the Legendre polynomial with the corresponding degree in the subscript, respectively. Equation B.4 can be expanded into four equations, each with a value of the collocation point to create the collocation matrix. Since there are four unknown values in Equation B.4, four equations are created to implicitly solve for the unknown values. Equation B.5 displays the four unknown equations in matrix form while Figure B-1 shows the collocation matrix. The first column of the collocation matrix describes the mean of k_ϕ while the second column to last columns of the collocation matrix describes the standard deviation of k_ϕ . For the particular case study, columns 3 and 4 contained a value that was far less than the value contained in the second column. Therefore, they were multiplied and assumed to be a value of 0. For this particular case

study, the value of k_1 is equal to the value of k_ϕ and the value of k_2 is equal to the value of k_ϕ divided by the uncertainty amplitude. The values for k_3 and k_4 are both equal to 0.

$$\begin{bmatrix} k(\xi_1) \\ k(\xi_2) \\ k(\xi_3) \\ k(\xi_4) \end{bmatrix} = \begin{bmatrix} \psi_0(\xi_1) & \psi_1(\xi_2) & \psi_2(\xi_3) & \psi_3(\xi_4) \\ \psi_0(\xi_1) & \psi_1(\xi_2) & \psi_2(\xi_3) & \psi_3(\xi_4) \\ \psi_0(\xi_1) & \psi_1(\xi_2) & \psi_2(\xi_3) & \psi_3(\xi_4) \\ \psi_0(\xi_1) & \psi_1(\xi_2) & \psi_2(\xi_3) & \psi_3(\xi_4) \end{bmatrix} \begin{bmatrix} k_1 \\ k_2 \\ k_3 \\ k_4 \end{bmatrix} \quad (B.5)$$

$$\begin{bmatrix} \psi_0(\xi_1) & \psi_1(\xi_2) & \psi_2(\xi_3) & \psi_3(\xi_4) \\ \psi_0(\xi_1) & \psi_1(\xi_2) & \psi_2(\xi_3) & \psi_3(\xi_4) \\ \psi_0(\xi_1) & \psi_1(\xi_2) & \psi_2(\xi_3) & \psi_3(\xi_4) \\ \psi_0(\xi_1) & \psi_1(\xi_2) & \psi_2(\xi_3) & \psi_3(\xi_4) \end{bmatrix} = \begin{bmatrix} 1 & -0.8611 & 0.6122 & -0.3046 \\ 1 & 0.8611 & 0.6122 & 0.3046 \\ 1 & -0.34 & -0.3266 & 0.4117 \\ 1 & -0.34 & -0.3266 & -0.4117 \end{bmatrix}$$

Figure B-1 Collocation matrix for stochastic soil model case study.

Once the values for $k(\xi_1)$ to $k(\xi_4)$ are calculated, Equation B.4 can be solved, which can allow Equation B.2 to be solved. The mean value and the standard deviation calculated from the polynomial chaos described are plotted. The PDF is also shown to validate the stochastic soil model. The MATLAB m-file is shown in the next section.

B.3 MATLAB m-file for creating stochastic soil models

This section shows the MATLAB m-file used to create the stochastic soil models. This MATLAB code was modified and updated from a previous code received from Dr. Lin Li.

MATLAB m-file:

```
clear all

syms x

%chaos dimension
polynomial_dimension=1;
polynomial_order=3;
chaos=factorial(polynomial_dimension+polynomial_order)/factorial(polynomial_d
imension)/factorial(polynomial_order);

%define parameters;
b=0.1; %unit [m], the smaller size of contact patch

%define pressure sinkage parameters
n=1.1;
Kc=0.99; %unit [kN/m^(n+1)]
Kphi=1528.43; %unit [kN/m^(n+2)]
```

```

%uncertainty amplitude
r=1;

npoint=200;
%initiate the sinkage
z=linspace(0,50,npoint); %unit [cm]

%errorbar interval
bars=1:20:npoint;

%%%%%%%%%%%%%%
%Deterministic%
%%%%%%%%%%%%%%

%calculate the pressure
Pdet=(Kc/b+Kphi)*(z/1000).^n;

%plot the figure of pressure versus sinkage
figure(1)
subplot(221)
plot(z,Pdet)
xlabel('Sinkage [mm]')
ylabel('Pressure [KPa]')
legend('Deterministic','location','SE');
tit=['Pressure at random Kphi value'];
title(tit)

save Result_Deterministic z Pdet

%%%%%%%%%%%%%%
%Monte Carlo%
%%%%%%%%%%%%%%

%Monte Carlo runs
NMC=1000;
xi_1=2*(rand(1,NMC)-0.5);
%calculate the results
disp('Start MonteCarlo Simulation')
timc=cputime;
for imc=1:NMC
    if (mod(imc,100)==0), fprintf('\nMC run no %d of %d',imc,NMC); end
%random coefficient

%uncertain Kphi
KphiMC=Kphi+Kphi*xi_1(imc)/r;

%calculate the pressure
Pmc1=(Kc/b+KphiMC)*(z/1000).^n;
Pmc_final1(imc,1:npoint)=Pmc1;
end

disp(['CPU MonteCarlo Seconds=',num2str((cputime-timc)/2)]);

```



```

%rearrange the data
Pmc_mean1=mean(Pmc_final1);
Pmc_std1=std(Pmc_final1);

save Result_Montecarlo z Pmc_final1 Pmc_mean1 Pmc_std1 NMC bars

%%plot the figure of pressure versus sinkage
subplot(222)
errorbar(z(bars),Pmc_mean1(bars),Pmc_std1(bars));
xlabel('Sinkage [mm]')
ylabel('Pressure [kN/m^2]')
legend('Monte Carlo(z^n)','location','SE');
tit=['Pressure at random Kphi value'];
title(tit)

subplot(223)
plot(z,Pdet,'b-'); hold on;

errorbar(z(bars),Pmc_mean1(bars),Pmc_std1(bars),'r-'); hold on
xlabel('Sinkage [mm]')
ylabel('Pressure [kN/m^2]')

legend('Deterministic','Monte Carlo(z^n)','location','SE');
tit=['Pressure at random Kphi value'];
title(tit)

%%%%%%%%%%%%%%
%Stochastic Approach%
%%%%%%%%%%%%%%

%uncertainty amplitude
r=1;
Kphi_pc(1)=Kphi;
Kphi_pc(2)=Kphi_pc(1)/r;
Kphi_pc(3:chaos)=0;

%calculate the orthogonality
%collocation roots
colroots=[-0.8611 0.8611 -0.34 0.34];
%calculate the collocation matrix
for k=1:chaos
    for l=1:chaos
        Acol(k,l)=subs(Legendre_polynomial(1,x),colroots(k));
        coeff(k,l)=Kphi_pc(l)*Acol(k,l);
    end
    Kphi_col(k)=sum(coeff(k,:));
end

%calculate the results
disp('Start PolyChaos Simulation')
timp=cputime;
%calculate the pressure
for k=1:chaos
    Ppc1(:,k)=(Kc/b+Kphi_col(k))*(z/1000).^n;

```

```

end
for nn=1:npoint
    Ppc1(nn,:)=Acol\Ppc1(nn,:);
end
disp(['CPU PolyChaos Seconds=',num2str(cputime-timp)]);
V2 = [1 0.33333 0.2 0.14286];
for ii=1:npoint
    Ppc_mean1(ii)=Ppc1(ii,1);
    Ppc_std1(ii)=sqrt((Ppc1(ii,2:chaos).^2)*V2(2:chaos)'/V2(1));
end

save Result_Polynomial Ppc1 Ppc_mean1 Ppc_std1 bars z chaos

%plot the figure of pressure versus sinkage
figure(2)
subplot(221)
plot(z(bars)/100,Pdet(bars),'b-'),hold on;
errorbar(z(bars)/100,Ppc_mean1(bars),Ppc_std1(bars),'r-'),hold on;
xlabel('Sinkage [m]')
ylabel('Pressure [KPa]')
legend('Deterministic','PolyChaos')
tit=['Pressure at random Kphi value'];
title(tit)

%%%%%
%PDF%
%%%%%
NPC = 5000;
Nedges = 200;
pressure_edges = linspace(0,1000,Nedges);
Map1 = [1;2;3;4];

xi=2*(rand(NPC,1)-0.5);

for i=1:npoint
    YPC=zeros(NPC,1);
    for ic = 1:chaos
        N = Map1(ic,:);
        aa = Legendre_polynomial(N(1),xi);
        YPC = YPC + Ppc1(i,ic).*aa;
    end
    PDF(1:Nedges,i)=histc(YPC,pressure_edges)/NPC/(pressure_edges(2)-
pressure_edges(1));
end

%%%%%%%%%%%%%%%%%%%%%%%%%%%%%%%%%%%%%%%%%%%%%%%%%%%%%%%%%%%%%%%%%%%%%%%%%%%%%%
% final ensemble from Monte Carlo simulation
%%%%%%%%%%%%%%%%%%%%%%%%%%%%%%%%%%%%%%%%%%%%%%%%%%%%%%%%%%%%%%%%%%%%%%%%%%%%%%
figure(3)
fz=12;

PDF(find(PDF<1.0e-4))=NaN;
cs = contourf(z/100,pressure_edges,log10(PDF),linspace(-3.5,-1.5,16));
colorbar('vert');
text(0.025,875,'Probability density','FontSize',fz);

```

```

text(0.025,775,'    (log scale)','FontSize',fz);
xlabel('Sinkage [m]','FontSize',fz,'FontWeight','bold');
ylabel('Pressure [kPa]','FontSize',fz,'FontWeight','bold');
zlabel(['Probability density'],'FontSize',fz,'FontWeight','bold');

figure(4)
errorbar(z(bars),Pmc_mean1(bars)+50,Pmc_std1(bars),'r--');hold on

errorbar(z(bars),Ppc_mean1(bars)+50,Ppc_std1(bars),'b:'),hold on;

%%GOBI's Challenge
gobi = 0.013*z.^2+3.437*z+48.55;
GobiSTD = [7.5763 11.7258 17.9796 21.9345 23.4638];
GobiZ = [5 15 25 35 45];
Gobiplot = 0.013*GobiZ.^2+3.437*GobiZ+48.55;
plot(z,gobi,'k-');
errorbar(GobiZ,Gobiplot,GobiSTD,'k-');

legend('Monte Carlo','PolyChaos','Experimental test')
xlabel('Sinkage [mm]')
ylabel('Pressure [kPa]')

```

Subroutine for “Legendre_polynomial.m”:

```

function f = Legendre_polynomial( n, x )
% x in [-1,1]. Not normalized.
% n = order + 1
switch n
    case 1, f = 1 ;
    case 2, f = x ;
    case 3, f = (-1 + 3*x.^2.)/2 ;
    case 4, f = (x.*(-3 + 5.*x.^2))./2 ;
    case 5, f = (3 - 30*x^2 + 35*x^4)/8 ;
end
% switch n

```

Appendix C

Appendix C shows all of the MATLAB m-files used to create the simulation frameworks shown in Chapter 5. Appendix C.1 shows the m-file for the rigid plate “stepping” on the deterministic surface. Appendix C.2 shows the m-file for the rigid wheel “stepping” on the deterministic surface. Appendix C.3 shows the m-file for the flexible wheel “stepping” on the deterministic surface. Appendix C.4 shows the m-file for the rigid wheel rolling on the deterministic (both the flat and semi-oval bump) surface. Appendix C.5 shows the m-file for the flexible wheel rolling on the deterministic (both the flat and semi-oval bump) surface. Appendices C.6 and C.7 shows the m-files for the rigid wheel and the flexible wheel rolling on a deterministic surface with stochastic soil, respectively. Appendices C.8 and C.9 gives descriptions on how to create the case studies for rolling on a stochastic surface and deterministic soil, and stochastic surface and stochastic soil, respectively.

C.1 MATLAB m-file for rigid plate “stepping” on deterministic surface

```
clear all

X=2; %distance of x-axis
Y=2; %distance of y-axis
imax=41;
jmax=41;
imin=1;
jmin=1;
dx=X/(imax-1);
dy=Y/(jmax-1);

%%Create surface
for i = imin:imax-1;
    for j = jmin:jmax-1;
        Z(i,j)=1; %%[m]
    end
end

xgrid=dx:dx:X;
ygrid=dy:dy:Y;

figure(1)
mesh(xgrid,ygrid,Z)
zlim([0.95 1.05])
xlabel('x, (m)')
ylabel('y, (m)')
zlabel('Height, (m)')

%%Assume Sandy Loam ***INPUT
```

```

kc = 5.27;    %% [kN/m^n+1]
kphi = 1515.04;    %% [kN/m^n+2]
n = 0.7;

%%INPUT number of cells for length of contact patch (odd number)
numblength = 13;
%%INPUT number of cells for width of contact patch (odd number)
numbwidth = 13;

%%width of contact patch
b = (numbwidth-1)*dx; %% [m]
%%length of contact patch
l = (numblength-1)*dy %% [m]

%%Input Force
F = 18.67; %% [kN]
A = b*l;
p = F/A;

sinkage = (p/((kc/b) + kphi))^(1/n);

Zold = Z;
for i = imin:numblength;
    for j = ((jmax-1)/2)-5:((jmax-1)/2)-6+numbwidth-1;
        Zold(i,j)=Z(i,j)-sinkage; %%[m]
    end
end

figure(2)
mesh(xgrid,ygrid,Zold)
zlim([0.95 1.05])
xlabel('x, (m)')
ylabel('y, (m)')
zlabel('Height, (m)')

Zold1 = Zold;
for i = numblength+1:numblength*2;
    for j = ((jmax-1)/2)-5:((jmax-1)/2)-6+numbwidth-1;
        Zold1(i,j)=Zold(i,j)-sinkage; %%[m]
    end
end

figure(3)
mesh(xgrid,ygrid,Zold1)
zlim([0.95 1.05])
xlabel('x, (m)')
ylabel('y, (m)')
zlabel('Height, (m)')

Zold2 = Zold1;
for i = (numblength*2)+1:numblength*3;
    for j = ((jmax-1)/2)-5:((jmax-1)/2)-6+numbwidth-1;
        Zold2(i,j)=Zold1(i,j)-sinkage; %%[m]
    end
end

```

```

figure(4)
mesh(xgrid,ygrid,Zold2)
zlim([0.95 1.05])
xlabel('x, (m)')
ylabel('y, (m)')
zlabel('Height, (m)')

```

```

figure(5)
plot(ygrid,Zold2)
ylim([0.985 1.002])
xlabel('y, (m)')
ylabel('Height, (m)')

```

C.2 MATLAB m-file for rigid wheel “stepping” on deterministic surface

```

clear all

X=2; %distance of x-axis
Y=2; %distance of y-axis
imax=41;
jmax=41;
imin=1;
jmin=1;
dx=X/(imax-1);
dy=Y/(jmax-1);

NoPts = imax-1;

%%Creating deterministic flat surface of 1m height
for i = imin:imax-1;
    for j = jmin:jmax-1;
        Z(i,j)=1; %%[m]
        P(i,j)=0;
    end
end

xgrid=dx:dx:X;
ygrid=dy:dy:Y;

figure(1)
mesh(xgrid,ygrid,Z)
zlim([0.95 1.05])
xlabel('x, (m)')
ylabel('y, (m)')
zlabel('Height, (m)')

%%INPUT number of cells for length of contact patch (odd number)
numlength = 13;
%%INPUT number of cells for width of contact patch (odd number)
numbwidth = 13;

%%Assume Sandy Loam ***INPUT
kc = 5.27; %% [kN/m^n+1]
kphi = 1515.04; %% [kN/m^n+2]

```

```

n = 0.7;

%%width of contact patch
bp = (numbwidth-1)*dx; %% [m]
%%length of contact patch
lp = (numblength-1)*dy %% [m]
%%longitudinal slip ratio
s = 0;
%%shape change factor
A1 = 1;

Fz = 18.67*1000; %% [kN]

zeta = 0:dy:lp;
term1 = ((4*Fz)/(pi*bp*lp));
term2 = (1+A1*s*(zeta-(lp/2)));
term3a = (zeta-(lp/2)).^2;
term3b = (lp/2)^2;
term3c = term3a/term3b;
term3 = sqrt(1-term3c);
p = ((term1.*term2.*term3)/1000)';

vectorzero(NoPts,1)=0;
Vold = vectorzero;
[M,N] = size(p);
Vold(1:M,1)=p(1:M);
Vold1 = Vold;
Vold1(M+1:(M*2),1)=p(1:M);
Vold2=Vold1;
Vold2((M*2)+1:(M*3),1)=p(1:M);

pvector = Vold2;
onevector = ones(1,NoPts);
pressure = pvector*onevector;

sinkage = (pressure./((kc/bp) + kphi)).^(1/n);

Zold = Z;
for i = imin:numblength;
    for j = ((jmax-1)/2)-5:((jmax-1)/2)-6+numbwidth-1;
        Zold(i,j)=Z(i,j)-sinkage(i,j); %%[m]
    end
end

figure(2)
%plot(xgrid,Zold)
mesh(xgrid,ygrid,Zold)
zlim([0.95 1.05])
xlabel('x, (m)')
ylabel('y, (m)')
zlabel('Height, (m)')

Zold1 = Zold;
for i = numblength+1:numblength*2;
    for j = ((jmax-1)/2)-5:((jmax-1)/2)-6+numbwidth-1;
        Zold1(i,j)=Zold(i,j)-sinkage(i,j); %%[m]
    end
end

```

```

        end
    end

    figure(3)
    mesh(xgrid,ygrid,Zold1)
    zlim([0.95 1.05])
    xlabel('x, (m)')
    ylabel('y, (m)')
    zlabel('Height, (m)')

    Zold2 = Zold1;
    for i = (numblength*2)+1:numblength*3;
        for j = ((jmax-1)/2)-5:((jmax-1)/2)-6+numbwidth-1;
            Zold2(i,j)=Zold1(i,j)-sinkage(i,j); %%[m]
        end
    end

    figure(4)
    mesh(xgrid,ygrid,Zold2)
    zlim([0.95 1.05])
    xlabel('x, (m)')
    ylabel('y, (m)')
    zlabel('Height, (m)')

    figure(5)
    plot(ygrid,Zold2)
    ylim([0.985 1.002])
    xlabel('y, (m)')
    ylabel('Height, (m)')

```

C.3 MATLAB m-file for flexible wheel “stepping” on deterministic surface

```

clear all

X=2; %distance of x-axis
Y=2; %distance of y-axis
imax=41;
jmax=41;
imin=1;
jmin=1;
dx=X/(imax-1);
dy=Y/(jmax-1);

NoPts = imax-1;

%%Creating deterministic flat surface of 1m height
for i = imin:imax-1;
    for j = jmin:jmax-1;
        Z(i,j)=1; %%[m]
        P(i,j)=0;
    end
end

xgrid=dx:dx:X;

```



```

ygrid=dy:dy:Y;

figure(1)
mesh(xgrid,ygrid,Z)
zlim([0.95 1.05])
xlabel('x, (m)')
ylabel('y, (m)')
zlabel('Height, (m)')

%%INPUT number of cells for length of contact patch (odd number)
numblength = 13;
%%INPUT number of cells for width of contact patch (odd number)
numbwidth = 13;

%%Assume Sandy Loam ***INPUT
kc = 5.27; %% [kN/m^n+1]
kphi = 1515.04; %% [kN/m^n+2]
n = 0.7;

%%width of contact patch
bp = (numbwidth-1)*dx; %% [m]
%%length of contact patch
lp = (numblength-1)*dy %% [m]
%%longitudinal slip ratio
s = 0;
%%shape change factor
A1 = 1;

Fz = 18.67*1000; %% [kN]

zeta = 0:dy:lp;
term1 = ((4*Fz)/(pi*bp*lp));
term2 = (1+A1*s*(zeta-(lp/2)));
term3a = (zeta-(lp/2)).^2;
term3b = (lp/2)^2;
term3c = term3a/term3b;
term3 = sqrt(1-term3c);
p = ((term1.*term2.*term3)/1000)';

vectorzero(NoPts,1)=0;
Vold = vectorzero;
[M,N] = size(p);
Vold(1:M,1)=p(1:M);
Vold1 = Vold;
Vold1(M+1:(M*2),1)=p(1:M);
Vold2=Vold1;
Vold2((M*2)+1:(M*3),1)=p(1:M);

pvector = Vold2;
onevector = ones(1,NoPts);
pressure = pvector*onevector;

sinkage = (pressure./((kc/bp) + kphi)).^(1/n);

%%deflection of pneumatic wheel
%%deflection is function of radius of wheel and sinkage

```

```

radius = (lp/2)*1000;

adeflection = -2;
bdeflection = 4.*radius-2.*sinkage;
cdeflection = -(lp.^2) + (2.*radius.*sinkage) - (sinkage.^2);
firstterm = sqrt(bdeflection.^2 - 4.*adeflection.*cdeflection);

deflectionplus = ((-bdeflection + firstterm)./(2*adeflection));
deflectionminus = (-bdeflection - firstterm)./(2*adeflection);

Zold = Z;
for i = imin:numblength;
    for j = ((jmax-1)/2)-5:((jmax-1)/2)-6+numbwidth-1;
        Zold(i,j)=Z(i,j)-sinkage(i,j)-deflectionplus(i,j); %%[m]
    end
end

figure(2)
%plot(xgrid,Zold)
mesh(xgrid,ygrid,Zold)
zlim([0.95 1.05])
xlabel('x, (m)')
ylabel('y, (m)')
zlabel('Height, (m)')

Zold1 = Zold;
for i = numblength+1:numblength*2;
    for j = ((jmax-1)/2)-5:((jmax-1)/2)-6+numbwidth-1;
        Zold1(i,j)=Zold(i,j)-sinkage(i,j)-deflectionplus(i,j); %%[m]
    end
end

figure(3)
mesh(xgrid,ygrid,Zold1)
zlim([0.95 1.05])
xlabel('x, (m)')
ylabel('y, (m)')
zlabel('Height, (m)')

Zold2 = Zold1;
for i = (numblength*2)+1:numblength*3;
    for j = ((jmax-1)/2)-5:((jmax-1)/2)-6+numbwidth-1;
        Zold2(i,j)=Zold1(i,j)-sinkage(i,j)-deflectionplus(i,j); %%[m]
    end
end

figure(4)
mesh(xgrid,ygrid,Zold2)
zlim([0.95 1.05])
xlabel('x, (m)')
ylabel('y, (m)')
zlabel('Height, (m)')

figure(5)
plot(ygrid,Zold2)
ylim([0.985 1.002])

```

```
xlabel('y, (m)')
ylabel('Height, (m)')
```

C.4 MATLAB m-file for rigid wheel rolling on deterministic surface

The MATLAB code that was created for the semi-oval bump was very similar. The only difference was that the deterministic flat surface was changed to the deterministic semi-oval bump created with the following code. This semi-oval bump was also created for the rolling of the flexible wheel case.

MATLAB m-file for semi-oval bump:

```
%Creating deterministic nonflat surface of 1m height
for i = imin:imax-1;
    for j = jmin:jmax-1;
        Z(i,j)=1; %%[m]
        S(i,j)=0;
    end
end
for i = 15:25;
    for j = jmin:jmax-1;
        Z(i,j)=1.004; %%[m]
    end
end
for i = 17:23;
    for j = jmin:jmax-1;
        Z(i,j)=1.008; %%[m]
    end
end
for i = 19:21;
    for j = jmin:jmax-1;
        Z(i,j)=1.012; %%[m]
    end
end

figure(1)
mesh(xgrid,ygrid,Z)
zlim([0.95 1.05])
xlabel('x')
ylabel('y')
zlabel('Height, (m)')
```

MATLAB m-file for simulation:

```
clear all

X=2; %distance of x-axis [m]
Y=2; %distance of y-axis [m]
```

```

imax=41;
jmax=41;
imin=1;
jmin=1;
dx=X/(imax-1);
dy=Y/(jmax-1);

xgrid=dx:dx:X;
ygrid=dy:dy:Y;

%%Creating deterministic flat surface of 1m height
for i = imin:imax-1;
    for j = jmin:jmax-1;
        Z(i,j)=1; %%[m]
        S(i,j)=0;
    end
end

figure(1)
mesh(xgrid,ygrid,Z)
zlim([0.95 1.05])
xlabel('x')
ylabel('y')
zlabel('Height, (m)')

%%INPUT number of cells for length of contact patch (odd number)
numblength = 13;
%%INPUT number of cells for width of contact patch (odd number)
numbwidth = 13;

%%Assume Sandy Loam ***INPUT
kc = 5.27; %% [kN/m^n+1]
kphi = 1515.04; %% [kN/m^n+2]
n = 0.7;

%%width of contact patch
bp = (numbwidth-1)*dx; %% [m]
%%length of contact patch
lp = (numblength-1)*dy; %% [m]
%%longitudinal slip ratio ***INPUT
s = 0;
%%shape change factor ***INPUT
A1 = 1;

%%Vertical Force
Fz = 18.67*1000; %% [kN]

zeta = 0:dy:lp;

p = (((4*Fz)/(pi*bp*lp)).*(1+A1*s*(zeta-(lp/2))).*sqrt(1-(((zeta-(lp/2)).^2)/((lp/2)^2))))/1000';
sinkage = (p./((kc/bp) + kphi)).^(1/n);

%%% Bottom left corner is now at (1,1)
%%%INPUT (add number to move up) **only effective for figure(2)
h = 1;

```

```

%%%INPUT (add number to move right)
k = 15;

%%move center in y direction
hc=((numblength+1)/2)+h;
%%move center in x direction
kc=((numbwidth-1)/2)+k;

n=2;
a=(numblength-1)/2; %number of points (length)
b=(numbwidth-1)/2; %number of points (width)
x=1+h:1:numblength+h;

y = b*(1-((x-hc)./a).^n).^(1/n)+kc;
yminus = -b*(1-((x-hc)./a).^n).^(1/n)+kc;

Y = round(y+1);
Yminus = round(yminus+1);

%%%Contact Patch for thesis
Xaxis = 0:1:numblength-1;
Ypaper1 = Yminus-16;
Ypaper2 = Y-16;
figure(2)
plot(Ypaper1,Xaxis,Ypaper2,Xaxis)
xlabel('Number of points in x direction')
ylabel('Number of points in y direction')
grid on

coordinates(numblength,3)=0;
coord = coordinates;
coord(1:numblength,1) = x(1:numblength);
coord(1:numblength,2) = Yminus(1:numblength);
coord(1:numblength,3) = Y(1:numblength);

Zold = Z;
Maximum = (numblength+1)/2;
for t = 1:Maximum
    for i = coord(t,1)-1
        for j = coord(t,2):coord(t,3)
            S(i,j) = sinkage(t);
        end
    end
end

NoIterations = 33;
for t = Maximum:NoIterations;
    for i = coord(Maximum,1)-1:NoIterations-1
        for j = coord(Maximum,2):coord(Maximum,3)
            S(i,j) = sinkage(Maximum);
        end
    end
end

for i = NoIterations
    for j = coord(7,2):coord(7,3);

```

```

        S(i,j) = sinkage(7);
    end
end

for i = NoIterations+1
    for j = coord(8,2):coord(8,3);
        S(i,j) = sinkage(8);
    end
end

for i = NoIterations+2
    for j = coord(9,2):coord(9,3);
        S(i,j) = sinkage(9);
    end
end

for i = NoIterations+3
    for j = coord(10,2):coord(10,3);
        S(i,j) = sinkage(10);
    end
end

for i = NoIterations+4
    for j = coord(11,2):coord(11,3);
        S(i,j) = sinkage(11);
    end
end

for i = NoIterations+5
    for j = coord(12,2):coord(12,3);
        S(i,j) = sinkage(12);
    end
end

for i = NoIterations+6
    for j = coord(13,2):coord(13,3);
        S(i,j) = sinkage(13);
    end
end

Zold=Z-S; %%[m]

figure(3)
mesh(xgrid,ygrid,Zold)
zlim([0.95 1.05])
xlabel('x, (m)')
ylabel('y, (m)')
zlabel('Height, (m)')

figure(5)
plot(ygrid,Zold)
ylim([0.985 1.002])
xlabel('y, (m)')
ylabel('Height, (m)')

```

C.5 MATLAB m-file for flexible wheel rolling on deterministic surface

```
clear all

X=2; %distance of x-axis [m]
Y=2; %distance of y-axis [m]
imax=41;
jmax=41;
imin=1;
jmin=1;
dx=X/(imax-1);
dy=Y/(jmax-1);

xgrid=dx:dx:X;
ygrid=dy:dy:Y;

%%Creating deterministic flat surface of 1m height
for i = imin:imax-1;
    for j = jmin:jmax-1;
        Z(i,j)=1; %%[m]
        S(i,j)=0;
    end
end

figure(1)
mesh(xgrid,ygrid,Z)
zlim([0.95 1.05])
xlabel('x')
ylabel('y')
zlabel('Height, (m)')

%%INPUT number of cells for length of contact patch (odd number)
numblength = 13;
%%INPUT number of cells for width of contact patch (odd number)
numbwidth = 13;

%%Assume Sandy Loam ***INPUT
kc = 5.27; %% [kN/m^n+1]
kphi = 1515.04; %% [kN/m^n+2]
n = 0.7;

%%width of contact patch
bp = (numbwidth-1)*dx; %% [m]
%%length of contact patch
lp = (numblength-1)*dy; %% [m]
%%longitudinal slip ratio ***INPUT
s = 0;
%%shape change factor ***INPUT
A1 = 1;

%%Vertical Force
Fz = 18.67*1000; %% [kN]

zeta = 0:dy:lp;
```

```

p = (((4*Fz)/(pi*bp*lp)).*(1+A1*s*(zeta-(lp/2))).*sqrt(1-(((zeta-(lp/2)).^2)/((lp/2)^2))))/1000';
sinkage = (p./((kc/bp) + kphi)).^(1/n);

%%deflection of pneumatic wheel
%%deflection is function of radius of wheel and sinkage
radius = (lp/2)*1000;

adeflection = -2;
bdeflection = 4.*radius-2.*sinkage;
cdeflection = -(lp.^2) + (2.*radius.*sinkage) - (sinkage.^2);
firstterm = sqrt(bdeflection.^2 - 4.*adeflection.*cdeflection);

deflectionplus = ((-bdeflection + firstterm)./(2*adeflection));
deflectionminus = (-bdeflection - firstterm)./(2*adeflection);

%%% Bottom left corner is now at (1,1)
%%%INPUT (add number to move up)  **only effective for figure(2)
h = 1;
%%%INPUT (add number to move right)
k = 15;

%%move center in y direction
hc=((numblength+1)/2)+h;
%%move center in x direction
kc=((numbwidth-1)/2)+k;

n=2;
a=(numblength-1)/2;  %number of points (length)
b=(numbwidth-1)/2;  %number of points (width)
x=1+h:1:numblength+h;

y = b*(1-((x-hc)./a).^n).^(1/n)+kc;
yminus = -b*(1-((x-hc)./a).^n).^(1/n)+kc;

Y = round(y+1);
Yminus = round(yminus+1);

%%%Contact Patch for thesis
Xaxis = 0:1:numblength-1;
Ypaper1 = Yminus-16;
Ypaper2 = Y-16;
figure(2)
plot(Ypaper1,Xaxis,Ypaper2,Xaxis)
xlabel('Number of points in x direction')
ylabel('Number of points in y direction')
grid on

coordinates(numblength,3)=0;
coord = coordinates;
coord(1:numblength,1) = x(1:numblength);
coord(1:numblength,2) = Yminus(1:numblength);
coord(1:numblength,3) = Y(1:numblength);

Zold = Z;
Maximum = (numblength+1)/2;

```



```

for t = 1:Maximum
    for i = coord(t,1)-1
        for j = coord(t,2):coord(t,3)
            S(i,j) = sinkage(t)+deflectionplus(t);
        end
    end
end

NoIterations = 33;
for t = Maximum:NoIterations;
    for i = coord(Maximum,1)-1:NoIterations-1
        for j = coord(Maximum,2):coord(Maximum,3)
            S(i,j) = sinkage(Maximum)+deflectionplus(Maximum);
        end
    end
end

for i = NoIterations
    for j = coord(7,2):coord(7,3);
        S(i,j) = sinkage(7)+deflectionplus(7);
    end
end

for i = NoIterations+1
    for j = coord(8,2):coord(8,3);
        S(i,j) = sinkage(8)+deflectionplus(8);
    end
end

for i = NoIterations+2
    for j = coord(9,2):coord(9,3);
        S(i,j) = sinkage(9)+deflectionplus(9);
    end
end

for i = NoIterations+3
    for j = coord(10,2):coord(10,3);
        S(i,j) = sinkage(10)+deflectionplus(10);
    end
end

for i = NoIterations+4
    for j = coord(11,2):coord(11,3);
        S(i,j) = sinkage(11)+deflectionplus(11);
    end
end

for i = NoIterations+5
    for j = coord(12,2):coord(12,3);
        S(i,j) = sinkage(12)+deflectionplus(12);
    end
end

for i = NoIterations+6
    for j = coord(13,2):coord(13,3);
        S(i,j) = sinkage(13)+deflectionplus(13);
    end
end

```

```

        end
    end

    Zold=Z-S; %%[m]

    figure(3)
    mesh(xgrid,ygrid,Zold)
    zlim([0.95 1.05])
    xlabel('x, (m)')
    ylabel('y, (m)')
    zlabel('Height, (m)')

    Zold1 = Zold
    figure(5)
    plot(xgrid,Zold1);
    ylim([0.985 1.002])
    xlabel('y, (m)')
    ylabel('Height, (m)')

```

C.6 MATLAB m-file for rigid wheel rolling on deterministic surface with stochastic soil

```

clear all

X=2; %distance of x-axis [m]
Y=2; %distance of y-axis [m]
imax=41;
jmax=41;
imin=1;
jmin=1;
dx=X/(imax-1);
dy=Y/(jmax-1);

xgrid=dx:dx:X;
ygrid=dy:dy:Y;

%%Creating deterministic flat surface of 1m height
for i = imin:imax-1;
    for j = jmin:jmax-1;
        Z(i,j)=1; %%[m]
        S(i,j)=0;
    end
end

figure(1)
mesh(xgrid,ygrid,Z)
zlim([0.95 1.05])
xlabel('x')
ylabel('y')
zlabel('Height, (m)')

%%INPUT number of cells for length of contact patch (odd number)
numblength = 13;
%%INPUT number of cells for width of contact patch (odd number)
numbwidth = 13;

```

```

%%Assume Sandy Loam ***INPUT
kc = 5.27; %% [kN/m^n+1]
kphi = 1515.04; %% [kN/m^n+2]
n = 0.7;

%%width of contact patch
bp = (numbwidth-1)*dx; %% [m]
%%length of contact patch
lp = (numblength-1)*dy; %% [m]
%%longitudinal slip ratio ***INPUT
s = 0;
%%shape change factor ***INPUT
A1 = 1;

%%Vertical Force
Fz = 18.67*1000; %% [kN]

zeta = 0:dy:lp;

p = (((4*Fz)/(pi*bp*lp)).*(1+A1*s*(zeta-(lp/2))).*sqrt(1-(((zeta-(lp/2)).^2)/((lp/2)^2))))/1000)';

%%% Bottom left corner is now at (1,1)
%%%INPUT (add number to move up) **only effective for figure(2)
h = 1;
%%%INPUT (add number to move right)
k = 15;

%%move center in y direction
hc=((numblength+1)/2)+h;
%%move center in x direction
kc=((numbwidth-1)/2)+k;

n=2;
a=(numblength-1)/2; %number of points (length)
b=(numbwidth-1)/2; %number of points (width)
x=1+h:1:numblength+h;

y = b*(1-((x-hc)./a).^n).^(1/n)+kc;
yminus = -b*(1-((x-hc)./a).^n).^(1/n)+kc;

Y = round(y+1);
Yminus = round(yminus+1);

%%%Contact Patch for thesis
Xaxis = 0:1:numblength-1;
Ypaper1 = Yminus-16;
Ypaper2 = Y-16;
figure(2)
plot(Ypaper1,Xaxis,Ypaper2,Xaxis)
xlabel('Number of points in x direction')
ylabel('Number of points in y direction')
grid on

coordinates(numblength,3)=0;
coord = coordinates;

```

```

coord(1:numblength,1) = x(1:numblength);
coord(1:numblength,2) = Yminus(1:numblength);
coord(1:numblength,3) = Y(1:numblength);

syms x
%chaos dimension
polynomial_dimension=1;
polynomial_order=3;
chaos=factorial(polynomial_dimension+polynomial_order)/factorial(polynomial_d
imension)/factorial(polynomial_order);
%uncertainty amplitude
r=5;
Kphi_pc(1)=Kphi;
Kphi_pc(2)=Kphi_pc(1)/r;
Kphi_pc(3:chaos)=0;

%calculate the orthogonality
%collocation roots
colroots=rand(1,4);
%calculate the collocation matrix
for k=1:chaos
    for l=1:chaos
        Acol(k,l)=subs(Legendre_polynomial(1,x),colroots(k));
        coeff(k,l)=Kphi_pc(l)*Acol(k,l);
    end
    Kphi_col(k)=sum(coeff(k,:));
end

for i = imin:imax-1;
    for j = jmin:jmax-1;
        kphis(i,j) = Kphi_col;
    end
end

Zold = Z;
Maximum = (numblength+1)/2;
for t = 1:Maximum
    for i = coord(t,1)-1
        for j = coord(t,2):coord(t,3)
            S(i,j) = ((p(t)./((kc/bp) + kphis(i,j))).^(1/n));
        end
    end
end

NoIterations = 33;
for t = Maximum:NoIterations;
    for i = coord(Maximum,1)-1:NoIterations-1
        for j = coord(Maximum,2):coord(Maximum,3)
            S(i,j) = ((p(Maximum)./((kc/bp) + kphis(i,j))).^(1/n));
        end
    end
end

for i = NoIterations
    for j = coord(7,2):coord(7,3);
        S(i,j) = ((p(7)./((kc/bp) + kphis(i,j))).^(1/n));
    end
end

```

```

end
end

for i = NoIterations+1
    for j = coord(8,2):coord(8,3);
        S(i,j) = ((p(8)./((kc/bp) + kphis(i,j))).^(1/n));
    end
end

for i = NoIterations+2
    for j = coord(9,2):coord(9,3);
        S(i,j) = ((p(9)./((kc/bp) + kphis(i,j))).^(1/n));
    end
end

for i = NoIterations+3
    for j = coord(10,2):coord(10,3);
        S(i,j) = ((p(10)./((kc/bp) + kphis(i,j))).^(1/n));
    end
end

for i = NoIterations+4
    for j = coord(11,2):coord(11,3);
        S(i,j) = ((p(11)./((kc/bp) + kphis(i,j))).^(1/n));
    end
end

for i = NoIterations+5
    for j = coord(12,2):coord(12,3);
        S(i,j) = ((p(12)./((kc/bp) + kphis(i,j))).^(1/n));
    end
end

for i = NoIterations+6
    for j = coord(13,2):coord(13,3);
        S(i,j) = ((p(13)./((kc/bp) + kphis(i,j))).^(1/n));
    end
end

Zold=Z-(S)/19; %%[m]

figure(3)
mesh(xgrid,ygrid,Zold)
zlim([0.95 1.05])
xlabel('x, (m)')
ylabel('y, (m)')
zlabel('Height, (m)')

figure(5)
plot(ygrid,Zold)
ylim([0.985 1.002])
xlabel('y, (m)')
ylabel('Height, (m)')

```

C.7 MATLAB m-file for flexible wheel rolling on deterministic surface, stochastic soil

```
clear all

X=2; %distance of x-axis [m]
Y=2; %distance of y-axis [m]
imax=41;
jmax=41;
imin=1;
jmin=1;
dx=X/(imax-1);
dy=Y/(jmax-1);

xgrid=dx:dx:X;
ygrid=dy:dy:Y;

%%Creating deterministic flat surface of 1m height
for i = imin:imax-1;
    for j = jmin:jmax-1;
        Z(i,j)=1; %%[m]
        S(i,j)=0;
    end
end

figure(1)
mesh(xgrid,ygrid,Z)
zlim([0.95 1.05])
xlabel('x')
ylabel('y')
zlabel('Height, (m)')

%%INPUT number of cells for length of contact patch (odd number)
numblength = 13;
%%INPUT number of cells for width of contact patch (odd number)
numbwidth = 13;

%%Assume Sandy Loam ***INPUT
kc = 5.27; %% [kN/m^n+1]
kphi = 1515.04; %% [kN/m^n+2]
n = 0.7;

%%width of contact patch
bp = (numbwidth-1)*dx; %% [m]
%%length of contact patch
lp = (numblength-1)*dy; %% [m]
%%longitudinal slip ratio ***INPUT
s = 0;
%%shape change factor ***INPUT
A1 = 1;

%%Vertical Force
Fz = 18.67*1000; %% [kN]

zeta = 0:dy:lp;
```

```

p = (((4*Fz)/(pi*bp*lp)).*(1+A1*s*(zeta-(lp/2))).*sqrt(1-(((zeta-
(lp/2)).^2)/((lp/2)^2))))/1000)';
sinkage = (p./((kc/bp) + kphi)).^(1/n);

%%deflection of pneumatic wheel
%%deflection is function of radius of wheel and sinkage
radius = (lp/2)*1000;

adeflection = -2;
bdeflection = 4.*radius-2.*sinkage;
cdeflection = -(lp.^2) + (2.*radius.*sinkage) - (sinkage.^2);
firstterm = sqrt(bdeflection.^2 - 4.*adeflection.*cdeflection);

deflectionplus = ((-bdeflection + firstterm)./(2*adeflection));
deflectionminus = (-bdeflection - firstterm)./(2*adeflection);

%% Bottom left corner is now at (1,1)
%%%INPUT (add number to move up) **only effective for figure(2)
h = 1;
%%%INPUT (add number to move right)
k = 15;

%%move center in y direction
hc=((numblength+1)/2)+h;
%%move center in x direction
kc=((numbwidth-1)/2)+k;

n=2;
a=(numblength-1)/2; %number of points (length)
b=(numbwidth-1)/2; %number of points (width)
x=1+h:1:numblength+h;

y = b*(1-((x-hc)./a).^n).^((1/n))+kc;
yminus = -b*(1-((x-hc)./a).^n).^((1/n))+kc;

Y = round(y+1);
Yminus = round(yminus+1);

%%Contact Patch for thesis
Xaxis = 0:1:numblength-1;
Ypaper1 = Yminus-16;
Ypaper2 = Y-16;
figure(2)
plot(Ypaper1,Xaxis,Ypaper2,Xaxis)
xlabel('Number of points in x direction')
ylabel('Number of points in y direction')
grid on

coordinates(numblength,3)=0;
coord = coordinates;
coord(1:numblength,1) = x(1:numblength);
coord(1:numblength,2) = Yminus(1:numblength);
coord(1:numblength,3) = Y(1:numblength);

syms x
%chaos dimension

```

```

polynomial_dimension=1;
polynomial_order=3;
chaos=factorial(polynomial_dimension+polynomial_order)/factorial(polynomial_d
imension)/factorial(polynomial_order);
%uncertainty amplitude
r=5;
Kphi_pc(1)=Kphi;
Kphi_pc(2)=Kphi_pc(1)/r;
Kphi_pc(3:chaos)=0;

%calculate the orthogonality
%collocation roots
colroots=rand(1,4);
%calculate the collocation matrix
for k=1:chaos
    for l=1:chaos
        Acol(k,l)=subs(Legendre_polynomial(1,x),colroots(k));
        coeff(k,l)=Kphi_pc(l)*Acol(k,l);
    end
    Kphi_col(k)=sum(coeff(k,:));
end

for i = imin:imax-1;
    for j = jmin:jmax-1;
        kphis(i,j) = Kphi_col;
    end
end

Zold = Z;
Maximum = (numblength+1)/2;
for t = 1:Maximum
    for i = coord(t,1)-1
        for j = coord(t,2):coord(t,3)
            S(i,j) = ((p(t)./((kc/bp) +
kphis(i,j))).^(1/n))+deflectionplus(t);
        end
    end
end

NoIterations = 33;
for t = Maximum:NoIterations;
    for i = coord(Maximum,1)-1:NoIterations-1
        for j = coord(Maximum,2):coord(Maximum,3)
            S(i,j) = ((p(Maximum)./((kc/bp) +
kphis(i,j))).^(1/n))+deflectionplus(Maximum);
        end
    end
end

for i = NoIterations
    for j = coord(7,2):coord(7,3);
        S(i,j) = ((p(7)./((kc/bp) + kphis(i,j))).^(1/n))+deflectionplus(7);
    end
end

for i = NoIterations+1

```



```

    for j = coord(8,2):coord(8,3);
        S(i,j) = ((p(8)./((kc/bp) + kphis(i,j))).^(1/n))+deflectionplus(8);
    end
end

for i = NoIterations+2
    for j = coord(9,2):coord(9,3);
        S(i,j) = ((p(9)./((kc/bp) + kphis(i,j))).^(1/n))+deflectionplus(9);
    end
end

for i = NoIterations+3
    for j = coord(10,2):coord(10,3);
        S(i,j) = ((p(10)./((kc/bp) + kphis(i,j))).^(1/n))+deflectionplus(10);
    end
end

for i = NoIterations+4
    for j = coord(11,2):coord(11,3);
        S(i,j) = ((p(11)./((kc/bp) + kphis(i,j))).^(1/n))+deflectionplus(11);
    end
end

for i = NoIterations+5
    for j = coord(12,2):coord(12,3);
        S(i,j) = ((p(12)./((kc/bp) + kphis(i,j))).^(1/n))+deflectionplus(12);
    end
end

for i = NoIterations+6
    for j = coord(13,2):coord(13,3);
        S(i,j) = ((p(13)./((kc/bp) + kphis(i,j))).^(1/n))+deflectionplus(13);
    end
end

Zold=Z-(S)/34; %%[m]

figure(3)
mesh(xgrid,ygrid,Zold)
zlim([0.95 1.05])
xlabel('x, (m)')
ylabel('y, (m)')
zlabel('Height, (m)')

figure(5)
plot(ygrid,Zold)
ylim([0.985 1.002])
xlabel('y, (m)')
ylabel('Height, (m)')

```

C.8 MATLAB m-file for rolling on stochastic surface with deterministic soil

The MATLAB m-file used to produce the simulation of a rigid wheel rolling on a stochastic surface with deterministic soil is similar to the MATLAB m-file displayed in Appendix C.4 (Simulation of rigid wheel rolling on deterministic terrain and deterministic soil parameters). The only difference is that the stochastic terrain profile method developed in this thesis is incorporated into the m-file instead of the flat deterministic terrain profile (MATLAB m-file introduced in Appendix A is inserted in MATLAB m-file simulation in Appendix C.4).

The MATLAB m-file used to produce the simulation of a flexible wheel rolling on a stochastic surface with deterministic soil is similar to the MATLAB m-file displayed in Appendix C.5 (Simulation of flexible wheel rolling on deterministic terrain and deterministic soil parameters). The only difference is that the stochastic terrain profile method developed in this thesis is incorporated into the m-file instead of the flat deterministic terrain profile (MATLAB m-file introduced in Appendix A is inserted in MATLAB m-file simulation in Appendix C.5).

C.9 MATLAB m-file for rolling on stochastic surface with stochastic soil

The MATLAB m-file used to produce the simulation of a rigid wheel rolling on a stochastic surface with stochastic soil is similar to the MATLAB m-file displayed in Appendix C.5 (Simulation of rigid wheel rolling on deterministic terrain and stochastic soil parameters). The only difference is that the stochastic terrain profile method developed in this thesis is incorporated into the m-file instead of the flat deterministic terrain profile (MATLAB m-file introduced in Appendix A is inserted in MATLAB m-file simulation in Appendix C.5).

The MATLAB m-file used to produce the simulation of a flexible wheel rolling on a stochastic surface with stochastic soil is similar to the MATLAB m-file displayed in Appendix C.6 (Simulation of flexible wheel rolling on deterministic terrain and stochastic soil parameters). The only difference is that the stochastic terrain profile method developed in this thesis is incorporated into the m-file instead of the flat deterministic terrain profile (MATLAB m-file introduced in Appendix A is inserted in MATLAB m-file simulation in Appendix C.6).